Utrecht University

A Colder Earth

Modelling carbon cycle perturbations to assess the course of the Eocene-Oligocene Transition

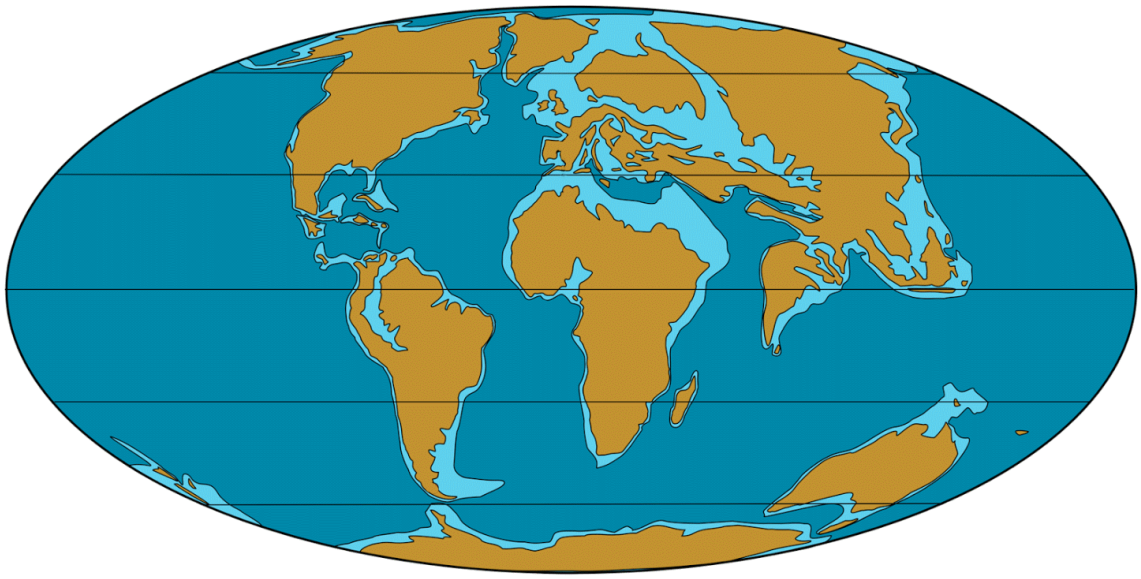

Eocene-Oligocene paleomap from Angst et al. (2013)

Master Thesis

Pieter Slomp

Utrecht University
Faculty of Earth Sciences
Master programme Earth, Life and Climate

Supervisors
dr. Anna von der Heydt
Prof. dr. Lucas Lourens

6 July 2022

Master Thesis

Pieter Slomp
Student no. 6240518

Utrecht University
Faculty of Earth Sciences
Master programme Earth, Life and Climate

Abstract

The Eocene-Oligocene Transition (EOT, ca. 34 Ma) marks an important point in geological history. Oxygen isotope shifts imply the formation of a large Antarctic ice cap, while carbon isotope shifts suggest this was paired with perturbations in the carbon cycle. In this research, these carbon cycle perturbations are brought under a closer look. Various hypotheses, which try to explain these carbon cycle perturbations, are tested using an adapted version of LOSCAR, a long-term carbon cycle ocean-atmosphere partitioning model. The model output was compared against carbonate compensation depth (CCD), benthic $\delta^{13}C$ and atmospheric pCO_2 reconstructions, among others. The model output brought forward three important implications: 1. Shelf-to-basin carbonate burial fractionation change explains best the two-step pattern and rapidness of CCD deepening. 2. Benthic $\delta^{13}C$ increase can be best explained by an increase in organic carbon burial due to increased (high latitude) biological productivity. 3. Increased silicate weathering needs to be invoked to explain the strong decline of atmospheric pCO_2 and subsequent "subduing" of any potential recovery. These implications were confronted with issues raised, to form eventually two synthesis scenarios which are proposed to be good contenders for the course of the EOT. The first synthesis scenario assumes a large shelf-to-basin carbonate burial fractionation change with a transient increase in carbonate weathering, highly enriched in $\delta^{13}C$. The second synthesis scenario assumes a pivotal role for organic carbon burial, with a transient increase in (high latitude) biological productivity besides increased ocean ventilation, coupled with a lesser carbonate burial fractionation and weathering change. Both synthesis scenarios include an increase in silicate weathering to explain major atmospheric pCO_2 decline. Ocean circulation change, by strengthening North Atlantic Deep Water (NADW) formation versus Southern Ocean Deep Water (SODW) formation, was also tested, to view the possible role of hypothesised ocean circulation change on the carbon cycle during the EOT. This (secondary) research proved less fruitful, as LOSCAR lacks a proper (dynamic) ocean circulation that is coupled with mechanisms. Nevertheless, the research offers insight to ocean circulation change and how it would fit with carbon cycle perturbations through a framework of "cascade tipping".

Contents

Appendices contents

1. Introduction

1.1. The Eocene-Oligocene Transition

The Eocene-Oligocene Transition (hereafter abbreviated as EOT) took place about 34 million years ago changing the Earth's climate system in the timespan of roughly half a million years. It marks the most important step from a Warmhouse to an Icehouse world during the Cenozoic (Westerhold et al., 2020; Zachos and Kump, 2005). $\delta^{18}O$, considered a proxy for global ice volume, shows a distinctive two-step pattern increase across the EOT (Pälike et al., 2006; Pearson et al., 2009). This increase in $\delta^{18}O$ (ca. 1.2 to 1.5‰) has been interpreted as marking the beginning of permanent glaciation of Antarctica, which in Eocene times was ice-free and lushly vegetated (Coxall and Pearson, 2007). This build-up of ice generated a lower eustatic sea level of about 70 metres (Hutchinson et al., 2021; Miller et al., 2020). The proxy $\delta^{13}C$ shows a similar path as $\delta^{18}O$, with a distinct two-stepped increase in values (ca. 0.7 to 1.0‰), suggesting that the build-up of the Antarctic ice sheet was paired with carbon cycle perturbation(s) (Coxall and Pearson, 2007; Coxall et al., 2005). Further evidence of perturbation(s) in the carbon cycle are shown in reconstructions of the carbonate compensation depth (CCD), which deepened with over a kilometre (e.g. van Andel, 1975; Rea and Lyle, 2005; Pälike et al., 2012), as well as declines in atmospheric pCO_2 in the order of several hundreds of ppm (Pearson et al., 2009; Heureux and Rickaby, 2015).

Two main hypothesises have been put forward to explain the cause of the EOT: ocean circulation change through gateway openings and long-term atmospheric pCO_2 drawdown (Kennedy et al., 2015). The former can be split into Northern and Southern gateway openings. The Southern gateway openings, the Tasman Strait and the Drake Passage, are hypothesised to have opened during the EOT, allowing for the formation of a strong (proto-)Antarctic Circumpolar Current (ACC), blocking or diminishing poleward warm waters to Antarctica, enabling ice growth (Kennedy et al., 2015; Coxall and Pearson, 2007). Some argue however, that the timing of these gateway openings is poorly constrained or otherwise not viable as cause for glaciation (e.g. Goldner et al., 2014). Some propose Northern gateway openings (such as the Greenland-Scotland Ridge), and presume a strengthened Atlantic Meridional Overturning Circulation (AMOC) and onset of North Atlantic Deep Water (NADW) formation, which, through enhanced ocean ventilation and biological productivity, primed Antarctic glaciation (e.g. Straume et al., 2022; Abelson and Erez, 2017). In the latter hypothesis, long-term drawdown of atmospheric pCO_2 caused rapid Antarctic glaciation (DeConto and Pollard, 2003). This drawdown already took place in the Eocene through silicate weathering and possibly lower continental crust production (Rynders, 2013), and was accelerated by Milankovitch cycles and ice-albedo feedback during the EOT (Coxall & Pearson, 2007). Eventually, a threshold atmospheric pCO_2 was reached, in the order of 2.4 to 2.8 times a pre-Industrial 280 ppm, which caused irreversible ice

growth in Antarctica (DeConto and Pollard, 2003). Through coupling with biological productivity feedback, Zachos and Kump (2005) showed that this hypothesis could explain the two-stepped pattern.

1.2. Research

Understanding the cause of the EOT requires understanding the course of the EOT, as the cause must be capable of explaining the course. Yet the exact course of the EOT remains elusive. Due to shifts in the environment and the speed of climate change, many sedimentary cores and proxy records contain hiatuses during the EOT timeframe (Hutchinson et al., 2021). Modelling the EOT offers an alternative. In this study, to better consider the course of the EOT, the carbon cycle perturbations during the EOT are investigated through modelling. Tested are various hypotheses, that try to link changes in the carbon cycle with climate system responses during the EOT (Coxall and Wilson, 2011). The study aims to answer how plausible these hypotheses are in explaining the proxy records, with a special focus on CCD reconstructions, and which hypothesis, or combination of, can explain best the carbon cycle perturbations during the EOT. Additionally, the role of a strengthening in the AMOC by a shift in deep water formation from South to North during the EOT is also investigated, to answer what the potential role it could have played in the carbon cycle perturbations during the EOT as well. With this, the study hopes to give a better insight into what the EOT actually entailed.

1.3. Thesis structure

In Section 2, background information regarding conditions (temperature and sea level, ocean circulation change, biological productivity and weathering) and terminology of the EOT will be given, as well as outlining proxy data. In Section 3, the methods will be elaborated: firstly, the model utilised in the study, LOSCAR, will be introduced, and what adaptations to it are implemented. Secondly, the model set-up and initial Late Eocene model state are delineated. Lastly, the scenarios that will test the hypotheses are elaborated. In Section 4, the results are shown, and in Section 5, discussion regarding these results and the model occurs. Lastly, in Section 6, the conclusion will be written.

2. Background

2.1. Terminology and conditions during the EOT

2.1.1. Terminology and timeframe

The period of interest for the EOT stretches a period of 500 to 790 kyr, around the Eocene-Oligocene boundary of 33.9 Ma (Hutchinson et al., 2021), previously set at 33.7 Ma (Coxall and Pearson, 2007). At 34.1 Ma, a so-called "precursor event" took place: this precursor event is seen as the first of important $\delta^{18}O$ increases (Katz et al., 2008; Miller et al., 2009). The same Miller et al. (2009) and Katz et al. (2008) denote the two main steps ($\delta^{18}O$ increases) of the EOT as EOT-1 and EOT-2, which occurred at 33.8 Ma and 33.63 Ma, respectively. Oi-1, during which most of Oligocene glaciation occurred, is set at 33.54 Ma by them. 34.1 Ma to 33.54 Ma gives a timeframe of roughly 500 kyr. However, Hutchinson et al. (2021) uses a different timing scheme for the EOT, extending the timeframe to 790 kyr. They argue that while Katz et al. (2008)'s EOT-1 arguably corresponds to Coxall and Pearson (2007)'s "Step 1" in the latter's review of the EOT, Katz et al. (2008)'s identification of EOT-2 is actually based on a separate feature in the St. Stephens Quarry record. Therefore, Hutchinson et al. (2021) do not use the term EOT-2 for the second step in Coxall and Pearson (2007). In their redefinition of the EOT, the EOT starts with the extinction of the tropical warm-water nannofossil *Discoaster saipanensis* (34.44 Ma), coincident with significant $\delta^{18}O$ increase, visible in many records and termed the "late Eocene event" (Hutchinson et al., 2021; Katz et al., 2008). Hutchinson et al. (2021) considered these biotic and climatic events that occurred during this event relevant for the EOT, thus expediting the start of the EOT, compared to the previous defined onset with the "precursor event" of 34.1 Ma. The precise age constraints of "Step 1", according to Hutchinson et al. (2021), have yet to be defined, and requires better-resolved records. However, "Step 1" (or EOT-1) is still an important and clear phase in the EOT terminology, to differentiate between cooling and ice growth phases. As Step 1 is defined in Hutchinson et al.'s terminology of the EOT as before the Eocene-Oligocene boundary (33.9 Ma), an approximate age of 34 Ma could be used. Following said terminology, the EOT ends at the "Earliest Oligocene oxygen isotope step" (EOIS) at ca. 33.65 Ma, and goes over into the 490 kyr long Early Oligocene Glacial Maximum (EOGM). This gives, from 34.44 Ma to 33.65 Ma, a period of roughly 790 kyr for the EOT.

2.1.2. Temperature and ice growth

In this research, Step 1 and EOIS are the subject of focus. It is therefore of importance to understand what happened during these events. Although Hutchinson et al. (2021) uses a different time frame for the EOT compared to Katz et al. (2008) and Miller et al. (2009), they all assert that the $\delta^{18}O$ proxy shift at Step 1 is the product of (ocean) cooling, with few to moderate ice growth. This is further collaborated by Lear et al. (2008). Throughout the entire EOT, bottom water temperatures declined with 3 to 5 degrees Celsius (Miller et al., 2009; Lauretano et al., 2021; Liu et al., 2009), while sea surface

temperatures declined with 4.8 to 5.4 degrees Celsius (Liu et al., 2009). Of this temperature decline, sea surface temperatures (SST) declined with 2.5 degrees Celsius during Step 1 (Lear et al., 2008; Miller et al., 2009), as well as a deep sea temperature decline of 2 degrees Celsius (Miller et al., 2009). The rest of the temperature drop must have occurred during the transient "EOT-2", with no (major) ocean cooling during EOIS (Houben et al., 2012), except for some deep sea temperature cooling (Kennedy et al., 2015). Besides temperature decline, some moderate ice growth is also interpreted to have occurred during Step 1, with a sea level drop of about 25 meters (Miller et al., 2009). In contrast to Step 1, EOIS (also called Oi-1), which occurred 300 kyr after Step 1 (Houben et al., 2012), shows mainly a $\delta^{18}O$ signal related to ice build-up (e.g. Galeotti et al., 2016). This ice-build up caused a sea level drop of about 50 to more than 100 meters, with a modern estimate of 80 meters, and a growth of up to 1.6 times the current Antarctic ice budget (Houben et al., 2012; Miller et al., 2009; Hutchinson et al., 2021; Coxall et al., 2005).

2.1.3. Ocean circulation and ventilation

From the Eocene towards the Oligocene, a change in ocean circulation is presumed to have occurred, from a main Southern deep water formation (SODW) towards a bipolar deep water formation with the onset of a (precursor of) Northern Atlantic Deep Water (NADW) formation (Borelli et al., 2016; Coxall and Pearson, 2007; Coxall et al., 2018). The NADW, and subsequently the Atlantic Meridional Overturning Circulation (AMOC), could have played an important role in initial cooling during the EOT by redistributing (cold) water masses (Hutchinson et al., 2019; Straume et al., 2020). The timing of NADW formation and to what degree remains elusive, however. Uncertainty arises for example on the timing of several Northern hemisphere gateway openings crucial for NADW formation, such as the Greenland-Scotland Ridge, Bering Strait and the Fram Strait (Straume et al., 2020). Closure of gateway openings, such as the Central American Strait and/or the Tethys Seaway, have been also invoked to explain the switch from a dominated SODW to a dominated NADW/AMOC circulation (Hamon et al., 2013; Zhang et al., 2011). Modelling shows the importance of especially the Greenland-Scotland Ridge and its role in initial ice growth (Straume et al., 2022).

In the latest Eocene, a precursor of the NADW, called the Northern Component Water (NCW), developed in the Northern Hemisphere (Coxall et al., 2018). Three ocean regimes regarding NCW near the Arctic have been interpreted from proxy records: 1. Arctic stratified conditions, implying Southern deep water formation, before 35.8 Ma. 2. After 35.8 Ma, a 1.5 to 2 Myr long pulse of NCW export. 3. A mature form of NCW, more ventilated, saline and denser, around 34.3 Ma. Since the NCW predates the EOT with 1 to 2 million years, it is also thought that the NCW played a role in preconditioning the Late Eocene for a greenhouse-icehouse transition by enhancing pCO_2-weathering feedbacks (Coxall et al., 2018). This preceding initiation of the NCW coincides with model evidence that showed the AMOC

intensified 1 to 0.5 million years prior to Antarctic glaciation (Hutchinson et al., 2019). An interhemispheric circulation role for the NADW and AMOC however likely only slightly preceded the EOT, with a major change in deep sea water structure 100 to 300 kyr before the EOT (Abelson and Erez, 2017).

During the EOT, the ocean ventilation/mixing is hypothesised to have increased due to enhanced salt rejection through Antarctic glaciation, forming the Antarctic Bottom Water, as well as increased meridional thermal gradients, stimulating stronger winds (Miller et al., 2009; Goldner et al., 2014; Coxall and Pearson, 2007). This ventilation increases entails enhanced Southern Ocean circulation, by creating a stronger northward transport of Antarctic Intermediate Water and Antarctic Bottom Water (Goldner et al., 2014). Increased ocean ventilation has also been tied to a change in overturning circulation (Abelson and Erez, 2017; Straume et al., 2022). Ocean ventilation could also have been influenced by paleogeographic changes, with modelling showing a 20 to 34% increase in global ocean ventilation as well, if a deepening in the Greenland-Scotland Ridge occurs, which deepened some time from the Late Eocene to the Early Oligocene (Straume et al., 2020; Straume et al., 2022).

2.1.4. Biological productivity

It is thought that biological productivity increased at the onset of Antarctic glaciation, likely by an increased continental run-off of nutrients (Diester-Haass and Zahn, 1996; Houben et al., 2013). The more vigorous ocean overturning at the earliest Oligocene also had a role in increasing productivity (Coxall and Pearson, 2007), just as the opening of the gateways (Drake Passage and Tasman Strait) by means of controlling the thermocline, although their role is somewhat ambiguous (Moore et al., 2014). Throughout the EOT, ecosystems also underwent profound changes and reorganisation in ecosystem and flora and fauna (Houben et al., 2013; Hutchinson et al., 2021). However, productivity increases were not equal across the globe: paleoproductivity proxies from the equator show a sharp decrease from relatively high values in the Eocene to low values during the Oligocene (Moore et al., 2014). For example, a high resolution barite accumulation rate record (a proxy for export) from the Eastern equatorial Pacific shows decreases synchronous with the two step oxygen isotope excursion during the EOT (Erhardt et al., 2013). This is in contrast to sites at high latitudes, which show a distinct increase during the EOT (Diester-Haass and Zahn, 2001; Coxall and Pearson, 2007). This has been explained as the result of a deepening of the thermocline and stability in the upper ocean of the tropics (Moore et al., 2014). Viewing Southern Ocean paleoproductivity, three stages can be determined: 1. Late Eocene oligotrophic conditions (37.5 Ma to 34.5 Ma), where high SST was coupled with low productivity. 2. Growth in phytoplankton productivity during the EOT (34.5 Ma to 33.6 Ma). 3. Earliest Oligocene eutrophic conditions (33.6 Ma to 31.5 Ma), where low SST were coupled with a high productivity (Plancq et al., 2014). Similarly, increased diatom production occurred from the Late

Eocene onwards in the high Southern latitudes, and likely peaked at 31.5 Ma (Egan et al., 2013). In general, records from the Southern Ocean suggest a several fold increase in net productivity and export, sustaining the growth for at least the duration of the EOGM (ca. 33.6 Ma to 33.15 Ma) (Diester-Haass and Zahn, 2001; Coxall and Pearson, 2007).

2.1.5. Weathering

Closely related to biological productivity, is the weathering and continental input, which increased during the EOT with a main shift from chemical weathering to physical weathering at high latitudes associated with cooling (Hutchinson et al., 2021; Pälike et al., 2012). Physical weathering is thought to promote more rapid silicate weathering, serving as possible positive feedback to promote further glaciation through associated production of alkalinity (Torres et al., 2017). Besides cooling-associated increases, Elsworth et al. (2017) suggest in their hypothesis that redistribution of regional temperature and precipitation patterns, due to a change in ocean circulation, intensified silicate weathering. Besides increased silicate weathering, proxy evidence suggest that the fall in global sea levels due to Antarctic glaciation led to exposure of carbonate shelves to weathering, directly increasing global carbonate weathering rates (Armstrong McKay et al., 2016). On Antarctica itself, lead isotope proxies suggest the weathering of East Antarctic neritic Cambrian shelves, due to an amplification in physical weathering associated with glaciation (Basak and Martin, 2013; Elsworth, 2015).

2.2. Proxy records

2.2.1. Benthic $\delta^{18}O$ record

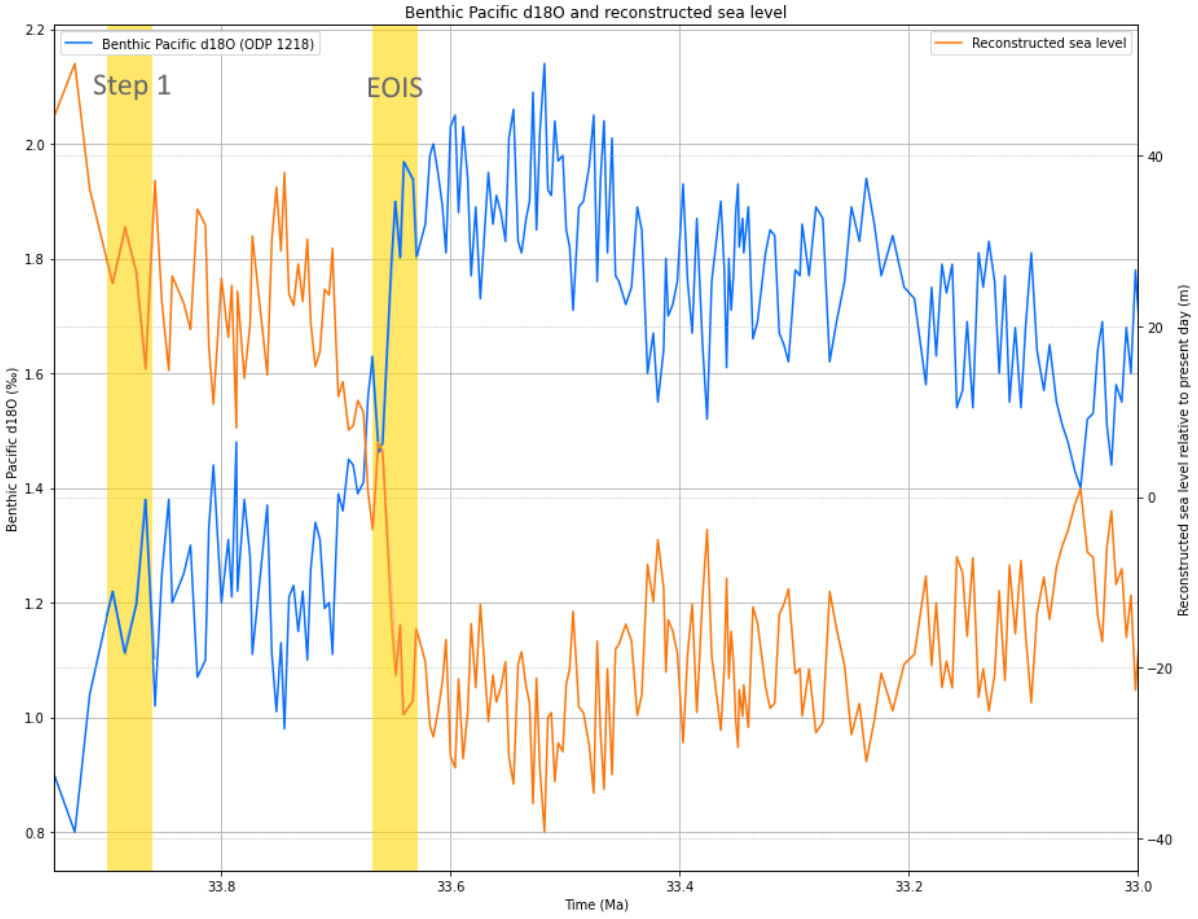

Figure 1. *Benthic Pacific $\delta^{18}O$ (blue) record at site ODP 1218 foraminifera Cibicidoides, in Eastern equatorial Pacific Ocean (Pälike et al., 2006). Besides the benthic $\delta^{18}O$ record, a reconstruction of eustatic sea level (orange) is shown (Miller et al., 2020), relative to present day. Note the mirroring of the two lines. Two yellow bars denoting Step 1 (ca. 33.9 Ma) and EOIS (ca. 33.65 Ma) respectively are visible.*

Although not actually used for proxy comparison (Section 4.2), it is worth showcasing the benthic $\delta^{18}O$ record (Fig. 1), as it is exemplary for the course of the EOT. The benthic $\delta^{18}O$ records symbolises a transition from Warmhouse to Coolhouse world during the EOT (Westerhold et al., 2020), and exhibits a clear two-stepped ca. 1.2 to 1.5‰ increase, especially at EOIS (Coxall and Pearson, 2007). $\delta^{18}O$ is a proxy for both sea level and temperature (Lisiecki and Raymo, 2005). As eustatic sea level is linked with ice growth (ice takes up isotopically light oxygen due to fractionation processes), $\delta^{18}O$ can be seen as a proxy for (global) ice volume (Ruddiman, 2014). Therefore, the enrichment in $\delta^{18}O$ during the EOT is generally regarded as showing the inception of major ice build-up on Antarctica (Coxall and Pearson, 2007). Relatively to benthic $\delta^{13}C$ (Section 2.6.3), benthic $\delta^{18}O$ shows a much longer period of increased values, with an extended Eocene-Oligocene Glacial Maximum period of 490 kyr (Hutchinson et al., 2021; Section 2.1.1)

2.2.2. Carbonate Compensation Depth (CCD)

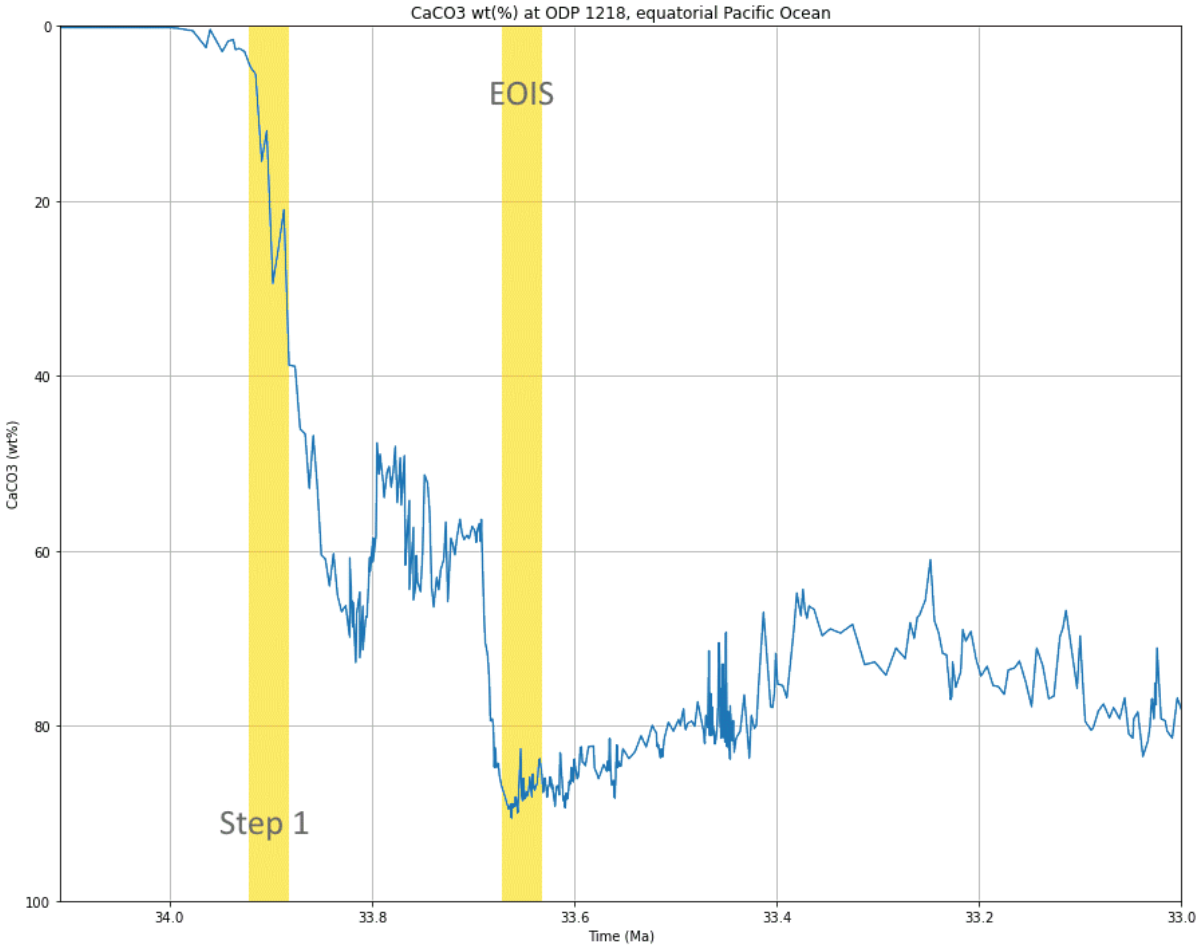

Figure 2. $CaCO_3$ *weight percentage in sediment at ODP 1218, equatorial Pacific, as a proxy for the position of the CCD (Coxall et al., 2005). ODP 1218 sits at a paleodepth of 3.7 to 4.0 km during the EOT (Pusz et al., 2011). The data has been flipped along the y-axis for visual reasons as* $CaCO_3$ *(wt%) shows an inverse relationship with the CCD position (Armstrong McKay et al., 2016); thus, an increase in* $CaCO_3$ *(wt%) can associated with a deepening of the CCD, hence showing a "deepening" here in the graph.*

One way to estimate the position of the CCD, is through $CaCO_3$ (wt%) reconstruction. For example, Pacific $CaCO_3$ (wt%) (Fig. 2) can be regarded as a qualitative proxy for Pacific CCD (Coxall et al., 2005), which is estimated to have deepen with 1200 meters (Rea and Lyle, 2005). Pälike et al. (2012) also made a reconstruction of the Pacific CCD throughout the Cenozoic, showing a deepening of about 3.5 km depth just before the EOT to 4.5 km depth after the EOT. Other reported changes in CCD are in regards to the Atlantic and Indian CCD (ca. 1 km and max. 700 meters, respectively; Coxall and Pearson, 2007 and references therein). Sedimentary depositional environment reconstructions across the oceans confirm the worldwide deepening in CCD (Wade et al., 2020). The two-step deepening in CCD, which potentially could have occurred in less than 300 kyr, led to a two to three fold increase in

carbonate accumulation area, based on hypsometry (Coxall et al., 2005; Bohaty et al., 2008; Rea and Lyle, 2005; Opdyke and Wilkinson, 1988).

Another proxy associated with the CCD is the carbonate ion concentration ($[CO_3^{-}]$), which determines together with the calcium ion concentration ($[Ca^{2+}]$) the saturation state of carbonate and subsequently the CCD position (Woosley, 2012). Research regarding the EOT has also developed an interest in determining $[CO_3^{-}]$ concentrations during the course of the EOT as it has an effect on magnesium to calcium concentrations, which in its turn is used as a temperature proxy to separate ice growth and temperature decline effects on $\delta^{18}O$ (see previous Section) (Pusz et al., 2011). Reported changes in $[CO_3^{-}]$ concentrations include a ca. 29 µmol increase in the South Atlantic (Peck et al., 2010) and a 37 µmol increase in the equatorial Pacific at ODP 1218, the same site as the $CaCO_3$ reconstruction of Figure 1 (Lear et al., 2010).

2.2.3 Benthic $\delta^{13}C$ records

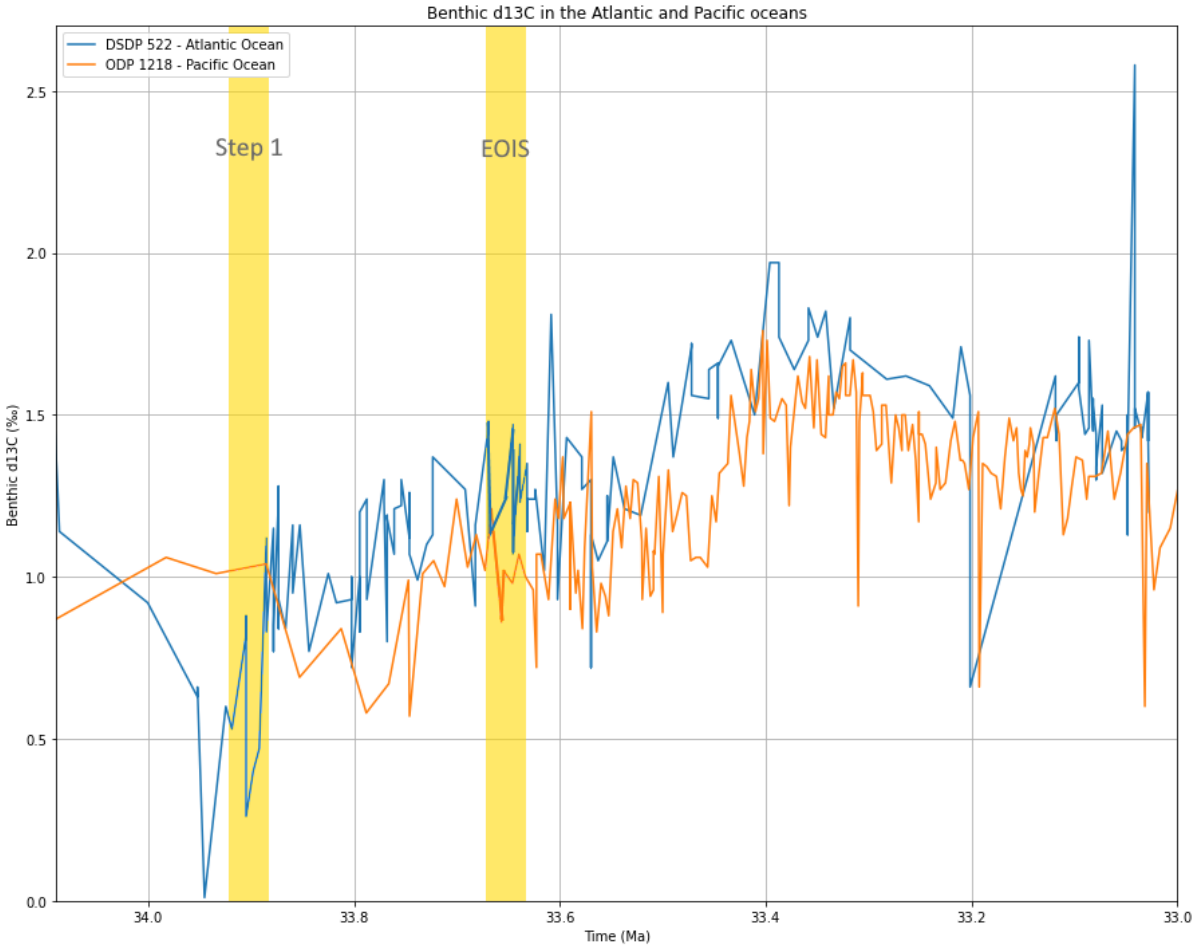

Figure 3. *Atlantic and Pacific benthic $\delta^{13}C$ from the foraminifera Cibicidoides (Cramer et al., 2009 and references therein). The extended timeframe alongside the EOT is shown (showing the EOGM, from 33.65 to ca. 33.15 Ma) as well. Highlighted are Step 1 (ca. 33.9 Ma) and Oi-1 (ca. 33.65 Ma).*

Useful for the study of the EOT, are proxy records such as benthic $\delta^{13}C$ in the Atlantic and Pacific (Cramer et al., 2009, and references therein) (Fig. 3). Long term benthic $\delta^{13}C$ is largely depended on internal oceanic processes, and surface $\delta^{13}C$. Long term surface $\delta^{13}C$ is in its term depended on weathering input and biological productivity (Kump, 1991). Biological productivity has an effect on $\delta^{13}C$ in dissolved inorganic carbon (DIC) in seawater, as DIC is used for photosynthesis by organic matter, during which lighter ^{12}C is preferred for biological uptake due to kinetic fractionation, enriching the surrounding waters by ^{13}C (Emerson and Hedges, 2016). Through an influx of carbon with different $\delta^{13}C$ signal, weathering plays a role in determining $\delta^{13}C$ (DIC) as well: for example, increased carbonate weathering of exposed platforms has been hypothesised to explain a positive incursion of (surface) $\delta^{13}C$ during the Late Devonian (Goddéris and Joachimski, 2004). Oceanic processes can circulate water masses of different $\delta^{13}C$, and oxidation plays a role in $\delta^{13}C$ for carbon fluxes through the water column (Kobayashi et al., 2015; Wefer et al., 1999).

Therefore, the benthic $\delta^{13}C$ record offers a look into various processes, such as weathering, ventilation/ocean circulation change and biological productivity, pertaining to the EOT. Regarding the benthic $\delta^{13}C$ record for the EOT, Figure 2 shows that both the Atlantic and Pacific benthic $\delta^{13}C$ increased after EOIS, with about 1.0‰ and 0.7‰ respectively. This climax was only reached after about 250 kyr after the EOIS, with a slow decline in $\delta^{13}C$ afterwards (see Fig. 2).

2.2.4 Atmospheric pCO_2

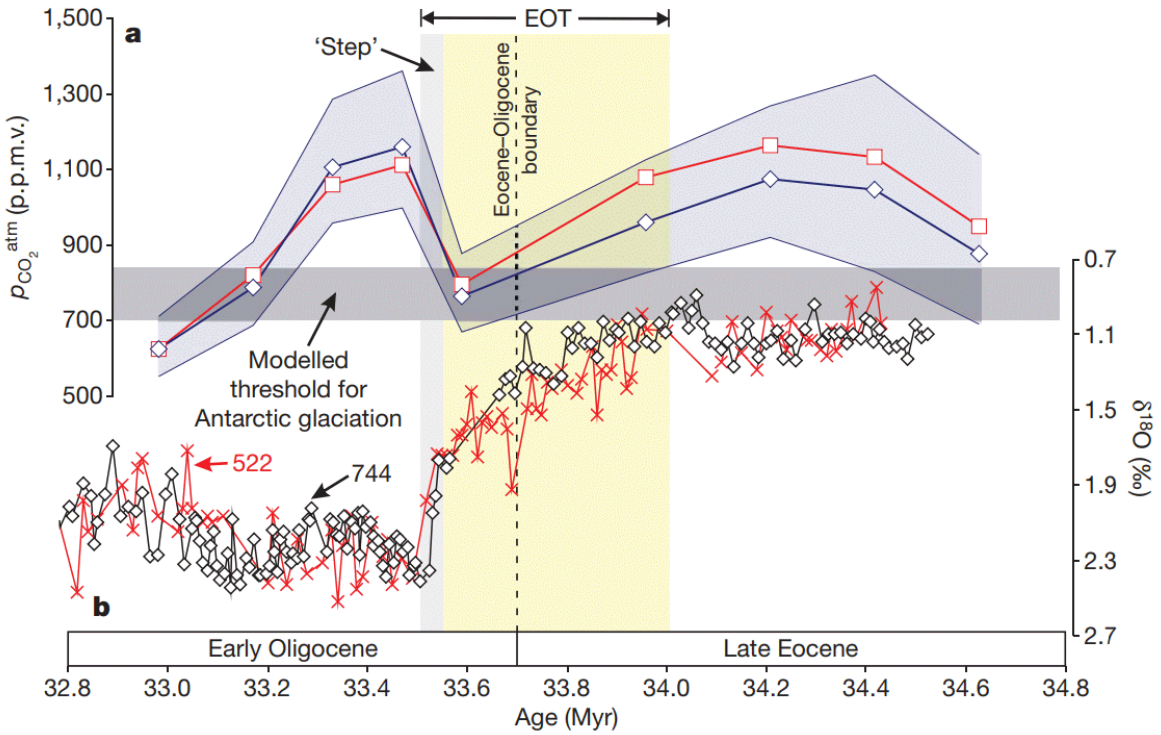

Figure 4. *From Pearson et al. (2009). Benthic $\delta^{18}O$ and atmospheric pCO_2 plotted against time. Note that the time axis is reversed compared to Figure 1 and Figure 2.*

Atmospheric pCO_2 proxy records show a decline during the EOT, from 1700 to 900 ppm initially to 800 to 700 ppm just prior the onset of EOIS (Heureux and Rickaby, 2015). Pearson et al. (2009) also made a reconstruction of atmospheric pCO_2 (Fig. 4), based on pH-reconstructions from Boron isotopes (pH basified from ca. 7.5 to 7.7 from 34.2 Ma to 33.0 Ma). Their findings are similar to Heureux and Rickaby (2015): a reduction from about 1100 ppm to 760 ppm, albeit with large uncertainties, from the Late Eocene to EOIS. This decline reaches modelled threshold for Antarctic glaciation, although this threshold has considerable uncertainty behind it and could range between 560 ppm to 920 ppm (Gasson et al., 2014). Atmospheric pCO_2 shows a rebound after the EOIS, but declines in the next 500 kyr to less than 700 ppm (in both Pearson et al., 2009 and Heureux and Rickaby, 2015).

2.3. Hypotheses regarding carbon cycle perturbations

Coxall and Wilson (2011) summarised various hypotheses from literature that try to link carbon cycle changes/perturbations (see proxies of Section 2.6) with climate changes (such as described in Section 2.2 to 2.5) during the EOT. Their list contained the following hypotheses: 1. Increased silicate weathering due to ice sheet coverage. 2. Increased marine organic carbon burial/cycling. 3. A global switch in the ecology of plankton to favour silicious organisms. 4. A shift in global carbonate

sedimentation from the shelf to the deep ocean. 5. Changing riverine chemical inputs. 6. An increase in the size or mean isotopic composition of the terrestrial biosphere. 7. Increases in the rain ratio of inorganic to organic carbon from the surface to the deep ocean. 8. Reduced ocean acidity due to increased ocean overturning.

In this study, several of these named hypotheses are tested, and will be provided with a more elaborate description.

3. Methods

3.1. LOSCAR

LOSCAR v.2.0.4.3 (*Long-term Ocean-atmosphere-Sediment CArbon cycle Reservoir Model*) is a computer model that aims to simulate climate and more specifically carbon partitioning over long-time scales with respect to ocean, atmosphere and sediments (Zeebe, 2012). An important characteristic of LOSCAR is that it incorporates a computationally efficient sediment module that is linked with the ocean-atmosphere equations. The model is divided into a pre-Industrial ("modern") version and a paleo version (based on the Paleocene-Eocene Thermal Maximum), however, the model can be run using any scenario. LOSCAR includes several boxes for the oceans, including a Tethys ocean in the paleo version, divided into a surface, an intermediate box and a deep box. In these boxes, ocean circulation is statically modelled using an upwelling and exporting variable per box. LOSCAR contains three possible ocean circulation modes: North Atlantic Deep Water Formation, North Pacific Deep Water Formation and, third, Southern Ocean Deep Water Formation. North Atlantic Deep Water Formation (NADW) and Southern Ocean Deep Water Formation (SODW) are of importance in this study (see Section 2.1.3, Section 3.6.2.1 and Fig. 5). These circulation modes assume a large role determining the fluxes of multiple tracers, such as DIC (dissolved inorganic carbon), ^{13}C of DIC, alkalinity, phosphate and oxygen between the boxes (see Section 3.2). Multiple other parameters are also modelled, such as pCO_2 (both ocean and atmosphere), pH, ocean temperature and of course the CCD. These parameters are calculated through various processes, such as air-sea gas exchange, biological pump, carbonate and silicate weathering and subsequent weathering feedbacks, as elaborated in Zeebe (2012). These included processes make LOSCAR a more than adequate model to simulate the CCD (Penman and Zachos, 2018). LOSCAR is also quick and able to simulate long-time scales (Zeebe, 2012) which is ideal for the 790 kyr long EOT.

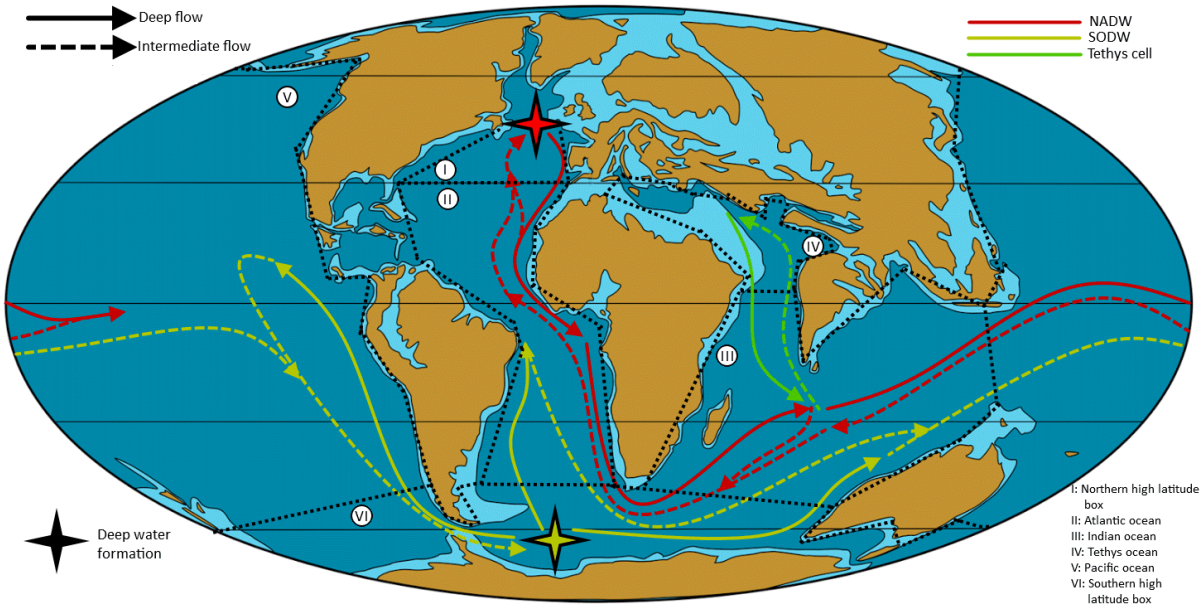

Figure 5. Edited from the paleomap of Angst et al. (2013). The map shows the concept of the thermohaline circulation in LOSCAR interpreted on an Eocene paleomap. Oceans and the high latitude boxes are crudely outlined. Both NADW and SODW circulation cells are shown. Deep water originates from the respective deep water formation location, and through intermediate water flows, the water returns to its deep water formation. Note that in the SODW circulation cell, deep water flows through the Drake Passage to the Pacific Ocean. This is, however, simply an artistic simplification; in LOSCAR, under a SODW circulation, deep water flows directly to the deep Atlantic, Indian and Pacific, from the Southern high latitude box which assumes the entirety of the Southern Ocean's surface. The Tethys cell is active under both NADW and SODW circulation, with no Tethys-Atlantic flow.

3.2. Carbon cycle in LOSCAR

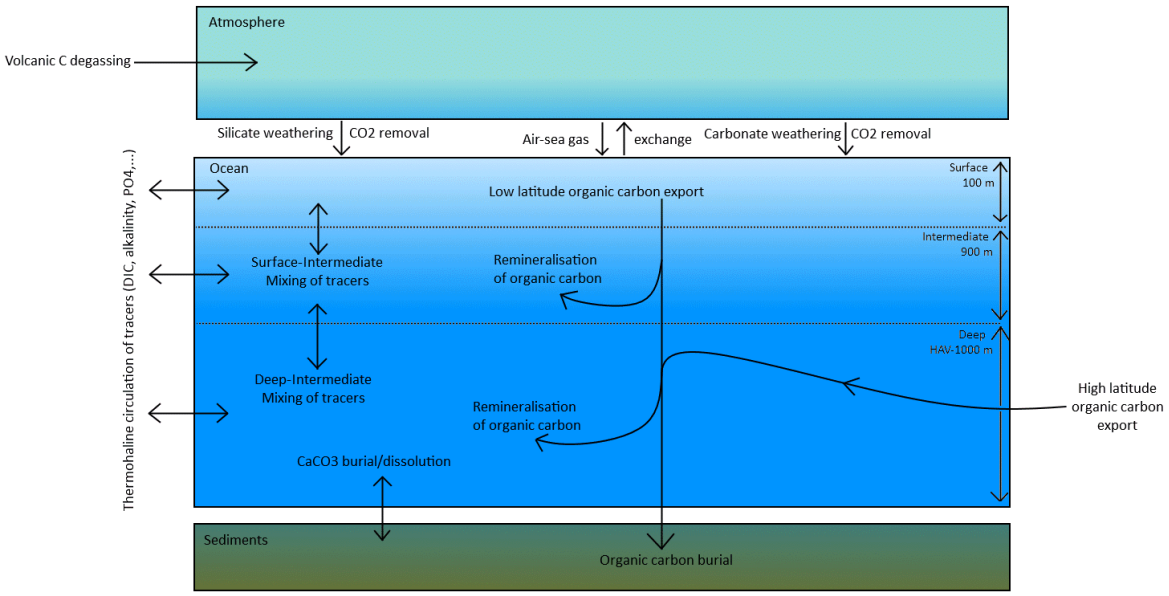

Figure 6. Carbon cycle in LOSCAR. In steady state, these fluxes are in balance. Thermohaline circulation allows for the transfer of tracers (DIC, alkalinity, PO4, etc.) between oceans, while mixing transfers the tracers between the depths. Organic carbon production takes up tracers such as DIC and PO4, and is exported to the intermediate and deep boxes. What is not remineralised, is buried. HAV is the average oceanic depth, depending on predefined surface and volume size in LOSCAR.

Figure 6 shows the carbon cycle in LOSCAR. The carbon cycle links carbon in sediments, ocean and atmosphere, with in steady state the fluxes being balanced. Atmospheric pCO_2 is controlled by volcanic degassing, weathering and air-sea gas exchange (Eq. 1).

$$\frac{dC_{atm}}{dt} = F_{volcanic} + F_{gas} - F_{carbonate\ weathering} - 2 \cdot F_{silicate\ weathering} \quad (1)$$

Here, $F_{volcanic}$ is the carbon degassing from volcanoes and F_{gas} is the net carbon flux to the atmosphere from air-sea gas exchange, following Henry's Law (Zeebe, 2012). Silicate weathering is multiplied by a factor of two times, as the weathering of a single mole CaSiO3 takes up two moles of atmospheric CO_2 (Eq. 2). Both carbonate (Eq. 3) and silicate weathering release two moles of carbon to the ocean after weathering one mole carbonate or calcium silicate.

$$CaSiO_3 + H_2O + 2 \cdot CO_2 \leftrightarrow Ca^{2+} + 2 \cdot HCO_3^- + SiO_2 \quad (2)$$

$$CaCO_3 + H_2O + CO_2 \leftrightarrow Ca^{2+} + 2 \cdot HCO_3^- \quad (3)$$

In steady state, burial (Eq. 3 reversed) equals influx, resulting in a net reaction (Eq. 4):

$$CaSiO_3 + CO_2 \leftrightarrow CaCO_3 + SiO_2 \quad (4)$$

Thus, the CO_2 that is degassed by volcanoes, is balanced by weathering of carbonate and silicate, and increased weathering will result in increased burial. Carbonate and silicate weathering fluxes (Eq. 5 and 6, respectively) are adjusted in LOSCAR to reach steady state (Zeebe, 2012):

$$F_{carbonate\ weathering} = F^0_{carbonate\ weathering} \cdot (\frac{pCO_2}{pCO_2^0})^{n_{cc}} \quad (5)$$

$$F_{silicate\ weathering} = F^0_{silicate\ weathering} \cdot (\frac{pCO_2}{pCO_2^0})^{n_{si}} \quad (6)$$

Here, pCO_2^0 is the steady state atmospheric CO_2 pressure, and pCO_2 the current atmospheric CO_2 pressure. The exponents n_{cc} and n_{si} determine the speed of the carbonate and silicate weathering feedbacks, and are initially 0.4 and 0.2, respectively, but have been upscaled to 0.6 and 0.4 (Section 3.4.2).

Carbon in the ocean is also regulated by ocean circulation/mixing: at every time step, boxes transfer tracer concentrations (such as DIC and alkalinity) to adjacent ocean boxes according to the defined ocean circulation (Fig. 5), which is modified depending on the model run. At the same time, mixing occurs between surface-intermediate and deep-intermediate boxes.

Further, biological productivity exerts an important control on carbon in LOSCAR. In LOSCAR, biological productivity is parameterised through PO4 concentrations. Via Redfield-ratio, organic carbon is made (C:P = 1:130), as well as oxygen (O:C = 165:130) and alkalinity. The latter depends on rain ratio of C_{org} to $CaCO_3$ to sediments as well as nitrate creation (N:C = 15:130). The low latitude organic carbon export flux, made in the Atlantic, Indian, Pacific and Tethys surface oceans, is displayed in a formula in Eq. 7:

$$F_{C_{org}low-lat_i} = \sum_{i=1}^{n=4} f_{eff} \cdot m_i \cdot [PO_4]_i \cdot 130 \quad (7)$$

In Eq. 7, f_{eff} represents the efficiency of the biological pump in low latitudes, set at 0.80. m_i represents the mixing from intermediate to surface ocean, while $[PO4]_i$ represents the phosphate concentration in the surface box of ocean *i*. To convert to carbon from phosphate, the formula is multiplied by 130, conform Redfield-ratio. Biological production also occurs in the high latitude surface boxes (two in the LOSCAR version used in this study, see Section 3.3.2), but this flux is set directly through the input file. High latitude organic carbon export directly transfers to the deep ocean. Eventually, 99% of both organic carbon export fluxes are remineralised, with only 1% being buried (Section 3.3.1).

This low latitude organic carbon flux determines the carbonate rain to sediments, following Eq. 8:

$$r_{carb} = F_{C_{org}low-lat}{}^{i} \cdot c_{rain\ ratio}{}^{-1} \cdot (1 - v_{wc}) \cdot k^* \quad (8)$$

In Eq. 8, the carbonate rain to sediments, r_{carb}, depends on the organic carbon flux F_{Corg} to sediment box *i*, the rain ratio $c_{rain\ ratio}$ of organic carbon to carbonate (a value of 6.7 used in this study), the fraction that is dissolved in the water column v_{wc} (0.31), and on a conversion factor k^* which makes the left hand side in m/year. r_{carb} is not the final carbonate rain to sediments however, and depends on the carbonate bottom water dissolution rate (based on Keir, 1982 and Sigman et al., 1998):

$$r_{diss} = \left(f_c^i\right)^{0.5} \cdot K_{sed} \cdot ([CO_3^{2-}]_{sat} - [CO_3^{2-}])^{n_{sd}} \cdot k^{**} \quad (9)$$

In Eq. 9, the bottom water carbonate dissolution rate r_{diss} depends on the calcite rain of the previous iteration f_c of sediment box *i*, on the effective dissolution rate K_{sed}, on both the saturated carbonate ion concentration (itself based on various parameters such as magnesium and calcium ion concentrations) and bottom water carbonate ion concentration, and the effective carbonate dissolution order n_{sd} and k^{**}, which makes the right hand side in m/year, just as with r_{carb}. Dissolution is zero if the bottom water carbonate ion concentration exceeds the saturated carbonate ion concentration. LOSCAR also includes erosion and variable porosity in sediments (Zeebe, 2012).

With this summary of the carbon cycle in LOSCAR, a general formula for the concentration of a tracer related to carbon (such as alkalinity, DIC, DIC-^{13}C, PO4, oxygen) per ocean box can be drawn up:

$$\frac{dy}{dt} = F_{weathering} + F_{mixing} + F_{ocean\ circulation} + c_{Redfield} \cdot c_{remin.} \cdot (F_{low-lat\ oc\ export} + F_{high-lat\ oc\ export}) + F_{diss} \quad (10)$$

In Eq. 10, the change in tracer *y*'s concentration thus depends on several fluxes. Carbonate and silicate weathering fluxes are of importance for DIC, DIC-^{13}C and alkalinity, following Eq. 2 and 3 in the surface boxes; besides carbonate and silicate weathering, a phosphate weathering flux (Section 3.4.2) adds PO4 to the surface boxes. Mixing and circulation fluxes are important to all tracers at any ocean box. The organic carbon export is multiplied by the appropriate Redfield-ratio and remineralisation rate to account for biological productivity; note, however, that organic carbon production takes up tracers at the surface level while releasing them in the intermediate and deep boxes through remineralisation, or burying them in the sediments. Finally, dissolution releases alkalinity, being balanced or enhanced by burial and erosion (Zeebe, 2012).

This Section only gives a slightly limited overview of the carbon cycle in LOSCAR, for a more complete overview, the reader is referred to Zeebe (2012).

3.3. Adaptations to LOSCAR

3.3.1. Incorporation of long-term organic carbon burial

Standard LOSCAR lacks a long-term coupling between organic carbon burial and biological productivity; effectively, all organic carbon is remineralised in the intermediate and deep boxes (Komar and Zeebe, 2017; Kocken et al., 2018). Instead, burial of the sediments is limited to carbonate and clay, with the $\delta^{13}C$ signal of organic carbon burial being transferred through a kerogen ^{13}C (DIC) flux. This is not unreasonable, as it has been shown that organic carbon burial rate is proportional to total sediment burial rate (Berner and Canfield, 1989). Nevertheless, to make the model more accurate in this regard, an adaption was implemented, loosely based on the "LOSCAR-P" adaption of LOSCAR (Komar and Zeebe, 2017). Like LOSCAR-P (which aims to include a long-term coupling between phosphorus and organic carbon burial), remineralisation is set at 99%, which results in a theoretical 1% burial of organic carbon. This is similar to actual observed organic carbon burial rates (Suess, 1980). Effectively, however, it results in the disappearance of 1% of organic carbon (and subsequently other tracers as well, linked through the Redfield-ratio) in LOSCAR. To make up for this disappearance, a weathering flux of PO4 is included in the model, just as in LOSCAR-P. This flux is distributed across the low-latitude surface boxes evenly. Through the means of an increased PO4 concentration, there is an increased organic carbon production, which results indirectly in increased alkalinity, DIC, and other tracers as well. Thus, burial presents a sink of tracers, while the PO4 weathering influx presents a source of tracers. This remineralisation and subsequent organic carbon burial is also applied to high-latitude carbon export to the deep waters. Just as in LOSCAR-P, remineralisation of phosphate is actually set at 99.5%, meaning the carbon to phosphate ratio in burial is twice as high as the Redfield-ratio in the surface, resulting in proportionally less phosphate burial, as PO4 burial depends greatly on the redox state in bottom waters (Komar and Zeebe, 2017). Unlike LOSCAR-P, however, the burial ratio between carbon and phosphate in the version used in this study is not variable depending on oxygen levels in the bottom waters, a simplification. The phosphate fluxes representing CaP and FeP burial are omitted as well.

3.3.2. Additional high latitude box

In standard LOSCAR, a single box represents the high latitude areas. Here, deep water formation and high latitude biological productivity occur. A theoretical problem arises, however, when ocean circulation change is implemented: the high latitude box assumes the role of a different high latitude area while (initially) keeping the parameter values associated with its previous area. To fix this issue, a second high latitude box is implemented. Two high latitude boxes allow for a more accurate representation of two separate deep water formation areas (a North Atlantic and Southern Ocean one) and its separate biological productivity. Geographically, the two high latitude boxes have the same dimensions (100 meters deep, and both occupying 10% of the ocean surface). Alkalinity, DIC and PO4

values were also adapted to make the two high latitude boxes more equal to each other , although these similarities are more or less simplifications.

The one tracer that differs moderately between the two high latitude boxes, is $\delta^{13}C$. In an SODW circulation state, $\delta^{13}C$ in the Northern high latitude box is 2.7‰, while in the Southern high latitude box, this amounts to 1.7‰. If NADW and SODW cells are equal in thermohaline strength, this difference is diminished to 0.25‰ in favour of the Northern high latitude box in equilibrium state. Increasing the Southern high latitude box's $\delta^{13}C$ to make up for this difference proved difficult: therefore, this offset of about 0.25‰ must be accounted for when comparing output between the different ocean circulation states. Nevertheless, it is not necessarily a bad addition: Antarctic intermediate $\delta^{13}C$ values are lower than that of deep Atlantic during the EOT (Katz et al., 2011).

In the Late Eocene steady state used in LOSCAR (see following Section), a Northern Component Water (precursor the NADW) was added (more information in next Section). This alters the $\delta^{13}C$ distribution across the oceans. In the SODW ocean circulation state including this NCW cell, the Northern high latitude box contains a $\delta^{13}C$ value of 2.4‰, while the Southern high latitude box contains a $\delta^{13}C$ value of 1.8‰. If the SODW and NADW are equal in strength (with still a NCW cell), the Northern high latitude box contains a $\delta^{13}C$ value of 2.0‰, while the Southern high latitude box contains a $\delta^{13}C$ value of 2.0‰ as well. Nevertheless, changes in $\delta^{13}C$ do occur, notably between the Atlantic and Pacific oceans (see Fig. 7), with the Atlantic containing higher $\delta^{13}C$ (in the order of 0.2 to 0.5‰), as is presently the case (Farmer et al., 2020).

3.4. Late Eocene steady state in LOSCAR

3.4.1. Steady state model set-up

The model was firstly run into a state representative of the latest Eocene, just prior the EOT. This included a main Southern Ocean deep water formation (Hutchinson et al., 2018), an atmospheric pCO_2 value of 1000 ppm (O'Brien et al., 2020; Heureux and Rickaby, 2015; Pearson et al., 2009) and seawater calcium, magnesium and sulfate-ion concentrations of 16, 36 and 19 millimoles per kg of H2O, respectively (Brennan et al., 2013). Ocean temperatures were also adapted to late Eocene standards: a general SST of 22 degrees Celsius was chosen (inferred from O'Brien et al., 2020), and deep water temperatures of 8 degrees Celsius (inferred from Rohling et al., 2021). Intermediate water temperatures of 14 degrees Celsius were chosen, keeping roughly the same proportion the different temperatures had in the paleo version of LOSCAR. Compared to the pre-Industrial set-up of LOSCAR, this gives a 2, 4 and 6 degrees warmer surface, intermediate and deep water temperatures, respectively. Tethys surface, intermediate and deep water temperature were chosen to be 16, 12 and 8 degrees Celsius, respectively. Considering that the model version which this study uses has a separate Northern high latitude box (Section 3.3.2), a Northern Component Water (precursor of the

NADW, see Section 2.1.3) was added to the standard ocean circulation, for a somewhat better representation (following Coxall et al., 2018). This extra circulation cell, with a thermohaline strength of 5 Sv, lets water flow from the Northern high latitude surface to the deep Atlantic, from where it flows to the Atlantic intermediate and returns to the Northern high latitude box. Further, the built-in bathymetry and hypsometry in LOSCAR were also adapted to the Late Eocene, using a linear interpolation from the values of the paleo version (representative of the PETM) and the pre-industrial version within LOSCAR (based on Bice and Marotzke, 2002 and Menard and Smith, 1966, respectively). Lastly, certain fluxes were adjusted (see following Section). For values of other parameters, those in the paleo version of LOSCAR were used. This LOSCAR version of the latest Eocene was run to equilibrium in 5 million model years.

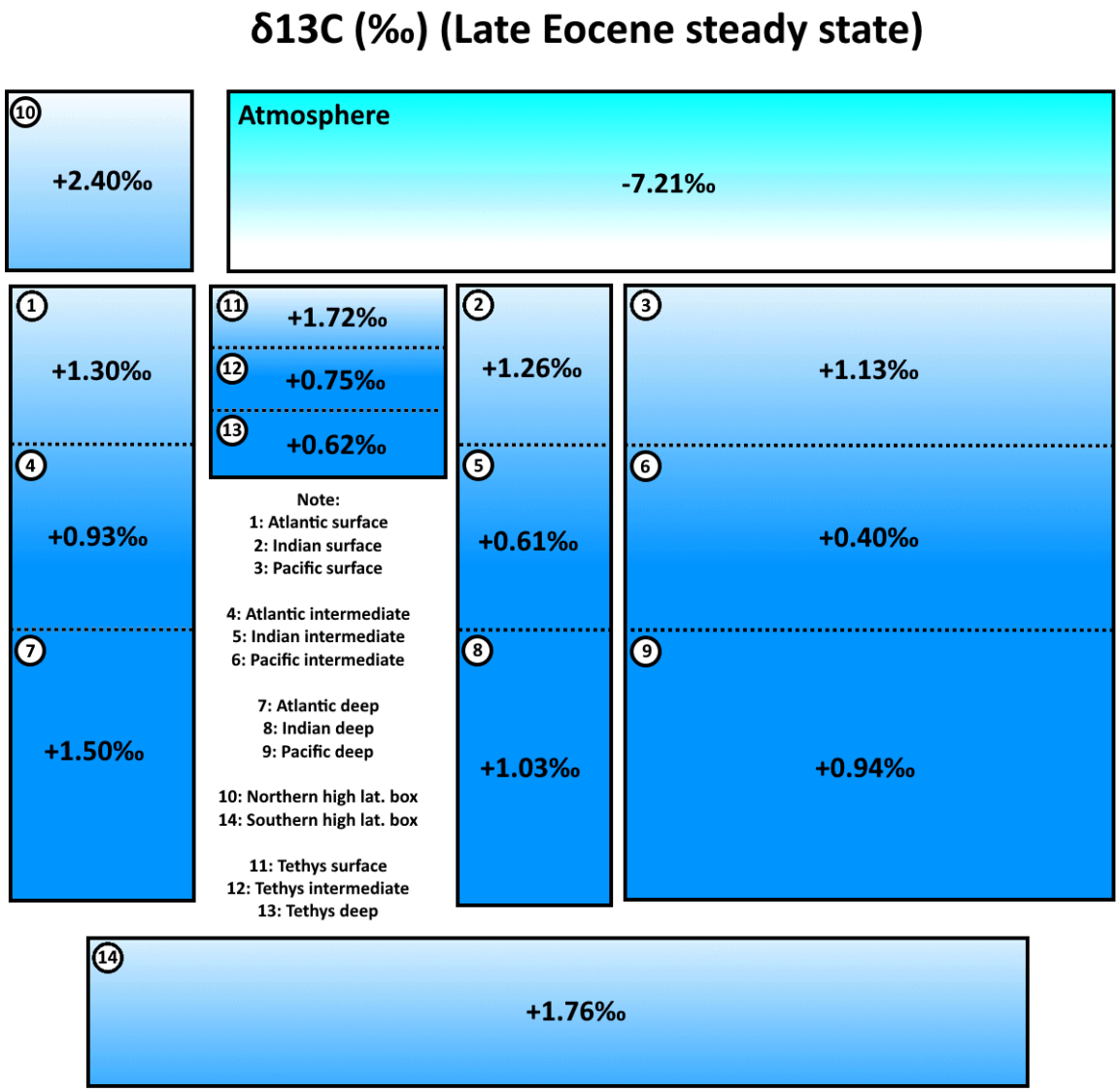

Figure 7. *$\delta^{13}C$ distribution in Late Eocene steady state in LOSCAR, under a SODW mode of circulation, including a NCW cell. The Figure also shows the box set-up in LOSCAR, with the additional Southern high latitude box. Box numbering follows intern LOSCAR numbering: first surface, then intermediate, then deep. The size of each ocean pictured is relative to their surface in LOSCAR: the larger the ocean pictured, the larger its surface is in LOSCAR. The high latitude boxes, as well as the atmosphere, are not to scale.*

3.4.2. Fluxes in steady state

A weathering flux of 15 gigamoles of PO4 per year was tuned to reach a steady-state (Section 3.3.1). However, this is not the actual weathering flux that gets used in the model, as it was prescribed that the weathering flux depends proportionally on weathered carbonate and silicate fluxes (Eq. 9), following the assumption that the weathering fluxes are related. As the pCO_2-Si from the input file was tuned to reach a pCO_2 of 1000 ppm in steady state (Section 3.4.1), carbonate, silicate and thus

phosphate weathering fluxes changed as well. To accelerate finding the steady state, carbonate and silicate weathering feedbacks were accelerated as well. In LOSCAR, carbonate and silicate weathering fluxes are calculated as prescribed in Equations 5 and 6. In standard LOSCAR, the coefficients n_{cc} and n_{si} are 0.4 and 0.2, respectively; in this version, these are increased to 0.6 and 0.4, respectively. This results in a stronger weathering feedback than the relatively weak standard weathering feedback (Uchikawa and Zeebe, 2008).

The phosphate weathering flux depends on changes in the weathering fluxes of carbonate and silicate, following Komar and Zeebe (2017):

$$F_{PO_4} = F^0_{PO_4} \cdot \frac{F_{carbonate}+F_{silicate}}{F^0_{carbonate}+F^0_{silicate}} \quad (11)$$

In Table 1, the fluxes that are present in the steady state (see Section 3.4.1) are visible. Note that the PO4 weathering flux differs from 15 gigamoles per year. Also note that silicate and volcanic C degassing fluxes differ: in steady state in standard LOSCAR, the fluxes are similar (Zeebe, 2012), but due to the addition of long-term organic carbon burial (see Section 3.3.1), an extra source of carbon sink was introduced, diminishing silicate and carbonate weathering fluxes and subsequent carbonate burial (see Eq. 4) to maintain carbon fluxes. Further, the (long term) organic carbon burial and carbonate burial differ from the set rain ratio in LOSCAR (C_{org}:$CaCO_3$ = 6.7), but the rain ratio in LOSCAR only determines the rain to sediments and does not include the carbonate share that dissolves in the bottom water.

Table 1. *Fluxes in Late Eocene model steady state*

Fluxes	Flux (amount)	d13C signature
PO4 weathering flux	8.452 gigamoles per year	-
Volcanic C degassing flux	6.598 teramoles per year	-4.0‰
Silicate weathering flux	4.283 teramoles per year	-
Carbonate weathering flux	7.323 teramoles per year	+2.0‰
Sea to air C degassing	9.291 teramoles per year (based on Eq. 1)	Following Mook (1986)
Carbonate burial	4.283 teramoles per year (based on Eq. 4)	$\delta^{13}C$ of deep water DIC
Organic carbon burial flux	2.188 teramoles per year	-33.0‰
Organic carbon export (low lat. + high lat.)	218.8 teramoles per year	-33.0‰
Organic carbon export (high lat.)	34.9 teramoles per year	-33.0‰

3.5. Sensitivity study

A sensitivity study of the parameters used to simulate the hypotheses was performed, not only to explore the effects of parameter changes but as well as to view the volatility/robustness of the adapted version of LOSCAR used in this study. More importantly, however, the sensitivity study was also undertaken to set as a base for the reasoning of parameter values used in the model runs. The parameters tested were changed in a range of differing values, excluding the value from steady state, both in negative and positive direction. In addition, a steady state with a permanent NADW circulation (80% of THC strength allocated to NADW, 20% SODW, see Section 3.6.2.1) also underwent parameter changes, to test the effect of a parameter change under a different circulation. As output, Atlantic and Pacific CCD and benthic $\delta^{13}C$ (DIC) were taken, as well as atmospheric pCO_2. As it is the nature of the climate system in LOSCAR to reach steady state (as in maintaining steady state pCO_2) through increased or diminished weathering and/or volcanic degassing (Zeebe, 2012), newly reached steady state values are perhaps not indicative for the shorter term changes a parameter change invokes. Therefore, output values were taken at 250 kyr after induced parameter changes, instead of running

the system to equilibrium (which could last millions of model years). 250 kyr is also roughly the time between Step 1 and EOIS (Section 2.1.1), giving a good approximation to the impact of a parameter change on EOT time scale. To gauge the role of a change in Southern deep water formation to a Northern (Atlantic) deep water formation in LOSCAR, the NCW cell (Section 3.4.1) was not yet implemented for the sensitivity study.

The results of the sensitivity study are on view in Appendix 1.

3.6. Scenario modelling

3.6.1. General model set-up

Five hypotheses, linking the carbon cycle to climate changes during the EOT, were tested, namely: Shelf-to-Basin carbonate fractionation change (SBFC), increased organic carbon burial through increased high latitude biological productivity (IHBP), increased ocean ventilation (IOV), increased carbonate weathering (ICW) and increased silicate weathering (ISW). Additionally, ocean circulation change (OCC) will be tested as a separate hypothesis. With the results of these scenarios, a combined scenario will be made. The output of the model runs will be compared to proxy data (Section 2.2) to shed light on the role of the various hypotheses on the course of the EOT.

Although Hutchinson et al. (2021) define the EOT as from 34.44 Ma to ca. 33.65 Ma, in this model a simplified timeframe will be used, spanning 1 myr and consisting of two main steps (Step 1 and EOIS, following Hutchinson et al., 2021's terminology) at which changes will occur. The first 100 kyr of the model run is a steady state run, with no changes. At 100 kyr, Step 1 occurs, lasting for 250 kyr when at 350 kyr EOIS initiates. The model continues for 700 kyr after EOIS for a total run of 1 myr.

All model runs will experience a decrease in sea temperature in both steps; twice a decline of 2.5 degrees Celsius in the surface waters, 2 degrees in the intermediate and deep waters. These temperature drops are based on findings described in Section 2.2. Although Miller et al. (2009) and Katz et al. (2008) have interpreted temperature declines in EOT-2, EOT-2 is not present in Hutchinson et al. (2021)'s terminology of the EOT; therefore these temperature declines are allocated to the second step, EOIS, in the model run. All hypotheses will run under a permanent SODW circulation, except for the OCC hypothesis, obviously. As a test run, the OCC hypothesis does include a permanent SODW circulation variant, which can therefore be considered as the null hypothesis, as it only includes temperature change which every model run includes.

3.6.2. Model set-up per hypothesis

3.6.2.1. Ocean circulation change (OCC)

Besides the carbon cycle hypotheses, the effect of circulation change, or better, strengthening of the NADW, is also tested, to attempt to ascertain whether NADW formation could have occurred and/or

explain the proxy data. The model will be statically adjusted in ocean circulation mode, as it is difficult to implement a dynamic ocean system such as a simple Stommel box (Stommel, 1961), which needs atmospheric temperature values and atmosphere-sea relaxation formulas which LOSCAR lacks (more discussion see Section 5.5.1). Circulation change occurs at Step 1, and the change is invoked instantly instead of gradually. As Section 2.1.3 elaborates, there is evidence for an increased/strengthened AMOC and initiation of NCW (predecessor of the NADW) 0.5 to 2 million years before the onset of the EOT; therefore a simple NCW circulation cell, as already told in Section 3.4.1, is added to the steady state. Besides this simple NCW circulation cell, ocean circulation at steady state follows SODW. When ocean circulation change occurs, this SODW circulation changes to a hybrid variant between the SODW and NADW circulations.

A point of discussion is the relative proportion of THC strength between the two circulations in the hybrid variant. As the North Atlantic was more narrow during the EOT than it is in the current day (e.g. Straume et al., 2020), one could wonder if NADW could sustain high levels of deep water formation comparable to SODW before (25 Sv in the pre-PETM set-up in LOSCAR). Therefore, three hybrid variants will be tested: 1. A weak NADW (20% of THC allocated to NADW cell), remainder SODW, 2. An equally strong NADW and SODW and lastly 3. A strong NADW (80% of THC strength), remainder SODW. THC strength is not increased, meaning that a stronger NADW results in a weaker SODW, under the assumption that NADW formation increased in strength while SODW weakened (through formation of Antarctic Circumpolar Current) due to the effects of closure and opening of gateway openings (e.g. Zhang et al., 2011).

Thus, four ocean circulation states will be tested. The ocean circulation states are summarized in Table 2:

Table 2. *Ocean circulation states that will be run, summarised*

Name	Circulation state
Permanent SODW	No ocean circulation change occurs. 100% of THC strength (25 Sv) fuels SODW circulation.
Weak NADW	Ocean circulation change occurs at Step 1: 20% of THC strength fuels NADW circulation, remainder SODW circulation
Equal NADW	Ocean circulation change occurs at Step 1: NADW and SODW cells are equally strong
Strong NADW	Ocean circulation change occurs at Step 1: 80% of THC strength fuels NADW circulation, remainder SODW circulation

3.6.2.2. Shelf-to-Basin carbonate fractionation change (SBFC)

The first hypothesis to be tested is shelf-to-basin fractionation change, which postulates that, as sea level dropped, carbonate sediment accumulation shifted to pelagic burial instead of shallow burial, due to the shallowing and exposure of shelves (e.g. Opdyke and Wilkinson, 1988). Such a transport of carbon to the deep sea elicits a deepening of the CCD, through a higher saturation of [Ca^{2+}] and [CO_3^{-}] at deeper depths (Woosley, 2012). It is thus a prime candidate for explaining the deepening of the CCD that occurred during the EOT. It has also been tested with other models in regards to the EOT, such as Armstrong McKay et al. (2016) and Merico et al. (2008), with promising results.

LOSCAR has an in-built parameter, called FSHLF, which modifies carbonate rain to sediments among the sediment boxes which lie at different depths. It is unitless and uses arbitrary values, and it is the relative proportion of carbonate rain on shelves (defined as shallower than 600 meters depth) versus in deep water. This means a lower FSHLF favours deeper carbonate rain, and vice versa (Zeebe, 2012). Komar and Zeebe (2021) (which also used LOSCAR) used the FHSLF parameter as an important control

on the CCD in their model reconstruction across the Cenozoic. In their research, an amplified FHSLF value was needed to accurately portray carbonate accumulation rates in the early Cenozoic, before the EOT. Their FSHLF record contained a dip from a value of circa 12 to 4.5 (see Supplementary Materials of Komar and Zeebe, 2021), to accommodate with observed carbonate mass accumulation rates that declined with a factor of 2 to 3 during the EOT (Opdyke and Wilkinson, 1988). However, this study will use an initial steady state value of 4.5 for FSHLF, as it only focusses on the EOT and not the entirety of the Cenozoic, and therefore it is deemed not necessary to use the inflated values for FSHLF. How FSHLF is related to carbonate rain in shelves and deep sea is formulised in Eq. 12 and 13:

$$F^{i}_{final\ carb.\ rain} = F^{i}_{carb.\ rain\ to\ sed.} \cdot FSHLF^{i} \quad (12)$$

In Eq. 10, the final carbonate rain to sediment box *i* depends on the carbonate rain to sediments (based on Eq. 8 and 9) and the FSHLF of sediment box *i*. FSHLF for shelves (<600 meters) is equal to the FSHLF set as input parameter (in steady state: 4.5). FSHLF for sediment boxes deeper than 600 meters is formulised in Eq. 11:

$$FSHLF_{deep} = 1 - FSHLF_{shelves} \cdot \sum_{i=1}^{n=nr\ of\ shelf\ boxes} Surface(fraction)_i \quad (13)$$

In Eq. 13, the deep FSHLF is equal to the fraction of sea surface that is not shelf (<600 m). It therefore depends on hypsometry (sea surface per depth interval). With a steady state input FSHLF of 4.5, and roughly 10.6% of the sea surface below 600 meters depth (based on the hypsometry/bathymetry used in this study, see Section 3.4.1), carbonate rain to shelves is proportionally more than 9 times as high as carbonate rain to pelagic areas in steady state.

Based on the sensitivity study (Appendix 1) and Komar and Zeebe's (2021) usage of the FSHLF parameter, a rough decrease in two-thirds in FSHLF value seems validated across the EOT. Thus, a decline of an initial 4.5 to 1.5 during the EOT, in FSHLF value, will be tested. As fractionation change is, indirectly, driven by sea level fall, it makes sense that the FSHLF decreases follow sea level. As read in Section 2.1.2, sea level fell with about 25 meters during Step 1, and with about 80 meters or more during EOIS (Miller et al., 2009). However, it is not as simple as using the sea level decline at Step 1 relative to total sea level decline as proportion for decline in FSHLF at Step 1. This is because FSHLF follows more precisely hypsometry changes, as shown in Eq. 13. Hypsometry is not linear or the same throughout the water column, and considering the nature of shelves, hypsometry of the shallow sea can differ quite significantly with lower sea level (Opdyke and Wilkinson, 1988; Rea and Lyle, 2005).

A change to a FSHLF of 1.5, under the same hypsometry (hypsometry is not changed in the model set-up), theoretically results in an increase of about 76% in pelagic carbonate rain to sediments and two-thirds decline in shallow carbonate rain (Eq. 13), the latter following carbonate accumulation rate

reconstructions (Opdyke and Wilkinson, 1988). This calculation does not incorporate the effect of a change in CCD and thus dissolution rate, however, on pelagic carbonate accumulation. As the uncertainty is mostly related to the fractionation change at Step 1, a range of FSHLF changes at Step 1 will be tested: a weak fractionation change (decline to 3.5), a medium fractionation change (decline to 3.0) and a strong fractionation change (decline to 2.5). After EOIS, FSHLF will further decline to 1.5.

3.6.2.3. Increased high latitude biological productivity (IHBP)

As elaborated in Section 2.1.4, high latitude biological productivity is hypothesised to have grown in size with the onset of Antarctic glaciation and increased ventilation, possibly several fold (e.g. Diester-Haass and Zahn, 2001; Coxall and Pearson, 2007). Regarding the EOT, the hypothesis assumes that through increased biological productivity, more organic carbon became sequestered to the deep ocean, deepening the CCD, but also taking out light $\delta^{13}C$ carbon of the ocean and burying it (Zachos and Kump, 2005; Coxall and Pearson, 2007). Therefore, biological productivity should be taken into account regarding modelling of the EOT.

LOSCAR allows the user to set directly the high latitude organic carbon flux to the deep ocean. This high latitude flux, or CBIOH as the parameter is called, takes up dissolved inorganic carbon, alkalinity and phosphate of the high latitude box, and releases 99% of it back to the deep ocean boxes; the remainder is buried. CBIOH is thus a good candidate for parameterising high latitude biological productivity. In steady state, CBIOH is set at 1 mole carbon per square meter per year (out of the high latitude box to the deep oceans). This is the equivalent of a high latitude organic carbon flux of 34.9 teramoles per year, or about 16% of the total organic carbon flux in this version of LOSCAR (Table 1). This also means a 100% increase in CBIOH will result in a 16% increase in (global) organic carbon burial.

CBIOH will be increased with 100% to 2 moles carbon per square meter per year, based on the sensitivity study (Appendix A), as the increase shows to have the potential to significantly affect pCO_2 and other values in the range proxies suggest (Section 2.2.4), as well as being in the ball park of an increase of several fold in high latitude biological productivity during the Earliest Oligocene (Diester-Haass and Zahn, 2001; Coxall and Pearson, 2007). As a 100% increase is the maximum tested in the sensitivity study, a lesser increase of 50% will also be tested (to 1.5 moles carbon per square meter per year) as well as an increase of 75% (to 1.75 moles carbon per square meter per year). CBIOH will be increased at EOIS, following Diester-Haass and Zahn (2001)'s paleoproductivity and export reconstruction of the Southern Ocean.

2.6.2.4. Increased ocean ventilation (IOV)

Increased salt rejection due to glaciation and a "spinning up" of the oceans due to increased meridional thermal gradients is hypothesised to have led to increased deep ocean ventilation (Miller et al., 2009), and is closely associated with higher biological productivity through increased upwelling of nutrients (Coxall and Pearson, 2007). Additionally, increased ventilation results in decreased residence times resulting in decreased acidity (Miller et al., 2009). Therefore, with regard to the carbon cycle, ocean ventilation increase is another hypothesis worth investigating in LOSCAR.

LOSCAR has two mixing vectors which govern the mixing rates between the surface, intermediate and deep boxes: one for surface to intermediate and vice versa, and one for deep to high latitude box(es) and vice versa. The mixing rates/flows are in Sverdrup (m^3 per year), and these will be altered in this study in LOSCAR. Although the EOT is associated with increased deep ventilation (Miller et al., 2009), intermediate to surface and vice versa mixing will also be increased, proportionally the same, as is it this mixing that imports phosphate (read: nutrients, in LOSCAR) to the surface for biological productivity. Initially, in steady state, the deep-high latitude box(es) mixing is 5, 5 and 8 Sv, while the surface-intermediate mixing amounts to 13, 13 and 27 Sv, for the Atlantic, Indian and Pacific oceans, respectively (Zeebe, 2012). There is also mixing for the Tethys Ocean, which will be increased as well.

Viewing the sensitivity study, it is clear that increased ocean ventilation produces shallower CCD and lower benthic $\delta^{13}C$ values compared to proxy records, and therefore basing increase values on the sensitivity study is not productive. It has to be kept in mind, however, that the sensitivity study only captures values 250 kyr after perturbation. Besides the sensitivity study, it is difficult to base increase values for ocean ventilation on data as constraints lack (Armstrong McKay et al., 2016). Still, to test increased ocean ventilation, a weakly increased ocean ventilation will be tested (+25%), a medium increased ocean ventilation (+75%) and finally a strongly increased ocean ventilation (+125%). On timing the ventilation changes in the model, a couple of points have to be taken into account. Firstly, ocean ventilation is associated with ocean circulation change (Straume et al., 2022), and as ocean circulation change is implemented at Step 1 (Section 3.6.2.1), it makes sense to also invoke increased ocean ventilation at Step 1 (although the non-OCC scenarios are run under a permanent SODW circulation state). Secondly, though, ventilation is also associated with a change in meridional temperature gradients, and thus being roughly in line with temperature declines which occur at both steps. It therefore also makes sense to increase mixing at both steps. Lastly, biological productivity increases at EOIS in the model (see previous Section), and as ventilation is seen as a driver for biological productivity, one could argue that increased ocean ventilation should be synchronous with biological productivity increases. As a compromise, ventilation increases are at both Step 1 and EOIS, with equal magnitude.

2.6.2.5. Increased carbonate weathering (ICW)

Weathering is suspected to have increased during the EOT as the result of falling sea levels and more exposure of shelves (Section 2.1.5). A stronger carbonate weathering results in a higher influx of [Ca^{2+}] and [CO_3^-] to the ocean, resulting in a higher carbonate saturation state and subsequent preservation, deepening the CCD (Griffith et al, 2011). In addition, the exposure of carbon isotope heavy neritic shelves would theoretically increase $\delta^{13}C$ of the ocean as well (Coxall and Wilson, 2011). Therefore, increased carbonate weathering is a plausible hypothesis to have occurred during the EOT, and worth investigating in LOSCAR.

LOSCAR includes a carbonate weathering feedback (Eq. 5), and it is this weathering that will be altered. Initially, in steady state, riverine carbonate weathering amounts to 7.858 teramoles per year (Table 1), which will be increased in this scenario. However, it must be taken into account that LOSCAR aims to return to steady state atmospheric pCO_2; therefore, the increased initial riverine carbonate weathering flux is not necessarily equal to the final riverine carbonate weathering flux. Nevertheless, testing, such as with the sensitivity study, shows that increased initial carbonate weathering flux roughly compares to the final carbonate weathering flux (e.g. a 33% increase in initial carbonate weathering flux resulted in a final 28% increased carbonate weathering flux after 250 kyr).

The sensitivity study (Appendix A) shows the best results compared to proxy data (Section 2.2) with a 25% increased carbonate weathering flux. A less strong carbonate weathering flux of 15% increased will also be considered, as well as a stronger one of 35% increased. The sensitivity study shows that increased carbonate weathering has almost negligible effect on (benthic) $\delta^{13}C$, as with FSHLF. To solve this issue, $\delta^{13}C$ of weathered carbonate will also be increased, in line with higher neritic $\delta^{13}C$ rates compared to pelagic sediments due to higher productivity rates (Basak and Martin, 2013; Swart and Eberli, 2005). A somewhat arbitrary value of +3.0 promille is chosen for the newly weathered carbonate (more discussion in Section 5.1.2). Following the assumption that increased weathering follows sea level fall, one-third (assuming one-third of total sea level drop during the EOT occurred at or around Step 1) of growth will occur at Step 1 and two-thirds at EOIS.

2.6.2.6. Increased silicate weathering (ISW)

Silicate weathering is associated with glaciation, due to a shift to physical weathering (Section 2.1.5), as well as an increasement in exposure of silicates due to sea level drop (Zachos and Kump, 2005). As the result of alkalinity changes with an increase in inflow of [Ca^{2+}], the CCD deepens (Griffith et al., 2011). Silicate weathering is also key in controlling atmospheric pCO_2 over long time-scales, and is hypothesised to have played an important role in the cause of EOT (Zachos and Kump, 2005; Kennedy et al., 2015). Therefore, incorporating increased silicate weathering into the study is interesting to see if LOSCAR agrees with these statements.

In LOSCAR, silicate weathering is quite similar to carbonate weathering (compare Eq. 5 and Eq. 6), and it is again the initial silicate weathering that is adjusted. Viewing the sensitivity study (Appendix A), it is not directly clear which range of values should be used for increased silicate weathering; CCD barely changes, while $\delta^{13}C$ shows opposite results compared to what would be expected from the proxy records (Section 2.2.3). Nonetheless, silicate weathering shows profound effect on atmospheric pCO_2, as expected; therefore, increased silicate weathering is still deemed interesting to include in the hypotheses. Basing on atmospheric pCO_2 outcomes, a 20% increase in (initial) silicate weathering, and the more heavy 40% increase in initial silicate weathering are picked. As with ICW, silicate weathering is expected to follow sea level fall, with one-third of growth occurring at Step 1, and the remainder at EOIS.

2.6.2.7. Summary of model set-ups of hypotheses tested

Table 3. *Summary of model set-ups of the hypotheses tested.*

Hypothesis	At Step 1 (at 100 kyr in model)	At EOIS (at 300 kyr in model)
Every hypothesis	Surface temperatures decline with 2.5 degrees Celsius, intermediate, deep and high latitude temperatures with 2 degrees.	Surface temperatures decline with 2.5 degrees Celsius, intermediate, deep and high latitude temperatures with 2 degrees.
OCC	No ocean circulation change (permanent SODW), or 20% of THC (weak NADW), 50% of THC (equal NADW) or 80% of THC (strong NADW) fueling the NADW, remainder SODW.	No changes.
SBFC	FSHLF parameter declines to either 3.5 (weak fractionation change), 3.0 (medium fractionation change) or 2.5 (strong fractionation change).	Further decline to a FSHLF value of 1.5.
IHBP	No change.	Increase in high latitude organic carbon export to deep oceans. Either with 50%, 75% or 100%.
IOV	Half of increase in ventilation occurs, either 25% (weak increase), 75% (moderate increase) or 125% (strong increase).	Remaining half in increase occurs.
ICW	One-third of increase in carbonate weathering (15%, 25%, 35%) as well as appropriate increase in $\delta^{13}C$ of weathered carbonate to make up for +3.0 promille $\delta^{13}C$ of newly weathered carbonate.	Remainder of increase occurs, as well as appropriate adjustment of $\delta^{13}C$ of weathered carbonate.
ISW	One-third of increase in silicate weathering (20% or 40%) occurring.	Remainder of increase occurring.

3.6.3. Combined scenarios

Aside from testing the hypotheses isolated from each other, three combined scenarios were also formed. This was done in order to explore the effect of multiple mechanisms alongside each other. It was also done, as one could argue that the various hypotheses tested are, to different degrees, associated with each other. The values used for parameter changes in the combined scenarios are actually based on the model output of the isolated hypotheses modelled, with the first two based on the medium variants of the hypotheses, and the last one (combination of all hypotheses) taking the weak variants of the hypotheses. All three combined scenarios will also be tested for ocean circulation change, following the OCC scenario (Section 3.6.2.1).

3.6.3.1. Carbonate fractionation and weathering change (CFW)

The first combined scenario to be tested, is carbonate fractionation and weathering change (CFW), which incorporates carbonate shelf-to-basin fractionation change (SBFC) and increased weathering (both ICW and ISW). A shelf-to-basin carbonate fractionation change due to sea level fall (as postulated in Section 3.6.2.2) also implies a simultaneous increase in weathering, following the explanation that weathering increased due to the exposure of shallow shelves as the result of sea level fall (as used as reasoning for increased weathering in Sections 3.6.2.5 and 3.6.2.6). LOSCAR artificially changes carbonate rain to sediments depending on sediment box depth through the parameter FSHLF but keeping the ocean carbonate budget intact, while increased carbonate weathering actually adds carbonate input to the ocean and various sediment boxes, and presents a new source of carbonate and $\delta^{13}\mathrm{C}$ but not necessarily the fractionation change associated with sea level fall. Therefore, the CFW scenario seeks to enhance the SBFC scenario, as well as the ICW and ISW scenarios. Carbonate and silicate weathering will be increased with 25% and 20%, respectively, with the extra weathered carbonate heaving a $\delta^{13}\mathrm{C}$ signature of 3.0 promille (as in the ICW scenario); this increase will be spread over Step 1 (one-third) and EOIS (remainder two-thirds) as with the ICW scenario. FSHLF will decline from 4.5 to 1.5, spread similarly over the two steps (medium fractionation change variant in the SBFC scenario).

3.6.3.2. Increased biological production and ocean ventilation (IBV)

The second combined scenario entails the combination of the IHBP and IOV scenarios (Sections 3.6.2.3 and 3.6.2.4, respectively), called increased biological production and ocean ventilation (IBV). As already mentioned in Section 2.1.4, biological productivity is thought to have been (partially) increased due to increased ventilation during the EOT, through increased upwelling of nutrients. It thus makes sense to include a scenario that combines the two hypotheses. IBV represents therefore a scenario that supplements the independent IHBP and IOV scenarios/hypotheses. Ventilation and biological productivity will be both increased with 75%, equally distributed at both Step 1 and EOIS.

3.6.3.3. Synthesis

The last combined scenario is the "synthesis" scenario. The synthesis scenario aims to produce the best fit with proxy data, considering every hypothesis/scenario tested. The synthesis scenario(s) will not be viewable in the Results (Section 4), as the synthesis scenario is based on the modelled output of the previous scenarios and therefore requires an explanation, which will be done in Section 5.2. The synthesis scenario(s) will be viewable in Appendix C, where a short summary of their set-up and output will be included as well.

4. Results

4.1. Model output

4.1.1. OCC

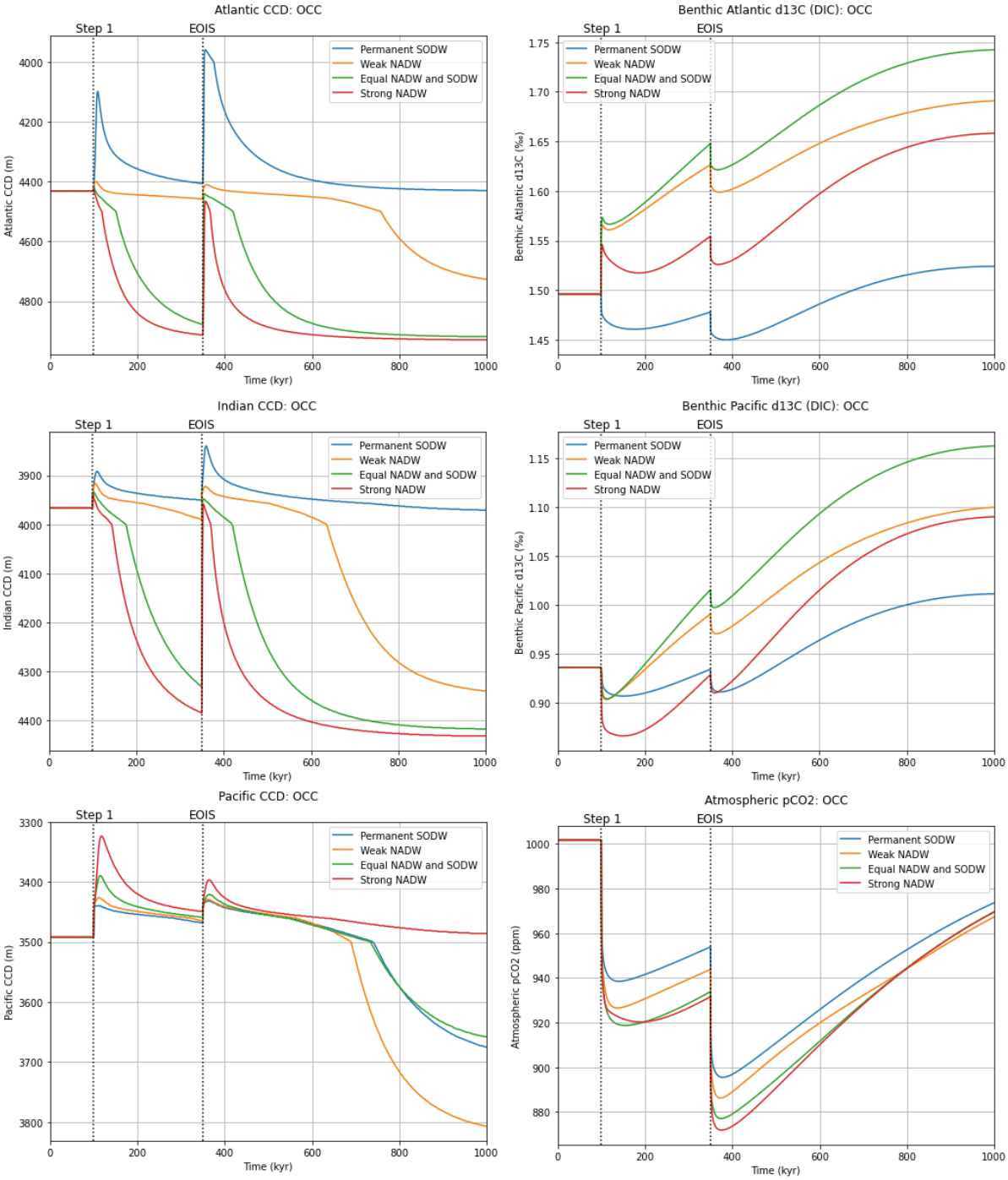

Figure 8. Modelling of Atlantic, Indian and Pacific CCD, as well as benthic Atlantic and Pacific $\delta^{13}C$ *(DIC) and atmospheric* pCO_2*, under the OCC hypothesis.*

Modelling of the OCC hypothesis (Fig. 8) shows interesting feats. Firstly, under a permanent SODW ("null hypothesis"), there are still drastic changes seen in CCD positions (shallowing of about 400 meters in the Atlantic at Step 1, and a deepening of about 200 meters in the Pacific) as well as

atmospheric pCO_2 (declines of about 60 ppm in both Step 1 and EOIS), even though the only change applied concerns temperature declines. It must be noted, however, that the short-term shallowings in CCD positions at Step 1 and EOIS quickly recover in a span of about 100 to 200 kyr. Secondly, the apparent non-linear behaviour of increasing NADW influence on benthic $\delta^{13}C$ is noticeable. Equally strong NADW and SODW circulation cells make benthic $\delta^{13}C$ the most heavy of all OCC simulations, whereas in the strong NADW simulation, a relatively lighter benthic $\delta^{13}C$ is modelled than even under a weak NADW. Thirdly, ocean circulation change has an almost negligible effect on declining atmospheric pCO_2, with atmospheric pCO_2 during the strong NADW simulation declining only with about 20 ppm more compared to the permanent SODW simulation.

Regarding benthic $\delta^{13}C$, the influence of even a weak NADW is significant, more so in the Atlantic Ocean than the Pacific Ocean. Compared to a permanent SODW, the inclusion of a weak NADW circulation cell already increases benthic Atlantic $\delta^{13}C$ with about 0.08‰ at Step 1. Interestingly, while in the Atlantic changes in benthic $\delta^{13}C$ occur instantly at Step 1 (adjoin the inputted instant ocean circulation change), the bulk of the positive change in benthic $\delta^{13}C$ in the Pacific Ocean occurs more gradually. The increase in benthic Pacific $\delta^{13}C$ in this gradual process (ca. 0.2‰) is roughly equal to the increase in benthic Atlantic $\delta^{13}C$ after Step 1, showing that in the short term the influence of NADW has a major impact on benthic Atlantic $\delta^{13}C$ while having little to no effect on benthic Pacific $\delta^{13}C$. In both Atlantic and Pacific Oceans, benthic $\delta^{13}C$ requires quite a bit of time to reach equilibrium, and seems to reach its apex just about at the end of the simulations.

Viewing CCD output, the inclusion of NADW seems to have a gradual opposing effect from the Atlantic to the Indian to the Pacific Ocean. In the Atlantic and Indian oceans, the stronger the input of the NADW circulation cell, the deeper the CCD eventually positions. In the Pacific Ocean, the effect of NADW seems to have completely turned around compared to the Atlantic and Indian, and a stronger NADW results in a lessened deepening of the CCD. This lessened deepening is quite significant, with a net difference between the end positions of the CCD under a permanent SODW and a strong NADW being more than 300 meters.

4.1.2. SBFC

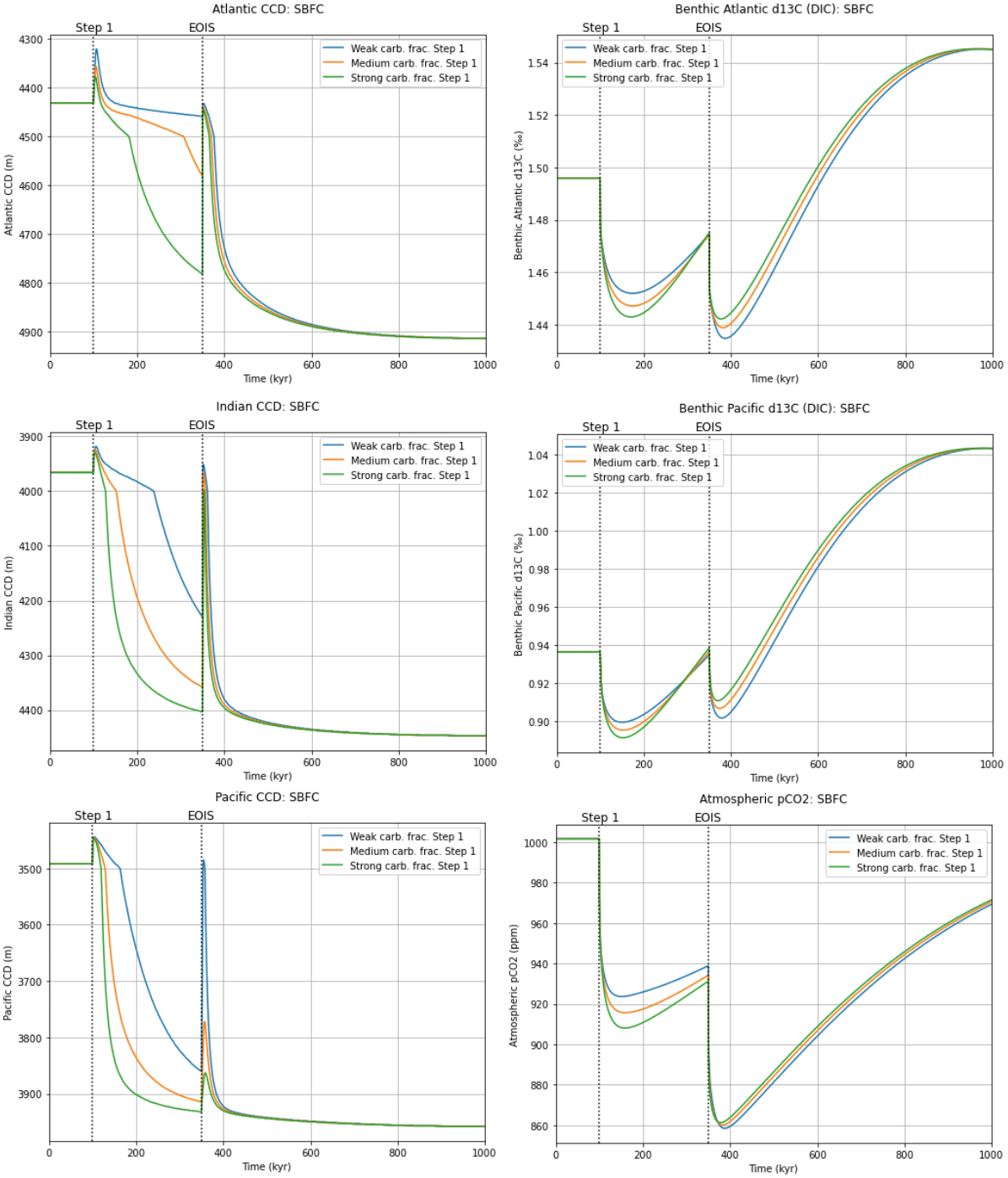

Figure 9. Modelling of Atlantic, Indian and Pacific CCD, as well as benthic Atlantic and Pacific $\delta^{13}C$ *(DIC) and atmospheric* pCO_2*, under the SBFC hypothesis.*

Modelling of the SBFC hypothesis through the FSHLF parameter (Fig. 9), shows that the FSHLF parameter has a large impact on CCD position, in all three oceans. In each ocean, CCD deepens with increased fractionation change, and the deepening shows quite a steep gradient. This deepening is not similar across the oceans: in the Atlantic, Step 1 carbonate fractionation change results in a relatively lower deepening than in the Indian or Pacific. Subsequently, deepening of the CCD in the

Atlantic primarily occurs after EOIS, while in the Indian and Pacific, most of the deepening occurs after Step 1.

In comparison, FSHLF has negligible effect on benthic Atlantic and Pacific $\delta^{13}C$, and shows basically no change compared to the permanent SODW circulation run (previous Section), which acts as null hypothesis. Atmospheric pCO_2 does seem to be impacted by FSHLF change, although to a minor degree, with an extra decline of about 15 ppm (compared to said null hypothesis). The different degrees of FSHLF change show some difference in effect on atmospheric pCO_2 between them, with a maximum difference of about 20 ppm between the most extreme variants at their climax.

4.1.3. IHBP

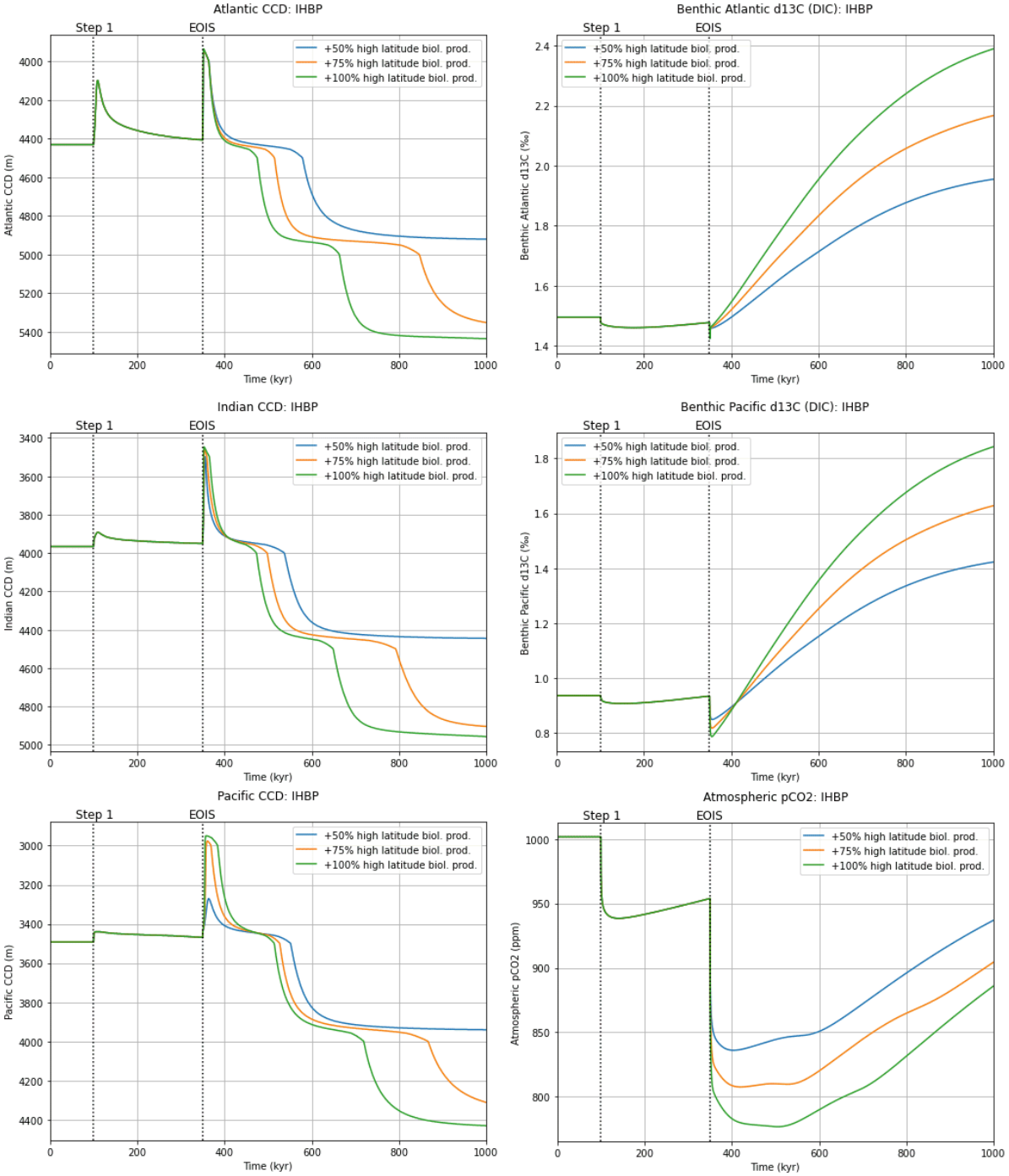

Figure 10. Modelling of Atlantic, Indian and Pacific CCD, as well as benthic Atlantic and Pacific $\delta^{13}C$ *(DIC) and atmospheric* pCO_2*, under the IHBP hypothesis.*

On all fronts, IHBP modelling (Fig. 10) shows a weighty influence. For example, regarding CCD output, the CCD deepens in all oceans with roughly a kilometre if high latitude biological productivity is increased with 100%. However, the CCD does not seem to easily reach equilibrium, with deepening occurring in multiple steps, and the position of the CCD at the end of model runs can therefore be misleading for its final equilibrium value. For example, the first "step" in CCD deepening after EOIS

shows a “delayed” response to biological productivity, with the CCD only deepening roughly 100 to 200 kyr after biological productivity is increased at EOIS. It does seem, however, that this delay in deepening is shortened with higher biological productivity increase.

Benthic $\delta^{13}C$ becomes significantly heavier with about 0.45 to 0.9‰, in both Atlantic and Pacific, depending on the increase in biological productivity, with the increase continuing in positive trend at the end of the model runs. A higher biological productivity thus results in an increase in benthic $\delta^{13}C$, and there is no real difference in this increase between the Atlantic and Pacific oceans. Atmospheric pCO_2 also declines considerably, up to 780 ppm depending on the simulation run. The range in decline in atmospheric pCO_2 between the varying runs is also quite wide, differing about 50 ppm. The magnitude of these declines seem to be roughly linearly related to the amount of increase in high latitude biological productivity, as seems the case for benthic $\delta^{13}C$.

4.1.4. IOV

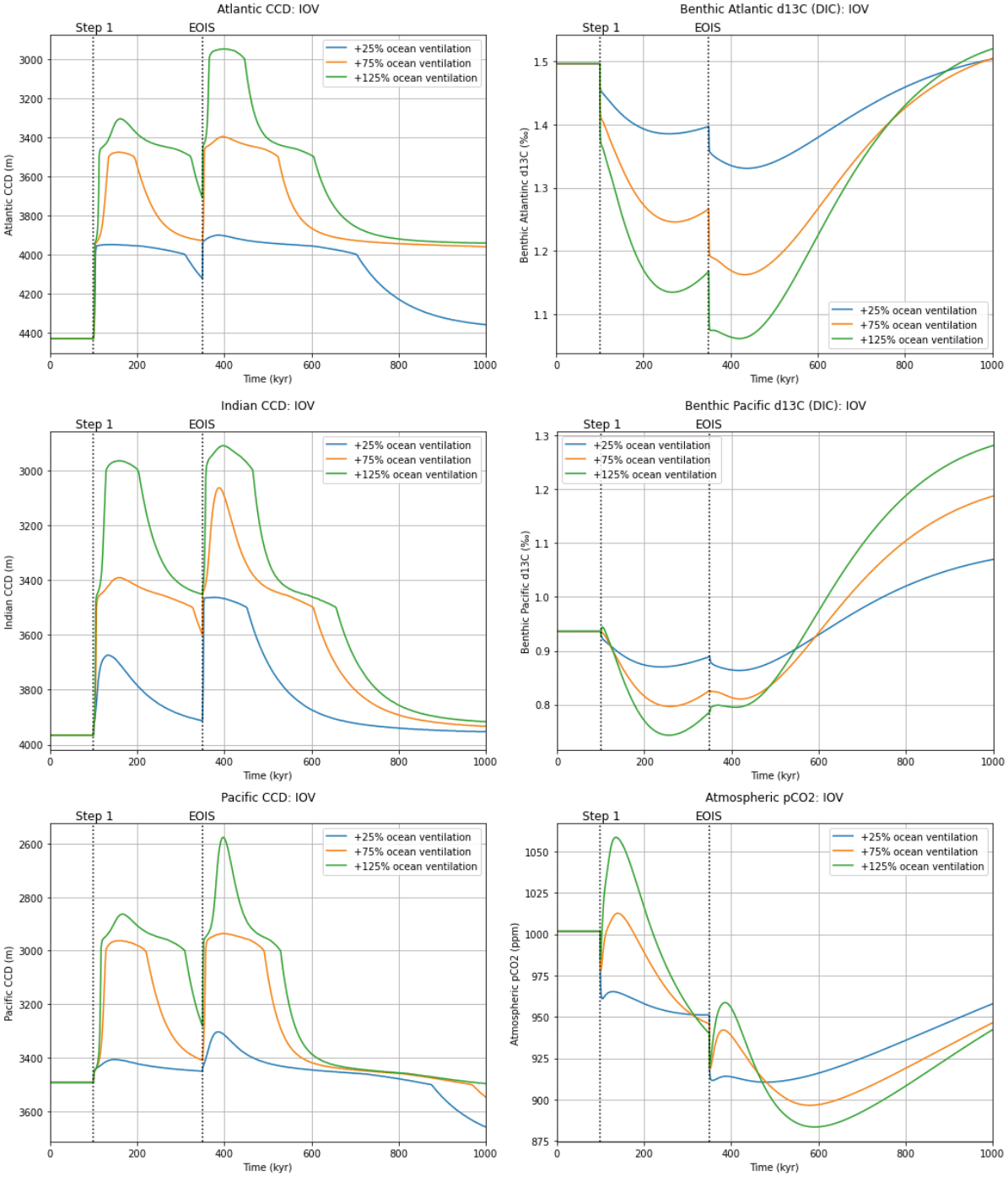

Figure 11. Modelling of Atlantic, Indian and Pacific CCD, as well as benthic Atlantic and Pacific $\delta^{13}C$ *(DIC) and atmospheric* pCO_2*, under the IOV hypothesis.*

Increased ocean ventilation (Fig. 11) shows pronounced impacts on the various modelled output parameters. Firstly, there is a clear difference in short-term versus long-term behaviour after an induced increase in mixing/ventilation rates. In the short term (100 to 200 kyr), increased ocean ventilation shows shallowings, decreases and increases in CCD, benthic $\delta^{13}C$ and atmospheric pCO_2, respectively. However, in the long term (>200 kyr after induced increased ocean ventilation), the CCD

deepens, benthic $\delta^{13}C$ increases, and atmospheric pCO_2 decreases. Compared to steady state, at the end of the simulations the CCD remains similar or is shallowed (400 meters, Atlantic) or deepened (100 to 200 meters, Pacific). Benthic $\delta^{13}C$ increases with up to 0.4‰ in the Pacific, while in the Atlantic benthic $\delta^{13}C$ takes a deep dive and only at the end of the simulations reaches levels higher than initial steady state. The final equilibrium value has not yet been reached at the end of the simulations (650 kyr after EOIS). Atmospheric pCO_2 shows at both steps a strong, almost instant (on 1 kyr scale) decrease, but after a ca. 100 kyr rebound in atmospheric pCO_2 levels. After this rebound, a stronger decrease commences, being more severe at Step 1 than at EOIS. Roughly 200 kyr after EOIS, the minimum in atmospheric pCO_2 is reached (to at most ca. 860 ppm), and a, slower, rebound occurs.

4.1.5. ICW

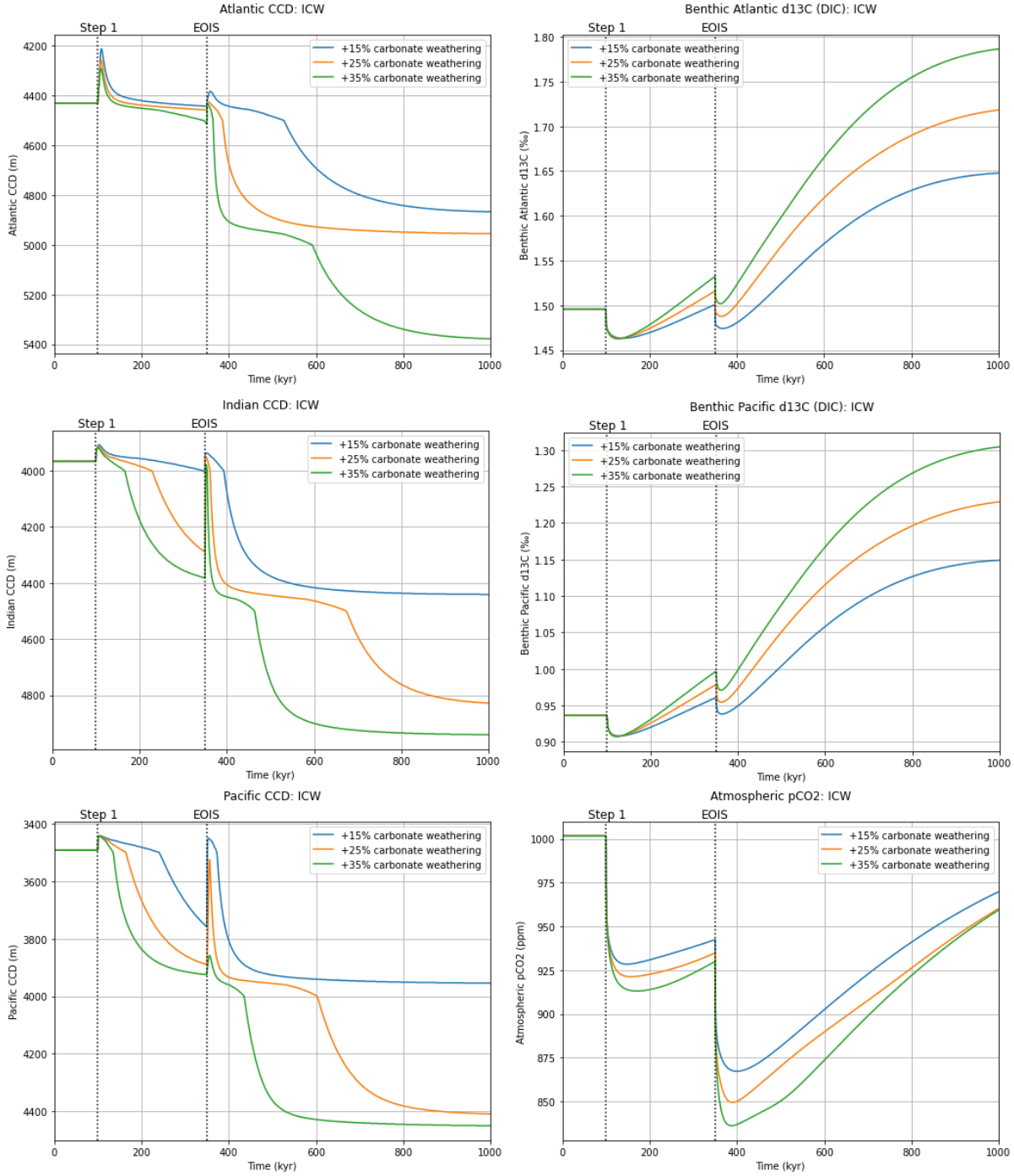

Figure 12. Modelling of Atlantic, Indian and Pacific CCD, as well as benthic Atlantic and Pacific $\delta^{13}C$ *(DIC) and atmospheric* pCO_2*, under the ICW hypothesis.*

The ICW hypothesis (Fig. 12) shows large impacts on the position of the CCD, in all three oceans. The CCD deepening shows a clear two-step deepening in the Pacific, while it is the deepening at Step 1 is less pronounced in the Indian Ocean and is almost non-existent in the Atlantic. Interestingly, similar to increased biological production (Section 4.1.3), the lower the increase in carbonate weathering, the more "delayed" the CCD response actually is. This delay is more noticeable after EOIS. For example,

for a 15% increased carbonate weathering, deepening only starts to significantly occur in the Atlantic CCD after almost 100 kyr after the EOIS, while for a 35% increase the deepening occurs instantly. Similarly to the IHBP scenario (Section 4.1.3), the CCD shows a stepped pattern because of this delay.

Benthic $\delta^{13}C$ increase at the end of the model run, compared to initial steady state, amounts to roughly 0.15‰ to 0.35‰, depending primarily on amount of increasement and secondly on the ocean. Atmospheric pCO_2 declines are, while not as large as in the modelling of the IHBP scenario (Section 4.1.3), still significant: under a 35% increase in carbonate weathering, pCO_2 declines to about 835 ppm.

4.1.6. ISW

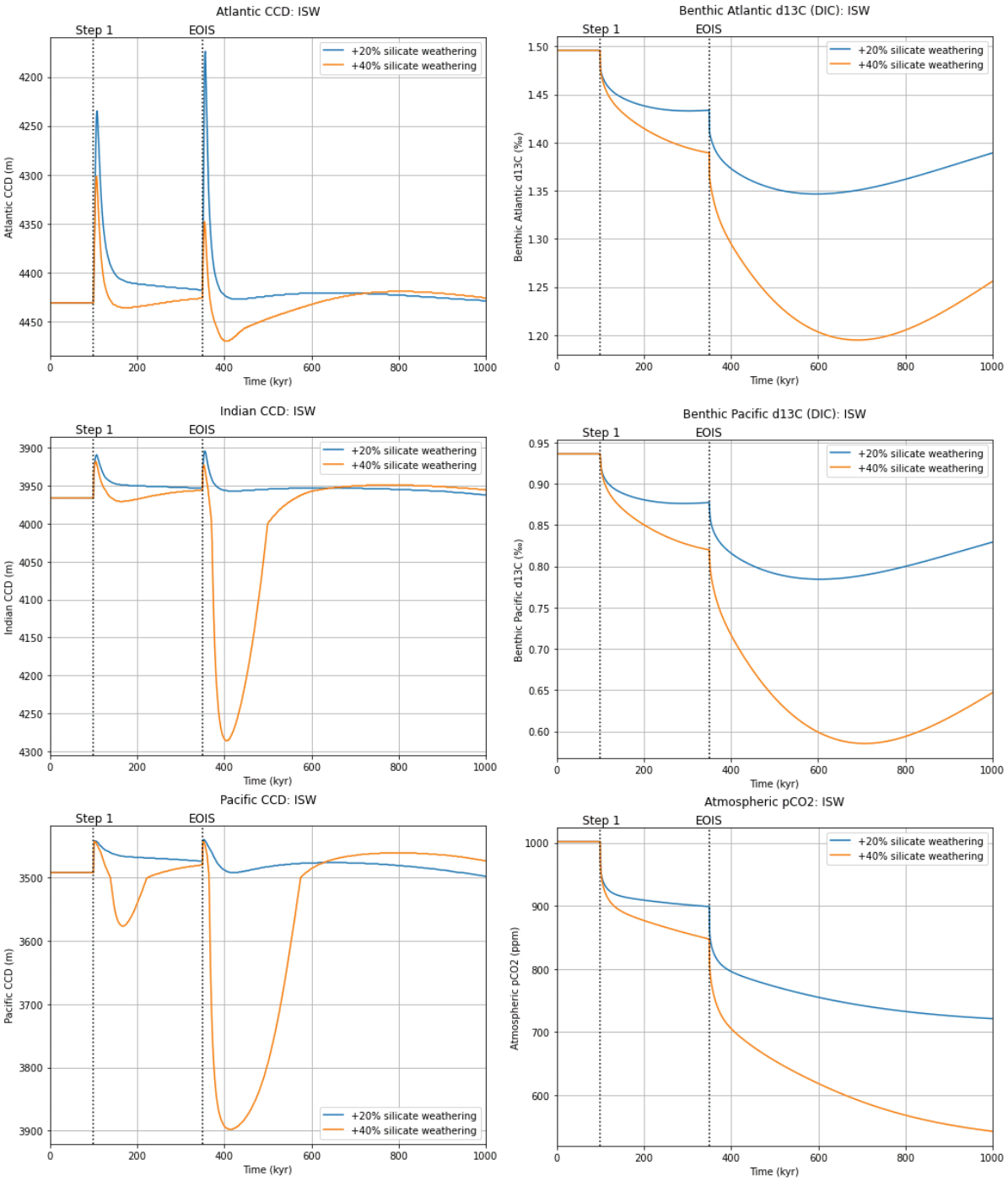

Figure 13. Modelling of Atlantic, Indian and Pacific CCD, as well as benthic Atlantic and Pacific $\delta^{13}C$ *(DIC) and atmospheric* pCO_2*, under the ISW hypothesis.*

Of all the hypotheses modelled, ISW (Fig. 13) shows the most restraint regarding CCD output. There is no major deepening in CCD, except for the Indian and Pacific who show a short temporary excursion of about 400 meters after EOIS (for a 40% increase). ISW is also the only hypothesis that actually records a decrease in benthic $\delta^{13}C$; the decline is fairly heavy, up to more than 0.4‰ for an increase of 40% in silicate weathering. However, about 350 kyr after EOIS, benthic $\delta^{13}C$ stabilises and increases,

although at a slow pace. Silicate weathering does have a strong effect on atmospheric pCO_2, with an increase of 40% in silicate weathering resulting in a decline of atmospheric pCO_2 to less than 600 ppm, with pCO_2 continuing to decrease at the end of the simulations. Of all the modelled hypotheses, ISW shows the strongest influence on atmospheric pCO_2.

4.1.7. CFW

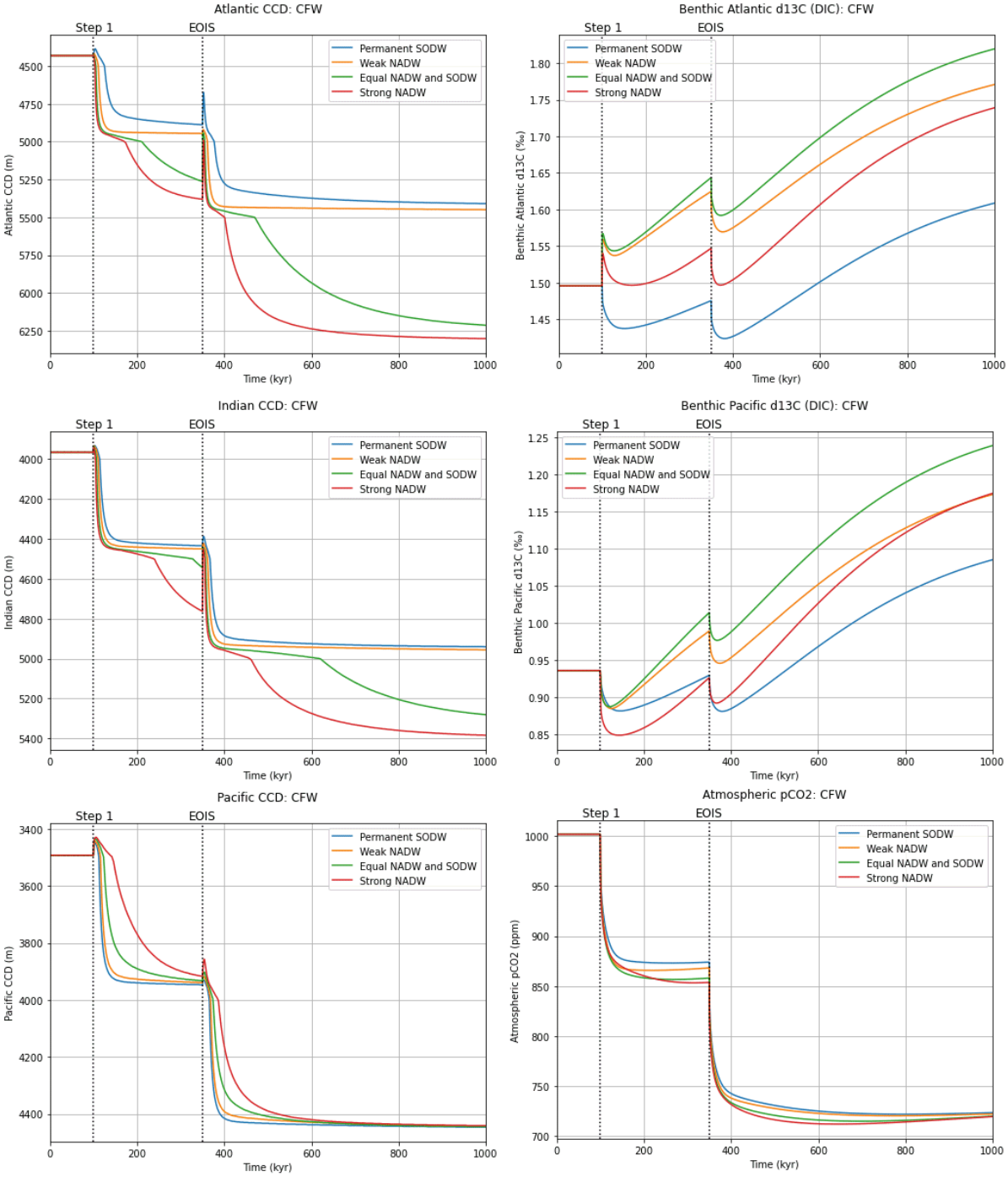

Figure 14. Carbonate fractionation change and weathering increase scenario. FSHLF was declined to 1.5 (with a decline to 3.0 at Step 1), and carbonate and silicate weathering were increased with 25% and 20%, respectively, in two steps. Just like the ICW scenario, the extra weathered carbonate has a $\delta^{13}C$ *of +3.0‰.*

The first combined scenario, CFW (Fig. 14), shows major changes in the position of the Atlantic (and Indian, but less pronounced) CCD depending on NADW strength: the Atlantic CCD is at the end of the simulation 900 meters deeper under a strong NADW than under a permanent SODW circulation. This is noteworthy as under a permanent SODW circulation the Atlantic CCD already deepens with almost

a kilometre in the CFW scenario. The eventual depth reached under a strong NADW is about 6300 meters, almost hitting the theoretical maximum of 6500 meters in LOSCAR (Zeebe, 2012). The Indian and Pacific CCDs do not deepen with more than 1000 or 900 meters, respectively, on the other hand. Interestingly, for a stronger NADW, the Pacific and Indian oceans require quite a bit of time for their CCDs to reach equilibrium, as a delay in deepening occurs, similarly to the CCD modelling in the ICW scenario (Section 4.1.5). All three oceans nevertheless show a clear two-stepped pattern deepening in CCD at Step 1 and EOIS.

In general, the benthic $\delta^{13}C$ follows a similar pattern as during the OCC modelling (Section 4.1.1), except that the values are somewhat higher, apparently as the result of increased carbonate weathering. In total, the increase amounts to about 0.3 promille in the Pacific and Atlantic under the equal NADW and SODW variants. As the OCC scenario showed that ocean circulation change barely influences atmospheric pCO_2 decline, the decline in the CFW modelling to about 720 ppm is the result of increased carbonate/silicate weathering and FSHLF decline together.

4.1.8. IBV

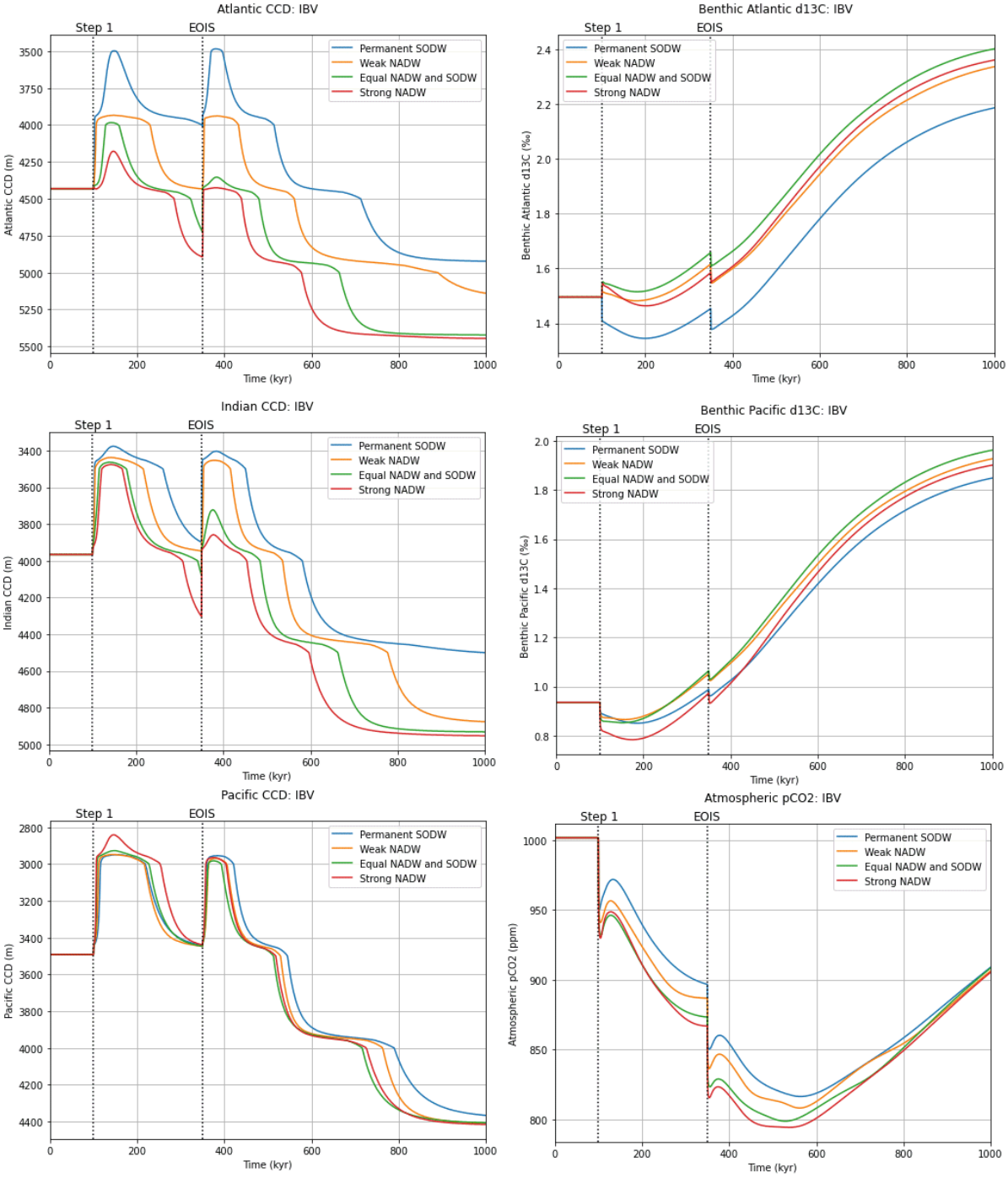

Figure 15. Modelling of the increased (high latitude) biological productivity and ocean ventilation scenario. High latitude biological productivity and ocean ventilation were both increased with 75%.

The IBV scenario (Fig. 15) has several interesting features. Firstly, the CCD output initially seems quite chaotic. At both steps, in each ocean, an initial shallowing of CCD occurs (with a magnitude of up to a kilometre) which takes in the order of 100 to 200 kyr to "settle", before deepening in CCD can occur. Of importance is that a deepening in CCD between Step 1 and EOIS does not occur, except for a minor deepening under a strong NADW circulation state in the Atlantic and Indian. Secondly, the impact of

a change in meridional overturning circulation (SODW to NADW based circulation) becomes progressively weaker from the Atlantic to the Pacific. In the Pacific Ocean, the CCD is barely affected by a (major) change in overturning circulation, while in the Atlantic Ocean, the difference in CCD position based on meridional overturning circulation can be up to 500 meters. Thirdly, all three oceans are capable of producing CCD deepenings in the order of 1 kilometre, but it requires a prolonged period of time to reach this deepening. Interestingly, in doing so, the CCD deepens with several steps: after EOIS, three of these "steps" (not to be confused with Step 1 and EOIS) can be identified.

The trajectory of benthic $\delta^{13}C$ on the other hand is much smoother, and does not contain such "steps". The magnitude in enrichment of benthic $\delta^{13}C$ is large: 0.7 to 1.0‰, depending ocean and NADW strength. In general, it seems that the Pacific enjoys slightly larger increases in benthic $\delta^{13}C$, although minor, while the Atlantic is more impacted by changes in the meridional overturning circulation. The increase in benthic $\delta^{13}C$ between Step 1 and EOIS on the other hand is minor to non-existent, most enrichment occurs after EOIS. At the end of the simulations (650 kyr after EOIS), the benthic $\delta^{13}C$ of both oceans has not reached equilibrium, but the gradient of increase has certainly slowed down. In contrast with benthic $\delta^{13}C$, atmospheric pCO_2 does show a strong change between Step 1 and EOIS, with actually most of the total decrease occurring before EOIS. After EOIS, the decline continues, with the minimum atmospheric pCO_2 being about 800 ppm under a strong NADW mode of circulation, reached roughly 200 kyr after EOIS. After this minimum, the atmospheric pCO_2 rebounds and linearly grows back to initial steady state value, albeit not reaching it before the simulations end.

4.2. Comparison to proxy data

4.2.1. CCD

CCD reconstructions from proxy records (see Section 2.2.2) showed a CCD deepening in the scale of kilometre in all oceans. Both CFW and IBV scenarios are capable of reaching these deepenings, but the other (isolated) scenarios are not able to produce such results, except for IHBP and and ICW. IHBP (Section 4.1.3) simulates deepenings in the order of 900 to 1000 meters for every ocean, but the deepening is spread over a long time (in some cases until the end of simulations, 900 kyr after Step 1) across multiple "steps" (not to confuse with Step 1 and EOIS), and differs thus from the rapid deepening (<300 kyr) Rea and Lyle (2005) and Pälike et al. (2012) reconstruct. In the ICW scenario, under a strong carbonate weathering rate (+35%), the CCD deepens with about 900 to 1000 meters, depending on ocean, again in steps such as with IHBP, but in a shorter timeframe. The problem, however, with the ICW scenario is that it does not reproduce a clear two-step deepening in CCD, differing from the interpretation that the CCD deepened across two steps (Coxall et al., 2005). The remaining, isolated, scenarios fail to simulate a deepening in the scale of a kilometre in CCD. In this sense, the CFW and IBV scenarios give a better fit. The IBV scenario is the more troublesome of the two, however. The IBV scenario shows a lengthy CCD deepening, occurring in multiple "steps" after EOIS, with the last of these three steps (not to confuse with Step 1 and EOIS) occurring roughly 200 to 400 kyr after EOIS. The CFW scenario on the other hand shows deepenings in much shorter time, with a very clear two-step pattern. The Atlantic CCD in the CFW scenario does become more deep when NADW is stronger rather than weak, with a deepening of about 1700 meters, similarly in the Indian CCD (deepening of about 1300 to 1400 meters). Nevertheless, the CFW scenario produces the best CCD output based on deepening (ca. 1 km), two-step growth (clear deepening in both Step 1 and EOIS) and deepening time (relatively quickly, <300 kyr).

4.2.2. Benthic $\delta^{13}C$

As Section 2.2.3 shows, benthic $\delta^{13}\mathrm{C}$ increased roughly in the order of 0.7 to 1.0‰ about 250 kyr after EOIS, after which it gradually declined. For the isolated scenarios, IHBP shows the most potential regarding benthic $\delta^{13}\mathrm{C}$, by far. For example, under a 100% increase in high latitude biological productivity, benthic $\delta^{13}\mathrm{C}$ in both Atlantic and Pacific enriches with 0.9‰. No other isolated scenario comes close to this: IOV (for the Pacific, not the Atlantic) and ICW are the closest with enrichments in $\delta^{13}\mathrm{C}$ of up to about 0.3 and 0.4‰, respectively. Modelled benthic $\delta^{13}\mathrm{C}$ in the IHBP scenario, however, takes a considerable amount of time (more than 650 kyr after EOIS, or well after the simulation ends) to reach a climax, which differs from the actual proxy record which shows a climax about 250 kyr after EOIS. In fact, the combined scenarios of CFW and IBV, which also show substantial enrichments in $\delta^{13}\mathrm{C}$, especially IBV (0.7 to 0.9‰, depending on ocean and mode of circulation), produce similar long climax times. It thus becomes clear that no scenario present here in the Results offer a good match with the

temporality of the increase in benthic $\delta^{13}C$ proxy record. Regarding CFW and IBV, the NADW has a positive effect on benthic $\delta^{13}C$ in both Atlantic and Pacific oceans. The size of the NADW seems to have a parabolic effect on benthic $\delta^{13}C$, with a weak NADW having a more positive effect on benthic $\delta^{13}C$ than a strong NADW, but less so than an equal NADW and SODW mode of circulation. The difference with no NADW formation (permanent SODW formation) and NADW inclusion can rise to about 0.2‰, with a stronger difference in the Atlantic than in the Pacific.

4.2.3. Atmospheric pCO_2

Section 2.2.4 mentions pCO_2 reconstructions made for the EOT, which both show a significant decline in atmospheric pCO_2 from the Late Eocene to EOIS, when major glaciation is hypothesised to have occurred. The decline would have reached a threshold value namely, modelled for Antarctic glaciation, in the order of 700 to 800 ppm. After EOIS, a short-lived positive incursion occurred, after which pCO_2 declines again. All scenarios, as well as the combined ones, fail to reproduce this exact timing of atmospheric pCO_2. At EOIS, the minimum reached pCO_2 is "only" about 850 ppm in the strong NADW variants of the CFW scenario. Nevertheless, the total decline in atmospheric pCO_2, after EOIS, is in most scenarios more than capable to reach the range of 700 to 800 ppm, or even less. Especially the ISW (+40% increase in silicate weathering) shows a very strong decline in atmospheric pCO_2 after EOIS, well below 700 ppm. Atmospheric pCO_2 reconstructions (such as Fig. 4) show a continuing decline to values hitting 600 ppm after a period longer than the modelled time period for the scenarios. Most scenarios, however, often show an eventual rebound, some quicker than others. This is quite likely the result of the in-built variable silicate and carbonate weathering rates in LOSCAR (Eq. 5 and 6). Especially the IOV and IBV scenarios show a quick rebound. Only two scenarios do not show a clear rebound: ISW and CFW scenarios. Of these two, the ISW scenario, especially under a 40% increase in silicate weathering, shows the most significant impact on pCO_2, with a very strong decrease in pCO_2 (hitting values below 600 ppm) which continues even after the simulations end. The CFW scenario includes increased silicate weathering (although at lower pace, +20%), and considering the ISW pCO_2 output, it is this silicate weathering which subdues any potential recovery in atmospheric pCO_2. Based on the substantial decline in atmospheric pCO_2 and this subduing of pCO_2 recovery, the ISW and CFW scenarios show the best fit with the reconstructed atmospheric pCO_2 record.

4.2.4. Other proxies

Although not plotted here, but in Appendix B, other proxies (briefly mentioned in Section 2.2) were modelled as well in the research, to enhance comparison. Benthic Pacific [CO_3^-] was modelled in order to compare with the reported 37 µmol/kg increase at ODP 1218 (Lear et al., 2010). This comparison proves fruitless, however, as the highest modelled increase in [CO_3^-] in the scenario amounts to about 12 µmol/kg. Quite importantly, however, [CO_3^-] depends greatly on depth (Elderfield et al., 2006), and

the modelled change in LOSCAR assumes the average of the entirety of the deep Pacific (1000 meters and deeper), while ODP 1218 sat at a paleodepth of 3.7 to 4.0 km during the EOT (Pusz et al., 2011). Nevertheless, modelled [CO_3^-] at steady state (ca. 41 µmol/kg) is roughly similar to the predicted Cenozoic deep sea [CO_3^-] concentrations around the EOT by the model used by Boudreau and Luo (2017), which do show a predicted increase in the order of 10 µmol/kg from EOT to ca. 30 Ma.

A further, more fruitful comparison can be made with the $CaCO_3$ wt(%) record of ODP 1218 (Coxall et al., 2005, viewable in Fig. 1), as the carbonate content in sediments at a depth of 3.5 to 4.0 km in the Pacific Ocean was modelled (Appendix B). Figure 1 (note the reversed y-axis) shows a clear two-step, 40 kyr increase in $CaCO_3$ wt(%), with at Step 1 an increase from virtually 0 to about 60%, after which values plateau to about 50% for about 100-200 kyr, and finally at EOIS a further increase to values reaching 90%. In the time span of about 250 kyr after EOIS, values dip again to about 70 to 80%. The modelling of pelagic Pacific $CaCO_3$ sediment content showed great results with this brief description of Figure 1. In Late Eocene steady state (Section 3.4.1), $CaCO_3$ wt(%) is virtually 0% as well, coherent with a Pacific CCD below 3500 meters. Only the CFW scenario shows a clear increase at Step 1 in $CaCO_3$ wt(%) in the order of 40 to 60% in a span of 40 kyr. The stronger the NADW, however, the more prolonged and lesser the increase becomes. Interestingly, while the ICW and SBFC scenarios show a quite modest gradient in increase of $CaCO_3$ wt(%) at Step 1, CFW (which is a combination of two scenarios) shows quite a rapid increase. CFW only really produces a clear plateauing in $CaCO_3$ wt(%) values between Step 1 and EOIS under a permanent SODW mode of circulation. At EOIS, the increase in $CaCO_3$ wt(%) is first preceded, in almost all scenarios by a short temporary decrease in values. The increase after EOIS is, however, more modest in the scenarios compared to the actual record: a value higher than 70% is not reached. Unlike at Step 1, the severity of the NADW does not seem to play a significant role in the increase in $CaCO_3$ wt(%) at EOIS. No scenario shows a rebound in values seen in the record. With regard to accuracy, CFW shows the best fit, but only really under a permanent SODW mode of circulation. The other combined scenario present here in the Results, the IBV scenario, exhibits a strong increase in $CaCO_3$ wt(%) after EOIS (to values hitting 70%), but completely fails to produce an adequate increase in $CaCO_3$ wt(%) after Step 1.

Finally, pH levels were modelled as well (Appendix B), to allow for a comparison with Pearson et al. (2009)'s reconstruction of pH levels during the EOT. Pearson et al. (2009) reconstructed pH levels in order to asses pCO_2 changes across the EOT, from boron isotopes of upper ocean dwelling foraminifera in Tanzania. The reconstruction showed an increase in pH levels, from ca. 7.5 (34.2 Ma), to ca. 7.64 (33.6 Ma) to finally 7.7 (33.0 Ma). Thus, increases of ca. 0.14 (Late Eocene to EOIS) and 0.06 (EOIS to Early Oligocene). In order to properly compare with these values, pH levels of the Indian intermediate (100 to 1000 meters depth) box were picked during modelling. In Late Eocene steady state (Section

3.4.1), pH levels were surprisingly similar to the reconstructed pH level of 7.5, with a modelled pH level of 7.56. CFW and IBV both show a strong fit with reconstructed pH record, and arguably the best of all scenarios. Both contain pH values of around 7.625-7.65 (CFW) and 7.65-7.675 (IBV) at EOIS, and at the end of the simulations (ca. 33.0 Ma) between 7.725-7.75 (CFW) to 7.75-7.78 (IBV), with higher values for a stronger NADW. Although the total increase from Late Eocene to Early Oligocene in the modelled pH of the CFW and IBV scenarios (increase of 0.16 to 0.22) is roughly similar to Pearson et al. (2009)'s reconstruction (increase of 0.20), most of pH increase occurs after EOIS, instead of before EOIS. Nevertheless, CFW and IBV remain the best fit, as other scenarios are not capable of reproducing this behaviour as well. The remaining scenarios show increases in pH, but not in the same magnitude. The one exception is for IHBP, which only shows substantial pH increase after EOIS (which makes sense as only at EOIS biological productivity increase is implemented), but with a large magnitude, depending on the amount of increase in biological productivity. For a 100% increase in high latitude biological productivity, pH increases to 7.73, for a total increase of 0.17.

5. Discussion

5.1. Model output

In order to determine the implications of the modelling on carbon cycle perturbations during the EOT, it is handy to have an overview of the proxy comparisons with modelled output of previous Sections (Table 4). Note that the [CO_3^{-}] comparison is not present as it did not allow for a proper comparison (see Section 4.2.4).

Table 4. *Summary of proxy comparisons with modelled output*

Proxy record	Best scenario(s) fit	Rationale
CCD reconstructions	CFW	Able to produce deepenings in the order of 1 km for every ocean, clear two step pattern and quick (<300 kyr)
Benthic $\delta^{13}C$ records	IHBP and IBV	Correct amplitude enrichment in $\delta^{13}C$ (0.7 to 0.9‰), although not able to reach a climax in 250 kyr
Atmospheric *pCO_2* reconstructions	ISW and CFW	Large declines in atmospheric pCO_2, to well below 700 ppm. Any potential recovery in pCO_2 stays subdued if increased silicate weathering is involved, following atmospheric pCO_2 reconstructions after EOT
Pelagic Pacific $CaCO_3$ wt(%) reconstruction	CFW	Clear two step growth (each ca. 40 kyr), with increases roughly in order of the reconstruction.
Upper Indian ocean pH reconstruction	CFW and IBV	Able to produce sufficient increase in pH coherent with reconstruction (ca. 0.2)

5.1.1. CCD

Regarding CCD output, CFW gives the best fit with CCD reconstructions and pelagic Pacific $CaCO_3$ wt(%) reconstruction, as it is the only scenario that fits within the three criteria (amplitude deepening, two-step pattern and rapidness). Thus, modelling with LOSCAR implies that CCD deepening and subsequent increase in carbonate in sediments is (primarily) the result of a shift from shelf to pelagic carbonate rain and increase in carbonate weathering. Both hypotheses (carbonate burial shift to pelagic and increased carbonate weathering) complement each other, as alone they are not able to explain the proxy data (Section 4.2). For example, increased carbonate weathering results in sufficient deepening, but in a prolonged fashion, while a fractionation change in burial from shelf to pelagic areas results in a quicker, but lessened, deepening of the CCD. Thus, increased carbonate weathering

is needed to adequately increase carbonate saturation state and subsequent carbonate burial while a shelf to pelagic carbonate burial fractionation change facilitates the increased transfer of this extra carbonate to the deep sea.

With a carbonate weathering increase of 25% and a FSHLF decline from 4.5 to 1.5 (as present in the CFW scenario), pelagic carbonate rain increases with about 100%. This is roughly in line with estimated Cenozoic pelagic carbonate burial rates increases from pre-EOT to post-EOT (Opdyke and Wilkinson, 1988; Boudreau and Luo, 2017). With a CCD deepening of about a kilometer, dissolution rates decline and allow for even higher carbonate burial rates, spread over a larger surface. Using the Pacific hypsometry in the model used as case, surface above the CCD increased from about 38% to 70% of total ocean surface, roughly in line with the estimation of an increase of 2.25 in surface (Rea and Lyle, 2005). Further testing shows pelagic burial of carbonate, including dissolution changes, increases with about 120% in LOSCAR with 25% increase in carbonate weathering and a FSHLF decline of 4.5 to 1.5. Therefore, the CFW scenario shows substantially increased pelagic carbonate burial. There is still some criticism about the role of shelf-to-basin fractionation change and weathering on CCD positions and pelagic carbonate burial, however, arguing that the sea level fall at both steps would have been too minor to cause significant CCD deepening through fractionation change alone and that Ca influx through weathering alone would be too small to sustain the CCD deepening (Rea and Lyle, 2005; Miller et al., 2009). More discussion pertaining shelf-to-basin fractionation-induced increased pelagic carbonate burial in LOSCAR follows in Section 5.5.2.

A small point to discuss is the relative deepening in CCD between the oceans. The Pacific CCD deepening is considered to be the largest in magnitude of all the oceans (Van Andel, 1975; Thunell and Corliss, 1986; Wade et al., 2020; Coxall and Pearson, 2007). However, the CCD model output shows (roughly) equal deepenings and often a stronger deepening in the Atlantic and Indian than in the Pacific Ocean (see CFW scenario output, Section 4.1.7). One answer for the reason of this difference lies in the lack of proper CCD reconstructions, for example Atlantic sites are still poorly covered for data pertaining to the CCD position (Van der Ploeg et al., 2019). Another answer lies in LOSCAR itself, and this study's interpretation of how mechanisms/processes, such as biological productivity, work per ocean (more discussion pertaining LOSCAR and this study's modelling of the EOT in Section 5.5). For example, shelf-to-basin carbonate fractionation change likely differed per ocean, due to differing hypsometries and shelf/pelagic carbonate production rates, yet in this study, for simplification reasons, the parameter FSHLF was changed equally per ocean. As the Pacific is on average deeper than the Atlantic and Indian oceans (based on the hypsometry used in this study), the relative surface of Pacific shallow sea is smaller. As the effect of the FSHLF is directly related to the relative size of the shallow sea (Eq. 13), shelf-to-basin carbonate fractionation change will favour the

Atlantic and Indian oceans in CCD deepening through higher increase in pelagic carbonate rain. This is not necessarily a bad result, but most of the shift in carbonate burial to pelagic areas could very well in reality occur on areas above the CCD already, in the Atlantic and Indian oceans. Therefore, a proper (and not a simplified) carbonate shelf-to-deep fractionation change scenario should tweak the FSHLF parameter carefully per ocean, based on hypsometry. Nevertheless, stronger deepenings in Atlantic and Indian CCD (compared to the Pacific CCD) do not occur that often (only really under a stronger than weak NADW, or for the Atlantic in the AI scenario), and the other deepenings modelled generally are in the same scale (ca. 1 km) as expected (Rea and Lyle, 2005; Coxall and Pearson, 2007). As the goal of this study is not to exactly reproduce the CCD position for each ocean as well (but more to determine the plausibility of the hypotheses), the modelled CCD positions are still deemed to be of interest.

5.1.2. Benthic $\delta^{13}C$

Only two scenarios were able to produce enrichments in benthic $\delta^{13}\mathrm{C}$ equal to the actual benthic $\delta^{13}\mathrm{C}$ record (0.7 to 1.0‰), namely IHBP and IBV. These two scenarios both include increased high latitude biological productivity, which exerts a much stronger control on benthic $\delta^{13}\mathrm{C}$ than increased ocean ventilation or increased carbonate weathering (Section 4.2.2). Therefore, the modelling in this study implies the importance of an increase in (high latitude) biological productivity during the EOT to match the benthic $\delta^{13}\mathrm{C}$ signal. Theoretically, increased carbonate weathering could also explain the increase in benthic $\delta^{13}\mathrm{C}$, but it would require either a substantially higher enrichment in $\delta^{13}\mathrm{C}$ for the newly weathered carbonate than used in the model (+3.0‰), or a much higher weathering rate. Considering the modelling output of the ICW and CFW scenarios, and the sensitivity study (Appendix A), a higher carbonate weathering rate would result in a too large deepening in CCD, and be therefore unlikely (more discussion about weathering in LOSCAR in Section 5.5.5). The other option would be that $\delta^{13}\mathrm{C}$ of the newly weathered carbonate is modelled too low; for example, aragonite-dominated carbonates have a high $\delta^{13}\mathrm{C}$, with sediments deposited on the Great Bahama Bank surface being almost 100% aragonite and containing $\delta^{13}\mathrm{C}$ values of +4.0 to +5.0‰ (Swart and Eberli, 2005). The weathered shelf carbonate $\delta^{13}\mathrm{C}$ also very much depends on age: for example, Late Carboniferous (ca. 300 Ma) limestones had high $\delta^{13}\mathrm{C}$ levels (in the order of +6.0‰) as coal swamps buried isotopically light carbon, leaving isotopically heavy carbon for carbonate precipitation in the oceans (Berner, 1987).

One point of notice was the time length to reach the apex (or maximum) in benthic $\delta^{13}\mathrm{C}$ (Section 4.2.2). The actual benthic $\delta^{13}\mathrm{C}$ record (Fig. 3) reaches its maximum at 33.4 Ma, or about 250 kyr after EOIS. None of the scenarios, as well as IBV and IHBP, reproduce this behaviour, and instead need the full time length of the simulations or longer to reach a climax. A possible reason for this mismatch, besides the omission of a factor/mechanism not included in the model, is that mechanism(s) should exhibit

transient instead of static behaviour. Instead of a permanent change in a mechanism, such as a 25% increase in weathering or 50% increase in biological productivity, a temporary and a more transient change could have, and more likely, occurred. In the case of weathering, enhanced weathering could occur after sea level fall but decline in the course of the EOT as more shelf carbonate eroded and less (and less weatherable) carbonate remained. It remains the question however, how much the initial increased weathering would decline over the course of the EOT and beyond.

High latitude biological productivity, more interestingly as the IHBP exerts the strongest control on modelled benthic $\delta^{13}C$, likely fluctuated as well across the EOT. For example, Site 1090 in the Southern Atlantic shows an increase in opal accumulation rates during EOIS but also a fall shortly after around 33.5 Ma, as well as a rise in reactive phosphorus concentrations (itself a proxy for organic carbon burial) at ca. 33.25 Ma after a minimum during the EOT (Anderson and Delaney, 2005). As another example, opal accumulation rates declined following benthic $\delta^{13}C$ decreases at Site 744 in the Southern Ocean in the Indian sector at the end of the EOT to ca. 33.0 Ma (Salamy and Zachos, 1999). On the other hand, it is also reported that Southern high latitude net productivity and export was at least sustained until the end of the EOGM (ca. 33.15 Ma), after the positive benthic $\delta^{13}C$ excursion had ended (Coxall and Pearson, 2007). This difference can lead to confusion that possibly originates in equating opal accumulation rates as a proxy for organic carbon export and burial, while the two differ (Anderson and Delaney, 2005). Standard LOSCAR does not include a proper diatom and subsequent opal production modelling component, but, speculatively, it could be that opal production and diatom populations played a role in the temporary benthic $\delta^{13}C$ record, as the silicate and (organic) carbon cycles are interconnected (e.g. Heinze et al., 1999).

All in all, the temporary positive benthic $\delta^{13}C$ excursion remains somewhat elusive, and more research is needed into the transient response of the weathering pulse and biological productivity during and after the EOT.

5.1.3. Atmospheric pCO_2

Regarding atmospheric pCO_2 output, the ISW and CFW scenarios show the best fit with atmospheric pCO_2 declines, with silicate weathering playing the most important role in this, as evidenced by the strong response of atmospheric pCO_2 with increased silicate weathering in the ISW scenario. Therefore, the ISW and CFW scenarios imply the importance of (increased) silicate weathering as a means to reach sufficient low atmospheric pCO_2 for a potential Antarctic glaciation. While atmospheric pCO_2 trajectories for the IBV, IHBP and IOV scenarios show a relatively quick recovery after the decline associated with EOIS, CFW and especially ISW do not. This has to do with the restoration time of silicate weathering after a perturbation, which is much longer than the carbonate one, with silicate weathering returning to steady state on a timescale of 10^5 to 10^6 kyr, present in

LOSCAR (Zeebe, 2012). In this regard, an increase in silicate weathering does fit better in the atmospheric pCO_2 reconstructions (Section 2.2.4) which show a decline in atmospheric pCO_2 continuing for hundreds of thousands of kyr after EOIS, than an increase in biological productivity or ocean ventilation.

A point of contention is about the timing of atmospheric pCO_2 fall, which shows pCO_2 declines up to glaciation threshold level at EOIS, and then a temporary increase to previous values (Pearson et al., 2009). None of the modelled scenarios actually match this timing, with the bulk of the decrease in atmospheric pCO_2 occurring after EOIS, with no temporary increase. pH values, closely related to atmospheric pCO_2 (Pearson et al, 2009), show similar behaviour, with most of the increase of modelled pH levels occurring after EOIS while the pH reconstruction by Pearson et al. (2009) shows most of the increase occurring before EOIS. This offset in timing with reconstructed atmospheric pCO_2 and pH levels has very likely to do with a wrong chosen timing for the tested hypotheses, or a factor not tested/considered in the modelling. For example, ocean ventilation and biological productivity increases could have occurred earlier than modelled, in accordance with Abelson and Erez (2017)'s finding that vertical mixing intensified 100 to 300 kyr before the EOT through a stronger AMOC. High latitude biological productivity exerts a strong impact on atmospheric pCO_2, as evidenced by the IHBP scenario (Section 4.1.3), and could therefore potentially be the trigger for major Antarctic glaciation at EOIS (Straume et al., 2022). Explaining the decline to glaciation threshold levels prior to the EOIS could also entail an increased silicate weathering long before it is implemented in the model runs, for example due to the said intensification of the AMOC (Elsworth et al., 2017). Explaining the rise in reconstructed atmospheric pCO_2 after EOIS is more speculative, however. The issue could lay in the reconstruction of the atmospheric pCO_2 record itself, or through processes such as ocean "venting" as the result of increased ocean overturning (Coxall and Wilson, 2011), although modelled increased ocean ventilation does not show enough of an increase in atmospheric pCO_2 after EOIS (see IOV scenario). Armstrong McKay et al. (2016), which also produced mismatches in the timing of atmospheric pCO_2 rise after EOIS with their modelling, speculate a regional process such as sea ice expansion in the Southern Ocean. Nonetheless, for an answer, more and higher resolution atmospheric pCO_2 records are needed to understand the exact timing and magnitude of atmospheric pCO_2 changes across the EOT.

5.2. Synthesis

Thus far, the modelling of the EOT in LOSCAR yielded several implications: 1. The CCD deepening is primarily the result of a change in shelf-to-basin fractionation and carbonate weathering. 2. The increase in benthic $\delta^{13}C$ in both the Atlantic and the Pacific oceans is primarily the result of increased high latitude biologic productivity and subsequent export to the deep oceans, or the weathering of

significantly $\delta^{13}C$ enriched neritic carbonates (>3.0‰ $\delta^{13}C$). 3. Atmospheric pCO_2 decline across the EOT and after must include enhanced silicate weathering to substantially decrease atmospheric pCO_2 but also to subdue any potential recovery in the long term.

There are problems however with or around these implications, noted in the discussion above: 1. There is criticism about the role of shelf-to-basin carbonate burial fractionation and weathering (more discussion in Section 5.5.2). 2. The temporariness of the positive benthic $\delta^{13}C$ excursion remains elusive, with the cause likely being related to a transient response of (carbonate) weathering pulse or biological productivity across and after the EOT, but these transient responses need (better) constraints. 3. The timing of atmospheric pCO_2 decline and the short temporary increase after EOIS is not matched with the output of the scenarios, with likely the cause laying in the timing/amplitude of mechanisms being wrong or the omission of a different (local) factor.

It is thus a challenge to form a synthesis from the implications and these problems. It could help to first make a synthesis based on the implications alone, and then alter the preliminary synthesis to deal with the problems. Making a synthesis scenario based on the implications alone, results in forming of two possible synthesis scenarios: 1. Shelf-to-basin carbonate burial fractionation change occurred in concert with increased carbonate weathering of exposed neritic shelves, substantially enriched in $\delta^{13}C$ (higher than 3.0‰), or 2. Increased high latitude biological productivity and ocean ventilation are included, at both steps, with lessened carbonate fractionation and weathering change at Step 1. In both, increased silicate weathering should be invoked to properly simulate the atmospheric pCO_2 levels. The rationale of these two "synthesis scenarios" is as follows: 1. The mechanisms included in the first scenario are capable of explaining the CCD data, but with the standard tested $\delta^{13}C$ (+3.0‰) for exposed neritic carbonate shelves the amplitude in increase of benthic $\delta^{13}C$ recorded is not reached. Increasing the amount of carbonate weathering results in too much deepening of the CCD and is therefore unlikely. 2. The IBV scenario is capable of producing the right amplitude in benthic $\delta^{13}C$ increase, but is not adequate enough in replicating the CCD and $CaCO_3$ wt(%) record, and needs a stronger response at Step 1 (by allocating a part of the increase in high latitude biological productivity to Step 1) and (possibly) a (lessened) shelf-to-basin carbonate burial fractionation (and subsequent carbonate weathering) to facilitate the rapidness in two step deepening of CCD.

In essence, the first synthesis scenario is an adapted version of the CFW scenario while the second synthesis scenario is an adapted version of the IBV scenario. To form a final synthesis, these two scenarios should be subjugated to the problems raised. Firstly, if the criticism about shelf-to-basin carbonate burial fractionation and subsequent increased neritic carbonate weathering holds any merit, the first synthesis scenario will be largely debunked and the choice for a lesser fractionation change

in the second synthesis scenario is validated. As said, more discussion about shelf-to-basin carbonate fractionation in LOSCAR is present in Section 5.5.2. Secondly, the temporary positive benthic $\delta^{13}C$ excursion is likely the result of transient behaviour of a mechanism, such as biological productivity or carbonate weathering, during and after the EOT. Therefore, the synthesis scenarios should include such a transient behaviour (by applying a gradual decrease in values after increase), although the exact nature of this transient behaviour is not yet constrained. Thirdly, and lastly, the timing of certain mechanisms should be shifted (compared to how they were implemented in the model set-up) to produce a better fit with the atmospheric pCO_2 and pH records. Considering the implied importance (Section 5.1.3) of silicate weathering, increased silicate weathering should be considered to commence sooner than implemented in the model set-up, following for example Elsworth et al. (2017)'s interpretation of linking the AMOC's intensifying with higher silicate weathering rates (instead of (only) linking silicate weathering with sea level decline as done in the model set-up, see Section 3.6.2.6). Applying an increase in high latitude biological productivity at Step 1 should not only produce a better CCD simulation for the second synthesis, but also further decrease atmospheric pCO_2 after Step 1. It would also follow the hypothesis that ocean ventilation and subsequent increased biological productivity played a role in reaching glaciation threshold values for atmospheric pCO_2 at EOIS (Straume et al., 2022).

Concluding, based on the model output, this study proposes two synthesis scenarios which are good contenders for the course of the EOT. They are adapted versions of the CFW and the AI scenarios, to comply with the issues raised in the Sections above. The first synthesis scenario (adapted from the CFW scenario) assumes a combination of shelf-to-sea carbonate burial change, with increased weathering of neritic carbonate shelves substantially enriched in $\delta^{13}C$ (>3.0‰). To allow for a temporary benthic $\delta^{13}C$ increase, the carbonate weathering pulse should be transient, with a decrease after its initial increase. The second synthesis scenario (adapted from the IBV scenario) includes increased high latitude biological productivity and ocean ventilation, but also a lessened shelf-to-basin carbonate fractionation change and increased carbonate weathering to facilitate the rapidness in the two step deepening of the CCD. Increased high latitude biological productivity should also be present at Step 1, to produce a stronger signal. To reproduce the benthic $\delta^{13}C$ temporary positive excursion, high latitude biological productivity should be transient (increasing and then decreasing). In both synthesis scenarios, increased silicate weathering should occur before the EOT to reach appropriate atmospheric pCO_2 glaciation threshold values (ca. 700 to 800 ppm) before EOIS.

These two synthesis scenarios are viewable in Appendix C, where a short summary regarding their model set-up and results is present. Both offer a good match with proxy records. In essence, the first synthesis scenario follows the conventional shelf-to-basin carbonate burial change hypothesis (e.g. in

Merico et al., 2008; Armstrong McKay et al., 2016), which assumes sea level fall due to cooling and Antarctic glaciation resulted in an increase in weathering and change in carbonate burial. The second synthesis scenario offers an alternative to this conventional hypothesis, and argues that increased organic carbon burial (through increased high latitude biological productivity and export) played a pivotal role in the EOT, with a lesser share of carbonate burial change.

5.3. Role of ocean circulation change

5.3.1. Effect of NADW strengthening in modelling output

In Sections 5.1 and 5.2, one important mechanism present in the modelling was not discussed, namely the role of the NADW. The complexity associated with ocean circulation warrants a separate section for this topic. Regarding the modelling output, by viewing the OCC and the combined scenarios where the role of the NADW was tested, the effect of ocean circulation is most noticeable on the CCD and secondarily on benthic $\delta^{13}C$. On the other hand, atmospheric pCO_2 does not seem to change much depending on the strength of the NADW, at most differing with ca. 20 ppm. A strengthening of the NADW favours CCD deepening in the Atlantic and Indian oceans over the Pacific (with up to 700 meters extra deepening under a strong NADW compared to a permanent SODW ocean circulation state), which is more discussed in detail in next Section. Viewing benthic $\delta^{13}C$ output, a strengthening of the NADW results in a further enrichment in benthic $\delta^{13}C$. Interestingly, a strong NADW (four times as strong as SODW formation) results in a stronger enrichment in benthic $\delta^{13}C$ than under a permanent SODW, but less so than under a NADW equal in strength to the SODW and even a weak NADW (four times as weak as SODW formation). This stronger enrichment is in the order of 0.1 to 0.25‰, depending on the strength of the NADW. An explanation for this non-linear behaviour of the strength of the NADW on Atlantic and Pacific benthic $\delta^{13}C$ is as follows: the Northern high latitude box is initially, under a SODW mode of circulation, highly enriched in $\delta^{13}C$ (Fig. 7). Under a stronger NADW cell, this $\delta^{13}C$ becomes less as DIC-^{13}C from it is distributed to the oceans, and with a subsequent weakened SODW cell, the Southern high latitude box becomes more enriched in $\delta^{13}C$. Eventually, when the NADW and SODW circulation cells are equal in strength, the $\delta^{13}C$ of both high latitude boxes are about equal (Section 3.3.2). If the NADW cell becomes even stronger, the Southern high latitude box will eclipse the Northern high latitude box in $\delta^{13}C$. This will result in a relatively lessened DIC-^{13}C flow to the oceans, as the main deep water source (the Northern high latitude box) contains a lighter $\delta^{13}C$ than the deep water source it replaces (the Southern high latitude box).

However, one should be careful with interpreting the role of the NADW based on the model output alone. This will be elaborated in the following Section 5.3.2, Section 5.3.3 and in Section 5.5.1.

5.3.2. Stronger Atlantic and Indian CCD deepening

The stronger deepening in Atlantic and Indian CCDs (compared to the Pacific CCD) under the influence of the NADW can be explained based on a change in fluxes. Fluxes per sea water volume (such as of carbonate weathering and high latitude organic carbon export, but also fluxes associated with ocean circulation) are depended in LOSCAR on the size of the reservoir, read box. The Atlantic and Indian ocean boxes are significantly smaller than the Pacific ocean box: Atlantic and Indian oceans represent together 35% of the ocean surface compared to 50% for the Pacific, in the LOSCAR version used in the study. As a reduction in SODW strength will mean an equal increase in NADW strength (Section 3.6.2.1), the extra increase in thermohaline flow into the deep Atlantic is compensated by reduced thermohaline flows into the deep Pacific, Indian and Atlantic oceans. This entails that the same flux that entered the Pacific, Indian and Atlantic is now distributed over a smaller, Atlantic volume. The fluxes are kept in balance through a lessened deep water flow to the Pacific and a stronger intermediate flow back to the deep Atlantic and Northern high latitude box. This produces an imbalance in tracer concentrations in the (deep) Atlantic, such as of $[CO_3^-]$, apparently increasing the saturation state of carbonate and deepening the CCD. As this version of LOSCAR uses two high latitude boxes instead of one, it is not entirely as simple as this, as the two high latitude boxes, from which deep water formation sources its tracers from, can differ in tracer concentrations. However, tracer concentrations are in (SODW) steady state roughly equal between the two (Section 3.3.2).

The stronger deepening in CCD as the result of the modelled NADW inclusion into the ocean circulation is not necessarily indicative of the hypothetical effect of NADW on Atlantic and Indian CCD. There are four reasons for this. Firstly, already touched upon, the geochemical tracer concentrations of the deep water fluxes into the deep Atlantic depend on the tracer concentrations of the Northern high latitude box, which as a simplification were made similar to those of the Southern high latitude box. Secondly, the timing of ocean circulation change is debatable, as elaborated in Section 2.1.3. For example, Abelson and Erez (2017) hypothesise, based on Southern Atlantic vertical $\delta^{13}\mathrm{C}$ gradients, an interhemispheric AMOC connection roughly 300 to 100 kyr before the onset of the EOT. Therefore, ocean circulation change could have already occurred before the EOT. A switch to a NADW based ocean circulation could very well have a positive deepening effect on Atlantic CCD, but this might be spread over a longer time and well before (or after) the EOT. Thirdly, a reduction in SODW strength would not necessarily meet with an instant subsequent (equal) strengthening in NADW, and this simplification used in this study can lead to confusion. Lastly, and following up on the third point, is that the modelled ocean circulation change in this study and in LOSCAR in general is statically determined, as well as parameters effected by ocean circulation such as temperature and salinity

which play a role in carbonate saturation state (Zeebe, 2012; Mucci, 1983). This will be discussed in greater detail in Section 5.5.1.

5.3.3. Interpreting ocean circulation change in a "cascading tipping" framework

A research question (Section 1.2) pertained to the role ocean circulation change could have played in carbon cycle perturbations during the EOT. The idea behind it is that ocean circulation change, although not directly related to the carbon cycle, exerts influence on the carbon cycle by enabling a "cascading tipping", a change in background state of different subsystems such as of the carbon cycle (Dekker et al., 2018). The OCC scenario, which only tested a simplified ocean circulation change, is itself not representative of actual ocean circulation change because of several issues. One of these issues is the flux balance that is disturbed in LOSCAR by such a change, mentioned in Section 5.3.2. A larger issue, discussed in Section 5.5.1, is the fact that ocean circulation change in LOSCAR is not dynamic and coupled with other mechanisms. Therefore, other scenarios need to be considered if one wants to assess the role of ocean circulation change on the carbon cycle during the EOT.

In LOSCAR, ocean ventilation/mixing and ocean circulation are not directly coupled. The strengthening of the AMOC and subsequently NADW formation is however hypothesised to have resulted in increased ventilation (e.g. Abelson and Erez, 2017; Straume et al., 2022). Mixing is also essential to an overturning circulation and depends on the temperatures and salinities of the different depths in the ocean (Vallis, 2012), which would, quite likely, change with an overturning circulation switch. The IOV and IBV scenarios simulated increased ocean ventilation and therefore offer an insight into the potential of increased ocean ventilation by the hands of a switch in overturning circulation. In Section 5.2, a synthesis scenario suggested to be a good contender for the course of the EOT was formed, which included increased ocean ventilation and biological productivity at Step 1. In the framework of a "cascading tipping" due to ocean circulation change, this synthesis scenario can be interpreted as following: a change in ocean circulation, and subsequent strengthening of the NADW, invokes a stronger ocean ventilation, which in its turn increases biological productivity by enhancing nutrient upwelling. Through the biological pump, atmospheric pCO_2 declines and reaches Antarctic glaciation threshold levels, allowing Antarctic glaciation. Antarctic glaciation further enhances ocean ventilation through salt rejection, as well as biological productivity by physical weathering of Antarctica and subsequent nutrient flow to the ocean.

Ocean circulation change is hypothesised to be synchronous with Southern high latitude cooling during the EOT (Tigchelaar et al., 2011), favouring ice growth and subsequent sea level fall. Sea level fall is in its turn linked to the carbon cycle perturbations during the EOT through shelf-to-basin carbonate burial fractionation change (e.g. Merico et al., 2008). In standard LOSCAR, sea level fall is not modelled, and therefore a coupling between ocean circulation change and shelf-to-basin

carbonate burial fractionation lacks. Such a coupling would depend on how sea ice and subsequent induced sea level fall and fractionation change are parameterised. Nevertheless, the CFW and the first synthesis scenarios can offer insight to the potential of sea level fall by ocean circulation change. Again an interpretation can be made, based on the framework of cascading tipping. An induced Southern high latitude cooling due to ocean circulation change could have increased ice growth on Antarctica, resulting in falling eustatic sea levels. This decline in sea levels would favour a shelf-to-basin carbonate burial fractionation change, as shelves became exposed. Through increased carbonate and silicate weathering, atmospheric pCO_2 was taken up and Antarctic glaciation threshold levels could be reached. Antarctic glaciation further increased carbonate burial fractionation change and weathering.

Concluding this Section, modelling of ocean circulation change in LOSCAR proved to be not suitable enough, which limits testing the effect of ocean circulation change on the carbon cycle during the EOT. Nevertheless, in the framework of cascading tipping, the two synthesis scenarios (Section 5.2), which were deemed good contenders for the course of the carbon cycle during the EOT, can be interpreted within the context of an ocean circulation change. Therefore, the synthesis scenarios (Appendix C) offer insight to how these interpretations could unfold. Better modelled ocean circulation is needed to properly test these cascading tipping interpretations, however (see Section 5.5.1). Of importance is that testing the plausibility of the inducing of these two synthesis scenarios by ocean circulation change would largely depend on how the various mechanisms are coupled to ocean circulation.

5.3.4. North Pacific Deep Water formation

One point of discussion of theoretical nature, involves the formation of North Pacific Deep Water (NPDW) in regards to the EOT, instead of NADW formation. The hypothesis that a change in the meridional overturning circulation from a unipolar to bipolar deep water formation explains the oxygen isotope shift at Step 1 (Tigchelaar et al., 2011) does not necessarily involve NADW. Therefore, other Northern deep water formations are of interest. The Pacific Meridional Overturning Circulation (PMOC) was (potentially) active during the EOT, with NPDW formation (Ferreira et al., 2018; Baatsen et al., 2018). In the context of the EOT, the role of the PMOC has been investigated as well (e.g. Su et al., 2018). In LOSCAR, the PMOC is modelled and one of the three meridional overturning circulations present (besides the AMOC and Southern Ocean meridional overturning circulation). The PMOC is modelled as a deep water flow (from the Northern high latitude box) to the deep Pacific, from where deep water flows to the Indian and eventually the Atlantic. Through an intermediate flow, the water returns. In essence, this modelled overturning circulation is similar to the modelled AMOC (Fig. 5) but with the Atlantic and Pacific switched. In regards to Section 5.2.2, this would prevent too much deepening in the Atlantic and Indian CCDs. Investigating the role of PMOC and subsequently the NPDW, has thus potential. It should be done however with appropriate modelling tools (Section 5.5.1).

5.4. Comparison with similar research

Two other studies also investigated various hypotheses as cause for carbon cycle perturbations during the EOT through modelling, namely Merico et al. (2008) and Armstrong McKay et al. (2016). It is thus of interest to compare the results of these two studies with those of this study. Both Merico et al. (2008) and Armstrong McKay et al. (2016) used the same biogeochemical box model, named MTW08 by the latter. It differs from LOSCAR most notably in that it only includes a single ocean, with no ocean circulation component. It does include a more comprehensive silicate cycle, which includes aeolian and hydrothermal transport of silicate and diatom productivity. For a more detailed overview of MTW08, the reader is referred to the supplementary files of both studies.

Merico et al. (2008) highlight the importance of shelf-to-basin carbonate burial fractionation, and regard it as the best hypothesis to explain the EOT. According to them, a sea level fall shifted the locus of carbonate burial from shallow to pelagic areas (99% reduction in shallow areas), with a transient response ("one-off dump") in increase in carbonate weathering (300% increase) through erosion. Armstrong McKay et al. (2016) expanded the MTW08 model to test more hypotheses. They formed two "end-member" scenarios as a best fit for the EOT: 1. A large shelf-to-basin carbonate fractionation change (80% reduction in shelf carbonate burial), with an increased carbonate weathering (100% increase) of highly enriched $\delta^{13}\mathrm{C}$ (+3.0‰), and carbon capacitor storage (in peatlands, tundra, etc.). 2. A lesser enriched neritic carbonate (+1.5‰), but with similar shelf-to-basin carbonate fractionation change, and an increase in ocean ventilation and carbon capacitor storage. It is unclear with how much ocean ventilation and carbon capacitor storage increases in these end-member scenarios.

Both studies therefore view shelf-to-basin carbonate burial fractionation change as the most important hypothesis to explain the EOT. Merico et al. (2008)'s fit and Armstrong McKay et al. (2016)'s first end-member scenario show analogue with the CFW scenario (Section 3.6.3.1), or the first synthesis scenario (Section 5.2). There are two large differences, though. Firstly, the carbonate burial in shallow areas is reduced by a larger margin: 99%/80% reduction versus a two-thirds reduction (FSHLF decline from 4.5 to 1.5). Secondly, the carbonate weathering increase is much larger: a 300%/100% increase versus a 15 to 35% increase (as used in the CFW scenario). Armstrong McKay et al. (2016) themselves state that the 99% reduction in shelf carbonate burial is implausible, with a 80% reduction more in line with Opdyke and Wilkinson (1988)'s reconstruction (50% to 66% decline). The difference in increase in carbonate weathering is even more pronounced. Both studies base the increase on reported increases in carbonate weathering during the Last Glacial Maximum (in the order of 25%) coupled with the higher prevalence of carbonate shelves during the Eocene. An explanation for this pronounced difference is as follows: the initial steady state flux of carbonate weathering in the MTW08 model is significantly higher (ca. 4x) compared to what is used in this study (Table 1), while

the silicate weathering flux is roughly similar. This has primed the MTW08 to a different steady state where flux alterations entail a different response. This follows sensitivity tests that shows MTW08 responding “robustly” to parameter changes (Merico et al., 2008), while the sensitivity study for LOSCAR (Appendix A) showed dramatic changes in say CCD position for changes in carbonate weathering. It shows that parameter changes are highly dependent on the model used, and should not be taken immediately at face value as true paleo-indicators. Merico et al. (2008) and Armstrong McKay et al. (2016) also tested temporary changes in parameter values; carbonate weathering was only temporarily increased. They do not specify the length of this temporariness; if it is relatively short, less than the time needed for the system in LOSCAR to reach equilibrium after a carbonate weathering perturbation, it might also explain the difference.

In regards to the second synthesis scenario formed in Section 5.2, which hypotheses a two-stepped increase in high latitude biological productivity and ocean ventilation to be the main drivers of the EOT, both studies showed less promising results. Merico et al. (2008) did not test biological productivity in concert with ocean ventilation: an efficiency increase in biological productivity did not produce a temporary benthic $\delta^{13}C$ increase, and a temporary increase in efficiency did not produce a permanent CCD deepening. Further, increasing riverine phosphorus run-off did produce a temporary increase in benthic $\delta^{13}C$ but a shallowing in CCD, while a 3.5-fold increase in ocean ventilation produces a temporary CCD deepening and a permanent benthic $\delta^{13}C$ increase. Armstrong McKay et al. (2016) also did not test increased biological productivity and ocean ventilation in concert, as they did not consider it to be a good fit for the paleorecords. Increased biological productivity was simulated in two ways: by increasing the rain ratio of C_{org} to $CaCO_3$, and by increasing organic carbon burial (from an initial 0.1%). The first method could only replicate the benthic $\delta^{13}C$ record if the rain ratio was substantially increased, but it would deepen the CCD with too much, and the rain ratio itself would conflict with paleorecords. The second method leads to a model fail as the carbon output exceeds the carbon input, draining the atmospheric pCO_2. Increasing ocean ventilation showed similar results as Merico et al. (2008).

For a discussion pertaining biological productivity and ocean ventilation in LOSCAR, view Sections 5.5.3 and 5.5.4.

5.5 LOSCAR discussion

5.5.1 Ocean circulation

Ocean circulation is modelled statically in LOSCAR (Zeebe, 2012). Further, temperature and salinity, crucial for thermohaline circulation (Vallis, 2012), are modelled statically as well. This limits testing the hypothesis that ocean circulation change induced cooling at Step 1 which primed Antarctic glaciation (Tigchelaar et al., 2011). To make ocean circulation more dynamic in LOSCAR using a Stommel box (Stommel, 1961), it would require several implementations. Firstly, it would require atmospheric temperatures, which standard LOSCAR lacks, likely over more than one atmospheric box to include latitudinal differences (standard LOSCAR has one atmospheric box, but the box set-up is customisable). Secondly, temperature and salinity need to be dynamical as well: LOSCAR allows the circulation of tracers, where temperature and salinity could be added to, but more formulas (to include the effect of precipitation and atmospheric-sea surface relaxation, among others) are required to simulate better temperature and salinity changes (such as present in Guan and Huang, 2008). Thirdly, there likely needs to be an ice component, which standard LOSCAR lacks, to simulate high latitude salt rejection and cooling during glaciation.

Such inclusion of a Stommel box would make ocean circulation more dynamical (after including a formula determining the relative share of a Northern versus a Southern meridional overturning circulation), but would still be decoupled from ocean ventilation and biological productivity among others in LOSCAR. This would require itself various further implementations (such as in Boot et al., 2021). Instead, this study opted for statically adjusting ocean circulation, and applying a scenario based approach to determine the effect of various hypotheses on the carbon cycle during the EOT. The OCC scenario should therefore be considered in light of the other scenarios, and not alone. If the hypothesis is that ocean circulation change (a strengthening of the AMOC and subsequent NADW) increased ocean ventilation and subsequently increased biological productivity (e.g. Straume et al., 2022), the IBV (Section 3.6.3.2) and the second synthesis scenarios (Section 5.2) should be studied. If the hypothesis is that ocean circulation change induced high latitude cooling and primed Antarctica for glaciation, after which sea level fell and a major shelf-to-basin carbonate burial fractionation occurred, the CFW (Section 3.6.3.1) and the first synthesis scenarios (Section 5.2) should be studied. A dynamic ocean circulation with coupled sea level fall, biological productivity and ocean ventilation, would give better results for the OCC scenario alone, but would also still depend on the parameterisations for the couplings used.

Aside from making the ocean circulation dynamic, the ocean circulation in LOSCAR could be enhanced by adding a Southern Ocean. Standard LOSCAR lacks a Southern Ocean, and intermediate water flows from the Atlantic to the Indian to the Pacific before returning the Southern high latitude box under a

SODW circulation (Fig. 5). A Southern Ocean, which would include an extra intermediate and deep box to LOSCAR (besides the Southern high latitude box which would represent the surface of the Southern Ocean), would allow for an intermediate flow from the three oceans straight to the Southern Ocean. The Southern Ocean acts then as a "mixing" place, interconnecting the Atlantic, Indian and Pacific oceans. It would allow for interesting simulations, such as the role of a strengthening in Antarctic Circumpolar Circulation during the EOT (Goldner et al., 2014), thermally isolating Antarctic and restricting Southern Ocean water flow from and to the Atlantic, Indian and Pacific oceans, and isolating themselves. Further, the role of a strengthened AMOC and subsequent NADW in allowing mixing between the oceans in such an "isolated Southern Ocean" case could be investigated more properly. A Southern Ocean would also present new boxes with different biogeochemical features, allowing for better comparisons with proxies from the Southern Ocean.

5.5.2 Shelf-to-basin carbonate burial fractionation

Although shelf-to-basin carbonate burial fractionation change (with increased carbonate weathering) shows promising results in explaining the course of the CCD during the EOT according to model output (see Section 5.1.1), its role has been called into question (Rea and Lyle, 2005; Miller et al., 2009). The criticism resolves around the increase in pelagic carbonate burial, arguing that sea level fall was too minor during both Step 1 and EOIS for exposing enough shelf carbonates for a ca. 1 kilometer deepening in CCD. Rea and Lyle (2005) estimate a 2.25 times increase in pelagic carbonate accumulation area (or 25% of the Earth's surface), with a CCD deepening of ca. 1 kilometer, while they estimate a sea level fall of about 50 meters would expose only about 3 to 4% of global surface. Therefore, the question arises why LOSCAR, despite the criticism, does show appropriate deepening in CCD with shelf-to-basin carbonate burial fractionation change, and if the mechanism is parameterised correctly through the FSHLF parameter.

A FSHLF decline from 4.5 to 1.5 results in a theoretical increase of about 60% in pelagic carbonate rain (Eq. 13), not including bottom water dissolution changes (Eq. 9), while shelf carbonate rain declines with two-thirds. The average carbonate rain stays the same, with no extra carbonate rain appearing out of thin air as the absolute loss in shelf carbonate rain (48% to 16% of total carbonate rain) is effectively replaced by an increase in pelagic rain (52% to 84%). However, the FSHLF parameter hinges on this mass balance, which is unrealistic: disregarding the possible extra carbonate weathering from exposed shelves, pelagic carbonate rain does not necessarily increase (or enough to compensate) if shelf carbonate rain decreases. Nevertheless, Opdyke and Wilkinson (1988) estimate a roughly two-fold increase in pelagic carbonate accumulation rates from pre-EOT to post-EOT (about 40 Ma to 30 Ma), and Boudreau and Luo (2017)'s pelagic burial reconstructions based on various CCD reconstructions show similar increases. If it is assumed that the increase of 60% in pelagic carbonate

rain is supplied fully by carbonate weathering of exposed shelves, so that it compensates the decline in shelf carbonate rain, carbonate weathering should increase with roughly 85% from the baseline carbonate weathering flux (Table 1). This calculation is based on Eq. 8, 12 and 13, and a low latitude organic carbon export of 18.9 teramoles per year and carbonate weathering flux of 7.323 teramoles per year (Table 1). Shelf-to-basin carbonate burial fractionation change in LOSCAR, through the FSHLF parameter, implicitly assumes thus a (substantial) increase in carbonate weathering to maintain global carbonate rain.

Rea and Lyle (2005) argue that such large (rapid) changes in continental Calcium ion input to the oceans through carbonate weathering (in the order of two-fold or more) are unlikely, and Miller et al. (2009) note that Cretaceous events with similar sea level fall did not include substantial CCD deepenings as during the EOT. The role of shelf-to-basin fractionation change therefore depends on research into weathering rates, and if these rates were tenable, during the EOT.

5.5.3 Biological productivity

Increased (high latitude) biological productivity has a strong impact on especially benthic $\delta^{13}C$ but also CCD position, albeit not rapidly (see IHBP scenario, Section 4.1.3). The second synthesis scenario (Section 5.2) envisions an increase in ventilation and high latitude biological productivity at both Step 1 and EOIS to explain the proxy data, besides a smaller shelf-to-basin carbonate fractionation change. Therefore, a closer look at biological productivity in LOSCAR is warranted.

High latitude biological productivity, or the parameter CBIOH in LOSCAR, creates organic carbon in the high latitude box and exports it to the deep boxes. There it adds to alkalinity, DIC and other tracers. A point of contention however lies in the high latitude box itself. In the LOSCAR version of this study, the origin of high latitude organic carbon export depends on the relative share between NADW and SODW. Under a permanent SODW circulation, all the organic export is created in the Southern high latitude box. Under an equal NADW and SODW strength, both high latitude boxes create an equal amount of organic carbon. This could be an erroneous assumption, as this study only relies on proxies in the Southern Ocean for biological productivity during the EOT (e.g. Diester-Haass and Zahn, 2001). Nevertheless, this issue only really matters for the high latitude boxes, as the export to the deep oceans remains unchanged and is not depended on the ocean circulation mode. For example, a change from permanent SODW to a strong NADW mode of circulation will result in less organic carbon production in the Southern high latitude box and subsequently less take up of phosphate, among others, but the high latitude organic carbon flux to the deep oceans remains similar as it is compensated by a higher organic carbon production in the Northern high latitude box. This sharing between the high latitude boxes in organic carbon production therefore likely does not influence the carbon cycle much, especially considering the two high latitude boxes are similar in size. It does not

make sense however that Northern (Atlantic) high latitude organic carbon production results in a direct organic carbon export to the deep Pacific. This mechanism of organic carbon export will also fail in simulating a potential isolated Southern Ocean.

The modelled increases in high latitude biological productivity show strong impacts on atmospheric pCO_2, [CO_3^-] and pH levels (see Section 4.1.3 and Appendix B). This follows the hypothesis that increased organic carbon sequesters atmospheric pCO_2 ("biological pump") and subsequently increases pH levels and [CO_3^-] concentrations, deepening the CCD (e.g. Merico et al., 2008). Merico et al. (2008) and Armstrong McKay et al. (2016) also tried to simulate this hypothesis (see Section 5.1.3), but not exactly as this study does. Armstrong McKay et al. (2016) did test increased organic carbon burial, but their model resulted in a model fail as more carbon left the system than entered the system. In this study, the "disappearance" of organic carbon that is buried is compensated by a phosphate weathering flux (Section 3.3.1), which reacts on changes in atmospheric pCO_2 through weathering rates (Eq. 11); this keeps the carbon cycle in this version of LOSCAR in balance. In this regard, this study's increased organic carbon burial is better than Armstrong McKay et al. (2016)'s application as it prevents model fail. However, the inclusion of diatom populations and subsequent opal production, which are present in the MTW08 model, would certainly be an enhancement for LOSCAR.

Currently, LOSCAR only uses one proper nutrient, namely phosphate. Adding other nutrients, such as iron and nitrate (e.g. in Boot et al., 2021) and coupling these with biological activity would allow for a better representation. It would open studies on bottlenecking of biological productivity and the role of riverine input of nutrients during the EOT. Lastly, Coxall and Wilson (2011) suggested that, similarly to carbonate shelf-basin fractionation, organic carbon burial should be appropriately distributed among shelves and pelagic areas in models. In this version of LOSCAR, organic carbon is simply removed from each ocean, without regard for areal burial distribution. Komar and Zeebe (2021), using a similar organic carbon burial mechanism as this study, experimented with such organic carbon burial distribution between shelves and pelagic areas, and found that it had negligible effect on model output (see Supplementary information of that paper). This makes sense, as the effect of organic carbon burial on model output is mainly indirect: for benthic $\delta^{13}C$ (DIC), the burial of isotopically light organic carbon, shelf or pelagic, will result in a net enrichment in $\delta^{13}C$ of DIC and through mixing/circulation be spread over the ocean. For CCD output, as formulated in previous paragraph, organic carbon burial, shelf or pelagic, will result in a drawdown of atmospheric pCO_2 to compensate for the carbon sink and deepen the CCD through increased [CO_3^-] concentrations.

5.5.4 Ocean ventilation

Ocean ventilation is hypothesised to deepen the CCD by decreasing deep ocean acidity (e.g. Miller et al., 2009), yet the IOV scenario (Section 4.1.4) shows on short-term (100 to 200 kyr) shallowings in

CCD. This is similar to Armstrong McKay et al. (2016)'s model output which also showed short-term shallowing in CCD with increased ocean ventilation. A possible explanation assumes a pivotal role of "venting"; increased degassing of pCO_2 at the sea surface. A higher ventilation rate will increase the intermediate-to-surface flux, allowing for higher sea surface DIC concentrations and subsequently higher oceanic pCO_2 levels, increasing degassing rate. This causes more carbon to be extracted from the ocean, decreasing DIC and subsequently carbonate saturation state. While increased ocean ventilation does increase biological productivity, which pulls carbon from the atmosphere to the ocean through the biological pump, testing shows that the increase in biological production, initially quite large in magnitude, diminishes very quickly to a much lower magnitude or even lower than initial steady state, possibly because of bottlenecking issues. This results in more carbon leaving the ocean, shallowing the CCD. Eventually, fluxes find balance again, and the impact of increased biological productivity on atmospheric pCO_2 will outweigh the venting of pCO_2. The short-term decline in benthic $\delta^{13}C$ values follows a somewhat different explanation: while increased venting is associated with an increase in surface $\delta^{13}C$ through fractionation processes (e.g. Mook, 1986), the temporary decrease in benthic $\delta^{13}C$ is likely the result of a higher mixing of isotopically light intermediate water $\delta^{13}C$ (Fig. 7) with the surface and deep waters.

5.5.5 Weathering

Carbonate weathering has already been somewhat discussed in Section 5.4, in that LOSCAR is sensitive to carbonate weathering pulses, more so than the MTW08 model used for similar research. A different point of discussion, not mentioned yet, discerns how carbonate (and silicate) weathering are parameterised in LOSCAR. Carbonate and silicate weathering are directly tied down to atmospheric pCO_2 (Eq. 5 and 6), and while used in other models as well, this parameterisation is not necessarily indicative of any actual relationship between atmospheric pCO_2 and weathering rates (Munhoven, 2011). The parameters of n_{cc} and n_{si} in Eq. 5 and 6 respectively, which determine the relative strength of the carbonate and silicate weathering feedback, have also been adjusted to somewhat arbitrary values (Section 3.4.2), and do not necessarily represent the actual strength of the weathering feedback. An additional, minor point concerns the addition of a phosphate weathering flux to LOSCAR, which is tied to the carbonate and silicate weathering fluxes (Eq. 11). With increased carbonate weathering, phosphate weathering increases as well, increasing biological productivity. In essence, the ICW and ISW scenarios thus simulate increased nutrient supply as well, but this relationship with phosphate weathering masks the actual impact of carbonate and silicate weathering alone. This study uses Komar and Zeebe (2017)'s parameterisation of the phosphate weathering flux, while Komar and Zeebe (2021) use a slightly different parameterisation, only involving the (initial) silicate weathering flux to

determine phosphate weathering flux. This latter parameterisation might therefore be better for testing carbonate weathering.

A further discussion point is about silicate weathering. Silicate weathering shows a strong control on atmospheric pCO_2 as it takes up two moles of CO_2 and has a long restoration time (Zeebe, 2012). The ISW scenario is also the only scenario which exhibits long-term declines in benthic $\delta^{13}C$ (Section 4.1.6), evidenced as well in sensitivity study (Appendix A). This is due to this strong control on atmospheric pCO_2, through which large isotopically light carbon from the atmosphere is taken to the ocean (Mook, 1986). Silicate weathering however, has much less effect on CCD (Section 4.1.6). Griffith et al. (2011) invoked silicate weathering as a means of deepening the CCD through an influx of calcium ions, however, there has been criticism regarding this hypothesis (Rea and Lyle, 2005). Rea and Lyle (2005) argue that a several fold increase in calcium ion input must occur to significantly alter the Late Eocene carbon cycle based on calcium residence times, and that such an increase seems implausible. The silicate weathering flux is small in LOSCAR (Table 1), and at most an increase of 40% is tested. This would therefore be not enough to realistically cause large CCD deepenings, which the ISW shows.

5.5.6 Temperature decline

Although not itself a scenario, it is worth discussing the effect of temperature decline on model output as temperature declines are enforced in every scenario. The effect of temperature decline on model output can be best studied observing the permanent SODW variant in the OCC scenario (Section 4.1.1), as this variant can be considered the "null hypothesis" as it only includes temperature declines. In the short-term (100 to 200 kyr), temperature declines (in the order of 2 to 2.5 degrees Celsius per step, see Section 3.6.1) produce CCD shallowings, small benthic $\delta^{13}C$ decreases and interestingly quite large atmospheric pCO_2 declines (ca. 60 ppm). Temperature has a negative correlation with apparent solubility of carbonate (Mucci, 1983), which means that a temperature decline will result in a higher solubility of carbonate and subsequently a decline in carbonate saturation state, shallowing the CCD (Woosley, 2012). The decline in atmospheric pCO_2 is more difficult to explain, but it could be connected to this shallowing of the CCD, as the shallowing of CCD and atmospheric pCO_2 decrease are synchronous. Possibly, sea surface to atmosphere carbon degassing decreases as more DIC can be stored in sea water. Lastly, benthic $\delta^{13}C$ decreases as temperature is positively correlated with $\delta^{13}C$ due to kinetic fractionation (Hesse et al., 2014; Mook, 1986), possibly balanced by said decrease in degassing, which would result in less uptake of isotopically light atmospheric carbon (Mook, 1986).

5.6 Future research

Future research is needed to unearth how weathering and biological productivity exactly developed during and after the EOT. Further, more precise atmospheric pCO_2 records are needed for comparison and in general for a better overview of the EOT. Regarding modelling, an ocean circulation that couples

various mechanisms (such as biological productivity, sea level, etc.) is needed to properly test the viability of ocean circulation change as "igniter" of the two synthesis scenarios. The ocean circulation in LOSCAR can also be enhanced by adding a Southern Ocean. A better biological productivity can also be modelled by including diatom populations and subsequent opal production, as well as more nutrient modelling. More hypotheses could also be tested, such as an increase in the carbon capacitor storage (Armstrong McKay et al., 2016). Other models should also be used to test the two synthesis scenarios, to rule out model-specific problems/sensitivity.

6. Conclusions

Various hypotheses, which try to explain the carbon cycle perturbations which occurred during the EOT, were tested in an adapted version of LOSCAR, a long term carbon ocean-atmosphere partitioning model. The model output contained several implications: firstly, to explain the rapidness and magnitude of CCD deepening and $CaCO_3$ wt(%) change, shelf-to-basin carbonate burial fractionation change and increased carbonate weathering should be invoked. Secondly, to explain the amplitude in benthic $\delta^{13}C$ increase, increased (high latitude) biological productivity and export should occur. Thirdly, to explain a strongly decreased atmospheric pCO_2 (<800 ppm), that stays subdued long after the EOT has ended, increased silicate weathering is needed. Besides these implications, some issues were raised: firstly, the shelf-to-basin carbonate burial fractionation with increased carbonate weathering hypothesis has been criticised, arguing that sea level fall was too minor to cause substantial carbonate weathering increase and subsequent burial fractionation change. Secondly, while scenarios could simulate the amplitude in benthic $\delta^{13}C$ increase, none were capable of simulating a temporary increase. Thirdly, atmospheric pCO_2 is capable of reaching Antarctic glaciation threshold levels (ca. 700 to 800 ppm), but only after EOIS, and not before. To reconcile the implications with these issues, two synthesis scenarios were formed. The first synthesis scenario assumes that shelf-to-basin carbonate burial fractionation change is viable, and includes increased silicate weathering and carbonate weathering significantly enriched in $\delta^{13}C$ (>3.0‰). The extra weathered carbonate follows a transient pattern, and decreases to initial steady state value after EOIS. The second synthesis scenario assumes a pivotal role for organic carbon burial, due to increased high latitude biological productivity and export. To force a more severe response at Step 1, which biological productivity and ocean ventilation fail to do, a (lesser) shelf-to-basin carbonate burial fractionation change is included. After EOIS, (high latitude) biological productivity follows a transient response to decline back to initial steady state levels.

Additionally, the role of ocean circulation on the carbon cycle was explored, and how it fits in the EOT. Ocean circulation change was tested on itself, by strengthening NADW and subsequently weakening SODW, as well as included in the combined scenarios. However, the role of ocean circulation change

is ambiguous and not clear-cut. There are namely several issues, most prominently that ocean circulation change is not dynamic and is not coupled with mechanisms such as ocean ventilation and biological productivity. Therefore, considering the model output, ocean circulation change should not be studied alone, but in light of other scenarios. The two synthesis scenarios were interpreted within a cascading tipping framework, which explains climate transitions through a "domino-effect" between climate subsystems. Ocean circulation change could have induced cooling and primed Antarctic glaciation, resulting in sea level fall and subsequent shelf-to-basin carbonate shelf fractionation change, linking ocean circulation change with synthesis scenario 1. The possible link between ocean circulation change and synthesis scenario 2 involves increased nutrient run-off due to physical weathering at Antarctica. These interpretations of a cascading tipping involving the synthesis scenarios and ocean circulation change remain hypotheses, but offer insight to how ocean circulation change could fit in the course of the EOT.

Future research should include testing the viability of the synthesis scenarios, not only with LOSCAR but also with other models. Including a dynamical ocean with mechanism coupling allows the testing of aforementioned cascading tipping interpretations. More research is also needed to the (possible) transient behaviour of weathering and biological productivity during and after the EOT, as well as the trajectory of atmospheric pCO_2, to enhance proxy record comparison.

Acknowledgments

I would like to thank my supervisors Anna von der Heydt and Lucas Lourens for enabling this thesis and the discussions I had regarding the master thesis. The thesis was originally focussed on ocean circulation change, Anna's expertise, but the focus shifted to a more "Earth Sciences" research on the carbon cycle. Even though it was not Anna's expertise, I would like to thank her for continuing this thesis as I very much enjoyed it. I would also like to thank Margot Cramwinckel for her help regarding LOSCAR, and Richard Zeebe himself for answering my emails. Finally, I'd like to thank my mother for improving the English of the thesis and helping with formatting.

References

Abelson, Meir, and Jonathan Erez. 2017. 'The Onset of Modern-like Atlantic Meridional Overturning Circulation at the Eocene-Oligocene Transition: Evidence, Causes, and Possible Implications for Global Cooling'. *Geochemistry, Geophysics, Geosystems* 18 (6): 2177–99. https://doi.org/10.1002/2017GC006826.

Anderson, L. D., and M. L. Delaney. 2005. 'Middle Eocene to Early Oligocene Paleoceanography from Agulhas Ridge, Southern Ocean (Ocean Drilling Program Leg 177, Site 1090)'. *Paleoceanography* 20 (1). https://doi.org/10.1029/2004PA001043.

Angst, Delphine, Eric Buffetaut, Christophe Lécuyer, and Romain Amiot. 2013. '"Terror Birds" (Phorusrhacidae) from the Eocene of Europe Imply Trans-Tethys Dispersal'. *PLOS ONE* 8 (11): e80357. https://doi.org/10.1371/journal.pone.0080357.

Armstrong McKay, David I., Toby Tyrrell, and Paul A. Wilson. 2016. 'Global Carbon Cycle Perturbation across the Eocene-Oligocene Climate Transition'. *Paleoceanography* 31 (2): 311–29. https://doi.org/10.1002/2015PA002818.

Baatsen, M. L. J., A. S. von der Heydt, M. Kliphuis, J. Viebahn, and H. A. Dijkstra. 2018. 'Multiple States in the Late Eocene Ocean Circulation'. *Global and Planetary Change* 163 (April): 18–28. https://doi.org/10.1016/j.gloplacha.2018.02.009.

Basak, Chandranath, and Ellen E. Martin. 2013. 'Antarctic Weathering and Carbonate Compensation at the Eocene–Oligocene Transition'. *Nature Geoscience* 6 (2): 121–24. https://doi.org/10.1038/ngeo1707.

Berner, Robert A. 1987. 'Models for carbon and sulfur cycles and atmospheric oxygen: Application to Paleozoic geologic history.' Amer. J. Sci. 281, 177-196.

Berner, Robert A., and Donald E. Canfield. 1989. 'A new model for atmospheric oxygen over Phanerozoic time.' *American Journal of Science* 289.4 (1989): 333-361.

Bice, Karen L., and Jochem Marotzke. 2002. 'Could Changing Ocean Circulation Have Destabilized Methane Hydrate at the Paleocene/Eocene Boundary?' *Paleoceanography* 17 (2): 8-1-8–12. https://doi.org/10.1029/2001PA000678.

Bohaty, Steven M., James C. Zachos, and Margaret L. Delaney. 2012. 'Foraminiferal Mg/Ca Evidence for Southern Ocean Cooling across the Eocene–Oligocene Transition'. *Earth and Planetary Science Letters* 317–318 (February): 251–61. https://doi.org/10.1016/j.epsl.2011.11.037.

Boot, Amber, Anna S. von der Heydt, and Henk A. Dijkstra. 2022. 'Effect of the Atlantic Meridional Overturning Circulation on Atmospheric pCO_2 Variations'. *Earth System Dynamics* 13 (3): 1041–58. https://doi.org/10.5194/esd-13-1041-2022.

Borrelli, Chiara, Benjamin S. Cramer, and Miriam E. Katz. 2014. 'Bipolar Atlantic Deepwater Circulation in the Middle-Late Eocene: Effects of Southern Ocean Gateway Openings'. *Paleoceanography* 29 (4): 308–27. https://doi.org/10.1002/2012PA002444.

Boudreau, Bernard P., and Yiming Luo. 2017. 'Retrodiction of Secular Variations in Deep-Sea CaCO3 Burial during the Cenozoic'. *Earth and Planetary Science Letters* 474 (September): 1–12. https://doi.org/10.1016/j.epsl.2017.06.005.

Brennan, Sean T., Tim K. Lowenstein, and Dioni I. Cendón. 2013. 'The Major-Ion Composition of Cenozoic Seawater: The Past 36 Million Years from Fluid Inclusions in Marine Halite'. *American Journal of Science* 313 (8): 713–75. https://doi.org/10.2475/08.2013.01.

Coxall, Helen K., Claire E. Huck, Matthew Huber, Caroline H. Lear, Alba Legarda-Lisarri, Matt O'Regan, Kasia K. Sliwinska, et al. 2018. 'Export of Nutrient Rich Northern Component Water Preceded Early Oligocene Antarctic Glaciation'. *Nature Geoscience* 11 (3): 190–96. https://doi.org/10.1038/s41561-018-0069-9.

Coxall, Helen K., and Paul A. Wilson. 2011. 'Early Oligocene Glaciation and Productivity in the Eastern Equatorial Pacific: Insights into Global Carbon Cycling'. *Paleoceanography* 26 (2). https://doi.org/10.1029/2010PA002021.

Coxall, Helen K., Paul A. Wilson, Heiko Pälike, Caroline H. Lear, and Jan Backman. 2005. 'Rapid Stepwise Onset of Antarctic Glaciation and Deeper Calcite Compensation in the Pacific Ocean'. *Nature* 433 (7021): 53–57. https://doi.org/10.1038/nature03135.

Coxall, Helen, and Paul Pearson. 2007. 'The Eocene-Oligocene Transition'. *Geological Society Special Publication* 2 (January): 351–87.

Cramer, B. S., J. R. Toggweiler, J. D. Wright, M. E. Katz, and K. G. Miller. 2009. 'Ocean Overturning since the Late Cretaceous: Inferences from a New Benthic Foraminiferal Isotope Compilation'. *Paleoceanography* 24 (4). https://doi.org/10.1029/2008PA001683.

DeConto, Robert M., and David Pollard. 2003. 'Rapid Cenozoic Glaciation of Antarctica Induced by Declining Atmospheric CO2'. *Nature* 421 (6920): 245–49. https://doi.org/10.1038/nature01290.

Dekker, Mark M., Anna S. von der Heydt, and Henk A. Dijkstra. 2018. 'Cascading Transitions in the Climate System'. *Earth System Dynamics* 9 (4): 1243–60. https://doi.org/10.5194/esd-9-1243-2018.

Diester-Haass, Liselotte, and Rainer Zahn. 1996. 'Eocene-Oligocene Transition in the Southern Ocean: History of Water Mass Circulation and Biological Productivity'. *Geology* 24 (2): 163–66. https://doi.org/10.1130/0091-7613(1996)024<0163:EOTITS>2.3.CO;2.

Diester-Haass, Liselotte, and Rainer Zahn. 2001. 'Paleoproductivity Increase at the Eocene–Oligocene Climatic Transition: ODP/DSDP Sites 763 and 592'. *Palaeogeography, Palaeoclimatology, Palaeoecology* 172 (1): 153–70. https://doi.org/10.1016/S0031-0182(01)00280-2.

Elderfield, H., J. Yu, P. Anand, T. Kiefer, and B. Nyland. 2006. 'Calibrations for Benthic Foraminiferal Mg/Ca Paleothermometry and the Carbonate Ion Hypothesis'. *Earth and Planetary Science Letters* 250 (3): 633–49. https://doi.org/10.1016/j.epsl.2006.07.041.

Elsworth, Genevieve. 2015. 'Global changes in paleoproductivity, biological export, and deep water oxygenation across the Eocene-Oligocene transition'. McGill University (Canada)

Elsworth, Geneviève, Eric Galbraith, Galen Halverson, and Simon Yang. 2017. 'Enhanced Weathering and CO2 Drawdown Caused by Latest Eocene Strengthening of the Atlantic Meridional Overturning Circulation'. *Nature Geoscience* 10 (3): 213–16. https://doi.org/10.1038/ngeo2888.

Farmer, J. R., J. E. Hertzberg, D. Cardinal, S. Fietz, K. Hendry, S. L. Jaccard, A. Paytan, et al. 2021. 'Assessment of C, N, and Si Isotopes as Tracers of Past Ocean Nutrient and Carbon Cycling'. *Global Biogeochemical Cycles* 35 (7): e2020GB006775. https://doi.org/10.1029/2020GB006775.

Ferreira, David, Paola Cessi, Helen K. Coxall, Agatha de Boer, Henk A. Dijkstra, Sybren S. Drijfhout, Tor Eldevik, et al. 2018. 'Atlantic-Pacific Asymmetry in Deep Water Formation'. *Annual Review of Earth and Planetary Sciences* 46 (1): 327–52. https://doi.org/10.1146/annurev-earth-082517-010045.

Galeotti, Simone, Robert DeConto, Timothy Naish, Paolo Stocchi, Fabio Florindo, Mark Pagani, Peter Barrett, et al. 2016. 'Antarctic Ice Sheet Variability across the Eocene-Oligocene Boundary Climate Transition'. *Science* 352 (6281): 76–80. https://doi.org/10.1126/science.aab0669.

Gasson, E., D. J. Lunt, R. DeConto, A. Goldner, M. Heinemann, M. Huber, A. N. LeGrande, et al. 2014. 'Uncertainties in the Modelled CO_2 Threshold for Antarctic Glaciation'. *Climate of the Past* 10 (2): 451–66. https://doi.org/10.5194/cp-10-451-2014.

Goddéris, Yves, and Michael M Joachimski. 2004. 'Global Change in the Late Devonian: Modelling the Frasnian–Famennian Short-Term Carbon Isotope Excursions'. *Palaeogeography, Palaeoclimatology, Palaeoecology* 202 (3): 309–29. https://doi.org/10.1016/S0031-0182(03)00641-2.

Goldner, A., N. Herold, and M. Huber. 2014. 'Antarctic Glaciation Caused Ocean Circulation Changes at the Eocene–Oligocene Transition'. *Nature* 511 (7511): 574–77. https://doi.org/10.1038/nature13597.

Griffith, Elizabeth M., Adina Paytan, Anton Eisenhauer, Thomas D. Bullen, and Ellen Thomas. 2011. 'Seawater Calcium Isotope Ratios across the Eocene-Oligocene Transition'. *Geology* 39 (7): 683–86. https://doi.org/10.1130/G31872.1.

Guan, Yu Ping, and Rui Xin Huang. 2008. 'Stommel's Box Model of Thermohaline Circulation Revisited—The Role of Mechanical Energy Supporting Mixing and the Wind-Driven Gyration'. *Journal of Physical Oceanography* 38 (4): 909–17. https://doi.org/10.1175/2007JPO3535.1.

Hamon, N., P. Sepulchre, V. Lefebvre, and G. Ramstein. 2013. 'The Role of Eastern Tethys Seaway Closure in the Middle Miocene Climatic Transition (ca. 14 Ma)'. *Climate of the Past* 9 (6): 2687–2702. https://doi.org/10.5194/cp-9-2687-2013.

Heinze, C., E. Maier-Reimer, A. M. E. Winguth, and D. Archer. 1999. 'A Global Oceanic Sediment Model for Long-Term Climate Studies'. *Global Biogeochemical Cycles* 13 (1): 221–50. https://doi.org/10.1029/98GB02812.

Hesse, T., D. Wolf-Gladrow, G. Lohmann, J. Bijma, A. Mackensen, and R. E. Zeebe. 2014. 'Modelling Δ13C in Benthic Foraminifera: Insights from Model Sensitivity Experiments'. *Marine Micropaleontology* 112 (October): 50–61. https://doi.org/10.1016/j.marmicro.2014.08.001.

Heureux, Ana M. C., and Rosalind E. M. Rickaby. 2015. 'Refining Our Estimate of Atmospheric CO2 across the Eocene–Oligocene Climatic Transition'. *Earth and Planetary Science Letters* 409 (January): 329–38. https://doi.org/10.1016/j.epsl.2014.10.036.

Houben, Alexander J. P., Peter K. Bijl, Jörg Pross, Steven M. Bohaty, Sandra Passchier, Catherine E. Stickley, Ursula Röhl, et al. 2013. 'Reorganization of Southern Ocean Plankton Ecosystem at the Onset of Antarctic Glaciation'. *Science* 340 (6130): 341–44. https://doi.org/10.1126/science.1223646.

Houben, Alexander J. P., Caroline A. van Mourik, Alessandro Montanari, Rodolfo Coccioni, and Henk Brinkhuis. 2012. 'The Eocene–Oligocene Transition: Changes in Sea Level, Temperature or Both?' *Palaeogeography, Palaeoclimatology, Palaeoecology*, Cenozoic Evolution of Antarctic Climates, Oceans and Ice Sheets, 335–336 (June): 75–83. https://doi.org/10.1016/j.palaeo.2011.04.008.

Hutchinson, David K., Helen K. Coxall, Daniel J. Lunt, Margret Steinthorsdottir, Agatha M. de Boer, Michiel Baatsen, Anna von der Heydt, et al. 2021. 'The Eocene–Oligocene Transition: A Review of Marine and Terrestrial Proxy Data, Models and Model–Data Comparisons'. *Climate of the Past* 17 (1): 269–315. https://doi.org/10.5194/cp-17-269-2021.

Hutchinson, David K., Helen K. Coxall, Matt O'Regan, Johan Nilsson, Rodrigo Caballero, and Agatha M. de Boer. 2019. 'Arctic Closure as a Trigger for Atlantic Overturning at the Eocene-Oligocene Transition'. *Nature Communications* 10 (1): 3797. https://doi.org/10.1038/s41467-019-11828-z.

Katz, Miriam E., Benjamin S. Cramer, J. R. Toggweiler, Gar Esmay, Chengjie Liu, Kenneth G. Miller, Yair Rosenthal, Bridget S. Wade, and James D. Wright. 2011. 'Impact of Antarctic Circumpolar Current Development on Late Paleogene Ocean Structure'. *Science* 332 (6033): 1076–79. https://doi.org/10.1126/science.1202122.

Katz, Miriam E., Kenneth G. Miller, James D. Wright, Bridget S. Wade, James V. Browning, Benjamin S. Cramer, and Yair Rosenthal. 2008. 'Stepwise Transition from the Eocene Greenhouse to the Oligocene Icehouse'. *Nature Geoscience* 1 (5): 329–34. https://doi.org/10.1038/ngeo179.

Keir, Robin S. 1982. 'Dissolution of calcite in the deep-sea; theoretical prediction for the case of uniform size particles settling into a well-mixed sediment.' *American Journal of Science* 282.3: 193-236.

Kennedy, A. T., A. Farnsworth, D. J. Lunt, C. H. Lear, and P. J. Markwick. 2015. 'Atmospheric and Oceanic Impacts of Antarctic Glaciation across the Eocene–Oligocene Transition'. *Philosophical Transactions of the Royal Society A: Mathematical, Physical and Engineering Sciences* 373 (2054): 20140419. https://doi.org/10.1098/rsta.2014.0419.

Kobayashi, Hidetaka, Ayako Abe-Ouchi, and Akira Oka. 2015. 'Role of Southern Ocean Stratification in Glacial Atmospheric CO2 Reduction Evaluated by a Three Dimensional Ocean General Circulation Model'. Paleoceanography 30, no. 9: 1202–16. https://doi.org/10.1002/2015PA002786.

Kocken, Ilja J., Margot J. Cramwinckel, Richard E. Zeebe, Jack J. Middelburg, and Appy Sluijs. 2019. 'The 405 Kyr and 2.4 Myr Eccentricity Components in Cenozoic Carbon Isotope Records'. *Climate of the Past* 15 (1): 91–104. https://doi.org/10.5194/cp-15-91-2019.

Komar, Nemanja, and Richard E. Zeebe. 2017. 'Redox-Controlled Carbon and Phosphorus Burial: A Mechanism for Enhanced Organic Carbon Sequestration during the PETM'. *Earth and Planetary Science Letters* 479 (December): 71–82. https://doi.org/10.1016/j.epsl.2017.09.011.

Komar, Nemanja, and Richard E. Zeebe. 2021. 'Reconciling Atmospheric CO2, Weathering, and Calcite Compensation Depth across the Cenozoic'. *Science Advances* 7 (4): eabd4876. https://doi.org/10.1126/sciadv.abd4876.

Kump, Lee R. 1991. 'Interpreting Carbon-Isotope Excursions: Strangelove Oceans'. *Geology* 19 (4): 299–302. https://doi.org/10.1130/0091-7613(1991)019<0299:ICIESO>2.3.CO;2.

Lauretano, Vittoria, Alan T. Kennedy-Asser, Vera A. Korasidis, Malcolm W. Wallace, Paul J. Valdes, Daniel J. Lunt, Richard D. Pancost, and B. David A. Naafs. 2021. 'Eocene to Oligocene Terrestrial

Southern Hemisphere Cooling Caused by Declining PCO2'. *Nature Geoscience* 14 (9): 659–64. https://doi.org/10.1038/s41561-021-00788-z.

Lear, Caroline H., Trevor R. Bailey, Paul N. Pearson, Helen K. Coxall, and Yair Rosenthal. 2008. 'Cooling and Ice Growth across the Eocene-Oligocene Transition'. *Geology* 36 (3): 251–54. https://doi.org/10.1130/G24584A.1.

Lear, Caroline H., Elaine M. Mawbey, and Yair Rosenthal. 2010. 'Cenozoic Benthic Foraminiferal Mg/Ca and Li/Ca Records: Toward Unlocking Temperatures and Saturation States'. *Paleoceanography* 25 (4). https://doi.org/10.1029/2009PA001880.

Lisiecki, Lorraine E., and Maureen E. Raymo. 2005. 'A Pliocene-Pleistocene Stack of 57 Globally Distributed Benthic Δ18O Records'. *Paleoceanography* 20 (1). https://doi.org/10.1029/2004PA001071.

Liu, Zhonghui, Mark Pagani, David Zinniker, Robert DeConto, Matthew Huber, Henk Brinkhuis, Sunita R. Shah, R. Mark Leckie, and Ann Pearson. 2009. 'Global Cooling During the Eocene-Oligocene Climate Transition'. *Science* 323 (5918): 1187–90. https://doi.org/10.1126/science.1166368.

Menard, Henry W., and Stuart M. Smith. 1966. 'Hypsometry of ocean basin provinces.' *Journal of Geophysical Research* 71.18: 4305-4325.

Merico, Agostino, Toby Tyrrell, and Paul A. Wilson. 2008. 'Eocene/Oligocene Ocean de-Acidification Linked to Antarctic Glaciation by Sea-Level Fall'. *Nature* 452 (7190): 979–82. https://doi.org/10.1038/nature06853.

Miller, Kenneth G., James V. Browning, W. John Schmelz, Robert E. Kopp, Gregory S. Mountain, and James D. Wright. 2020. 'Cenozoic Sea-Level and Cryospheric Evolution from Deep-Sea Geochemical and Continental Margin Records'. *Science Advances* 6 (20): eaaz1346. https://doi.org/10.1126/sciadv.aaz1346.

Miller, Kenneth G., James D. Wright, Miriam E. Katz, Bridget S. Wade, James V. Browning, Benjamin S. Cramer, and Yair Rosenthal. 2009. 'Climate Threshold at the Eocene-Oligocene Transition: Antarctic Ice Sheet Influence on Ocean Circulation', April. https://doi.org/10.1130/2009.2452(11).

Mook, W. G. 1986. '13C in Atmospheric CO2'. *Netherlands Journal of Sea Research* 20 (2): 211–23. https://doi.org/10.1016/0077-7579(86)90043-8.

Moore Jr., T. C., Bridget S. Wade, Thomas Westerhold, Andrea M. Erhardt, Helen K. Coxall, Jack Baldauf, and Meghan Wagner. 2014. 'Equatorial Pacific Productivity Changes near the Eocene-Oligocene Boundary'. *Paleoceanography* 29 (9): 825–44. https://doi.org/10.1002/2014PA002656.

Mucci, A. 1983. 'The solubility of calcite and aragonite in seawater at various salinities, temperatures, and one atmosphere total pressure', Am. J. Sci., 283, 780–799.

Munhoven, G. 2011. 'Interactive Comment on "LOSCAR: Long-Term Ocean-Atmosphere-Sediment CArbon Cycle Reservoir Model" by R. E. Zeebe'. *Discussion Paper*, 15.

O'Brien, Charlotte L., Matthew Huber, Ellen Thomas, Mark Pagani, James R. Super, Leanne E. Elder, and Pincelli M. Hull. 2020. 'The Enigma of Oligocene Climate and Global Surface Temperature Evolution'. *Proceedings of the National Academy of Sciences* 117 (41): 25302–9. https://doi.org/10.1073/pnas.2003914117.

Opdyke, Bradley N., and Bruce H. Wilkinson. 1988. 'Surface Area Control of Shallow Cratonic to Deep Marine Carbonate Accumulation'. *Paleoceanography* 3 (6): 685–703. https://doi.org/10.1029/PA003i006p00685.

Pälike, Heiko, Mitchell W. Lyle, Hiroshi Nishi, Isabella Raffi, Andy Ridgwell, Kusali Gamage, Adam Klaus, et al. 2012. 'A Cenozoic Record of the Equatorial Pacific Carbonate Compensation Depth'. *Nature* 488 (7413): 609–14. https://doi.org/10.1038/nature11360.

Pälike, Heiko, Richard D. Norris, Jens O. Herrle, Paul A. Wilson, Helen K. Coxall, Caroline H. Lear, Nicholas J. Shackleton, Aradhna K. Tripati, and Bridget S. Wade. 2006. 'The Heartbeat of the Oligocene Climate System'. *Science* 314 (5807): 1894–98. https://doi.org/10.1126/science.1133822.

Pearson, Paul N., Gavin L. Foster, and Bridget S. Wade. 2009. 'Atmospheric Carbon Dioxide through the Eocene–Oligocene Climate Transition'. *Nature* 461 (7267): 1110–13. https://doi.org/10.1038/nature08447.

Peck, V. L., J. Yu, S. Kender, and C. R. Riesselman. 2010. 'Shifting Ocean Carbonate Chemistry during the Eocene-Oligocene Climate Transition: Implications for Deep-Ocean Mg/Ca Paleothermometry'. *Paleoceanography* 25 (4). https://doi.org/10.1029/2009PA001906.

Penman, Donald E., and James C. Zachos. 2018. 'New Constraints on Massive Carbon Release and Recovery Processes during the Paleocene-Eocene Thermal Maximum'. *Environmental Research Letters* 13 (10): 105008. https://doi.org/10.1088/1748-9326/aae285.

Plancq, Julien, Emanuela Mattioli, Bernard Pittet, Laurent Simon, and Vincent Grossi. 2014. 'Productivity and Sea-Surface Temperature Changes Recorded during the Late Eocene–Early Oligocene at DSDP Site 511 (South Atlantic)'. *Palaeogeography, Palaeoclimatology, Palaeoecology* 407 (August): 34–44. https://doi.org/10.1016/j.palaeo.2014.04.016.

Ploeg, Robin van der, Bernard P. Boudreau, Jack J. Middelburg, and Appy Sluijs. 2019. 'Cenozoic Carbonate Burial along Continental Margins'. *Geology* 47 (11): 1025–28. https://doi.org/10.1130/G46418.1.

Pusz, A. E., R. C. Thunell, and K. G. Miller. 2011. 'Deep Water Temperature, Carbonate Ion, and Ice Volume Changes across the Eocene-Oligocene Climate Transition'. *Paleoceanography* 26 (2). https://doi.org/10.1029/2010PA001950.

Rea, David K., and Mitchell W. Lyle. 2005. 'Paleogene Calcite Compensation Depth in the Eastern Subtropical Pacific: Answers and Questions'. *Paleoceanography* 20 (1). https://doi.org/10.1029/2004PA001064.

Rohling, Eelco J., Jimin Yu, David Heslop, Gavin L. Foster, Bradley Opdyke, and Andrew P. Roberts. 2021. 'Sea Level and Deep-Sea Temperature Reconstructions Suggest Quasi-Stable States and Critical Transitions over the Past 40 Million Years'. *Science Advances* 7 (26): eabf5326. https://doi.org/10.1126/sciadv.abf5326.

Rynders, Stefanie. 2013. 'Ocean circulation and carbon cycles changes around the Eocene-Oligocene boundary'. Master thesis, *Utrecht University*

Salamy, Karen A., and James C. Zachos. 1999. 'Latest Eocene–Early Oligocene Climate Change and Southern Ocean Fertility: Inferences from Sediment Accumulation and Stable Isotope Data'. *Palaeogeography, Palaeoclimatology, Palaeoecology* 145 (1): 61–77. https://doi.org/10.1016/S0031-0182(98)00093-5.

Sigman, Daniel M., Daniel C. McCorkle, and William R. Martin. 1998. 'The Calcite Lysocline as a Constraint on Glacial/Interglacial Low-Latitude Production Changes'. *Global Biogeochemical Cycles* 12 (3): 409–27. https://doi.org/10.1029/98GB01184.

Stommel, Henry. 1961. 'Thermohaline Convection with Two Stable Regimes of Flow'. *Tellus* 13 (2): 224–30. https://doi.org/10.1111/j.2153-3490.1961.tb00079.x.

Straume, E. O., C. Gaina, S. Medvedev, and K. H. Nisancioglu. 2020. 'Global Cenozoic Paleobathymetry with a Focus on the Northern Hemisphere Oceanic Gateways'. *Gondwana Research* 86 (October): 126–43. https://doi.org/10.1016/j.gr.2020.05.011.

Straume, Eivind O., Aleksi Nummelin, Carmen Gaina, and Kerim H. Nisancioglu. 2022. 'Climate Transition at the Eocene–Oligocene Influenced by Bathymetric Changes to the Atlantic–Arctic Oceanic Gateways'. *Proceedings of the National Academy of Sciences* 119 (17): e2115346119. https://doi.org/10.1073/pnas.2115346119.

Su, Baohuang, Dabang Jiang, Ran Zhang, Pierre Sepulchre, and Gilles Ramstein. 2018. 'Difference between the North Atlantic and Pacific Meridional Overturning Circulation in Response to the Uplift of the Tibetan Plateau'. *Climate of the Past* 14 (6): 751–62. https://doi.org/10.5194/cp-14-751-2018.

Suess, Erwin. 1980. 'Particulate Organic Carbon Flux in the Oceans—Surface Productivity and Oxygen Utilization'. *Nature* 288 (5788): 260–63. https://doi.org/10.1038/288260a0.

Swart, Peter K., and Gregor Eberli. 2005. 'The Nature of the Δ13C of Periplatform Sediments: Implications for Stratigraphy and the Global Carbon Cycle'. *Sedimentary Geology*, Sedimentology in the 21st Century - A Tribute to Wolfgang Schlager, 175 (1): 115–29. https://doi.org/10.1016/j.sedgeo.2004.12.029.

Thunell, Robert C., and Bruce H. Corliss. 1986. 'Late Eocene-Early Oligocene Carbonate Sedimentation in the Deep Sea'. In *Developments in Palaeontology and Stratigraphy*, edited by Ch. Pomerol and I. Premoli-Silva, 9:363–80. Termbal Eocene Events. Elsevier. https://doi.org/10.1016/S0920-5446(08)70140-7.

Tigchelaar, M., A. S. von der Heydt, and H. A. Dijkstra. 2011. 'A New Mechanism for the Two-Step δ^{18}O Signal at the Eocene-Oligocene Boundary'. *Climate of the Past* 7 (1): 235–47. https://doi.org/10.5194/cp-7-235-2011.

Torres, Mark A., Nils Moosdorf, Jens Hartmann, Jess F. Adkins, and A. Joshua West. 2017. 'Glacial Weathering, Sulfide Oxidation, and Global Carbon Cycle Feedbacks'. *Proceedings of the National Academy of Sciences* 114 (33): 8716–21. https://doi.org/10.1073/pnas.1702953114.

Uchikawa, Joji, and Richard E. Zeebe. 2008. 'Influence of Terrestrial Weathering on Ocean Acidification and the next Glacial Inception'. *Geophysical Research Letters* 35 (23). https://doi.org/10.1029/2008GL035963.

Vallis, Geoffrey K. 2012. 'Climate and the Oceans'. *Primers in Climate by Princeton University Press.*

Van Andel, Tjeerd H. 1975. 'Mesozoic/Cenozoic Calcite Compensation Depth and the Global Distribution of Calcareous Sediments'. *Earth and Planetary Science Letters* 26 (2): 187–94. https://doi.org/10.1016/0012-821X(75)90086-2.

Wade, Bridget S., James F. O'Neill, Chawisa Phujareanchaiwon, Imran Ali, Mitchell Lyle, and Jakub Witkowski. 2020. 'Evolution of Deep-Sea Sediments across the Paleocene-Eocene and Eocene-Oligocene Boundaries'. *Earth-Science Reviews* 211 (December): 103403. https://doi.org/10.1016/j.earscirev.2020.103403.

Westerhold, Thomas, Norbert Marwan, Anna Joy Drury, Diederik Liebrand, Claudia Agnini, Eleni Anagnostou, James S. K. Barnet, et al. 2020. 'An Astronomically Dated Record of Earth's Climate and Its Predictability over the Last 66 Million Years'. *Science* 369 (6509): 1383–87. https://doi.org/10.1126/science.aba6853.

Wefer, G., W.H. Berger, J. Bijma, and G. Fischer. 1999. 'Clues to Ocean History: A Brief Overview of Proxies'. Paleoceanography, https://doi.org/10.1007/978-3- 642-58646-0_1

Woosley, Ryan. 2016. 'Carbonate Compensation Depth'. In *Encyclopedia of Earth Sciences Series*. https://doi.org/10.1007/978-3-319-39193-9_85-1.

Zachos, James C., and Lee R. Kump. 2005. 'Carbon Cycle Feedbacks and the Initiation of Antarctic Glaciation in the Earliest Oligocene'. *Global and Planetary Change* 47 (1): 51–66. https://doi.org/10.1016/j.gloplacha.2005.01.001.

Zeebe, R. E. 2012. 'LOSCAR: Long-Term Ocean-Atmosphere-Sediment CArbon Cycle Reservoir Model v2.0.4'. *Geoscientific Model Development* 5 (1): 149–66. https://doi.org/10.5194/gmd-5-149-2012.

Zhang, Z., K. H. Nisancioglu, F. Flatøy, M. Bentsen, I. Bethke, and H. Wang. 2011. 'Tropical Seaways Played a More Important Role than High Latitude Seaways in Cenozoic Cooling'. *Climate of the Past* 7 (3): 801–13. https://doi.org/10.5194/cp-7-801-2011.

Appendix A: Sensitivity study

The sensitivity study was performed on every mechanism invoked in the main study. The output was retrieved 250 kyr after perturbation (roughly the time between Step 1 and EOIS), instead of to equilibrium, to get a more transient picture of LOSCAR's response. Each sensitivity run was run from initial Late Eocene steady state as described in the main study. To test the effect of a strong NADW (and weak SODW), the system was also run to equilibrium with a prescribed strong NADW and weak SODW. From here, the sensitivity study was repeated. Note however that the Northern Component Water (NCW) circulation cell was not added in the sensitivity study, to view the severity of circulation change on output parameters.

The sensitivity study output is divided per model output and not per mechanism.

Atlantic CCD

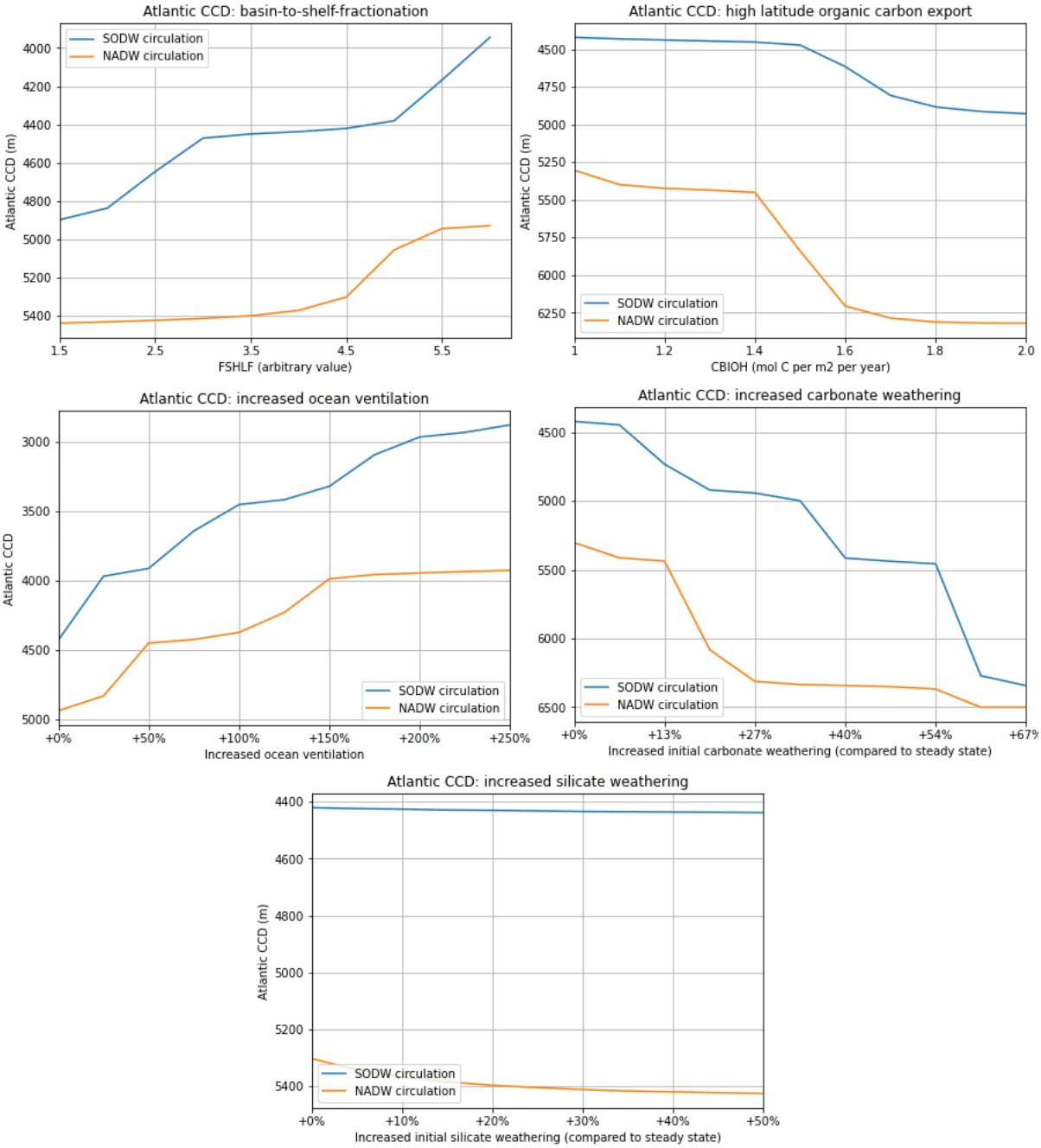

Indian CCD

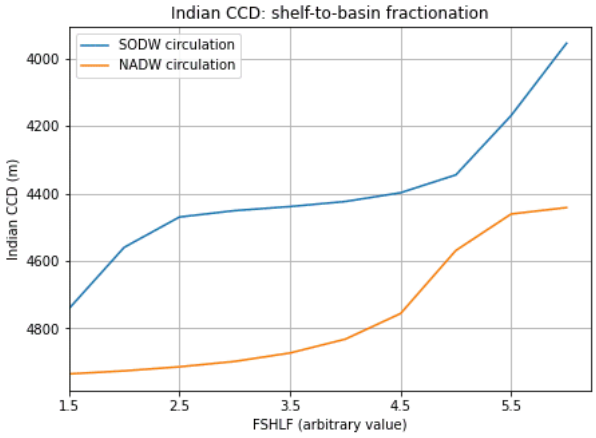
Indian CCD: shelf-to-basin fractionation
SODW circulation
NADW circulation
Indian CCD (m)
4000
4200
4400
4600
4800
1.5
2.5
3.5
4.5
5.5
FSHLF (arbitrary value)

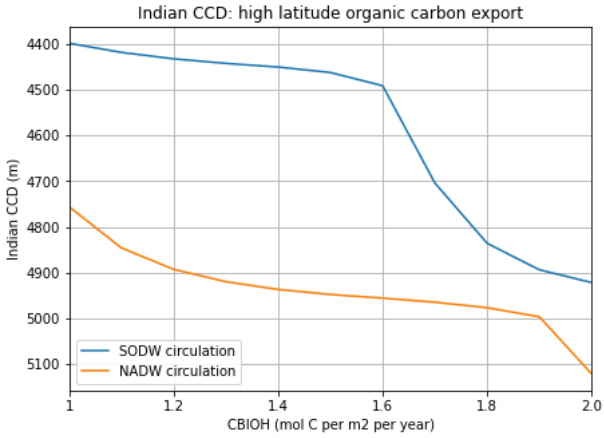
Indian CCD: high latitude organic carbon export
Indian CCD (m)
4400
4500
4600
4700
4800
4900
5000
5100
SODW circulation
NADW circulation
1
1.2
1.4
1.6
1.8
2.0
CBIOH (mol C per m2 per year)

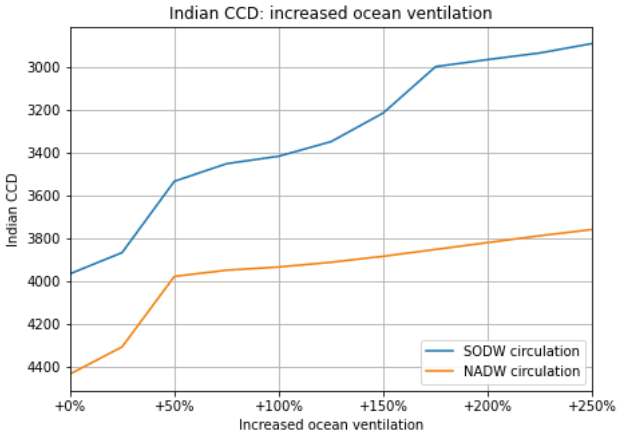
Indian CCD: increased ocean ventilation
Indian CCD
3000
3200
3400
3600
3800
4000
4200
4400
SODW circulation
NADW circulation
+0%
+50%
+100%
+150%
+200%
+250%
Increased ocean ventilation

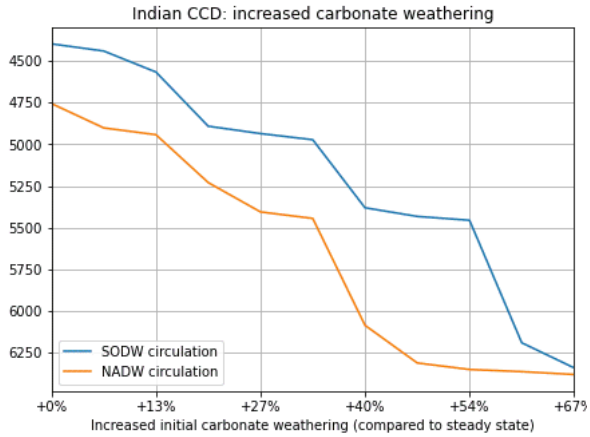
Indian CCD: increased carbonate weathering
4500
4750
5000
5250
5500
5750
6000
6250
SODW circulation
NADW circulation
+0%
+13%
+27%
+40%
+54%
+67%
Increased initial carbonate weathering (compared to steady state)

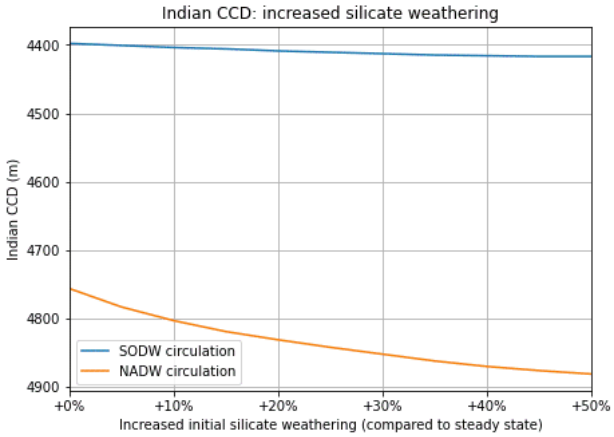
Indian CCD: increased silicate weathering
Indian CCD (m)
4400
4500
4600
4700
4800
4900
SODW circulation
NADW circulation
+0%
+10%
+20%
+30%
+40%
+50%
Increased initial silicate weathering (compared to steady state)

Pacific CCD

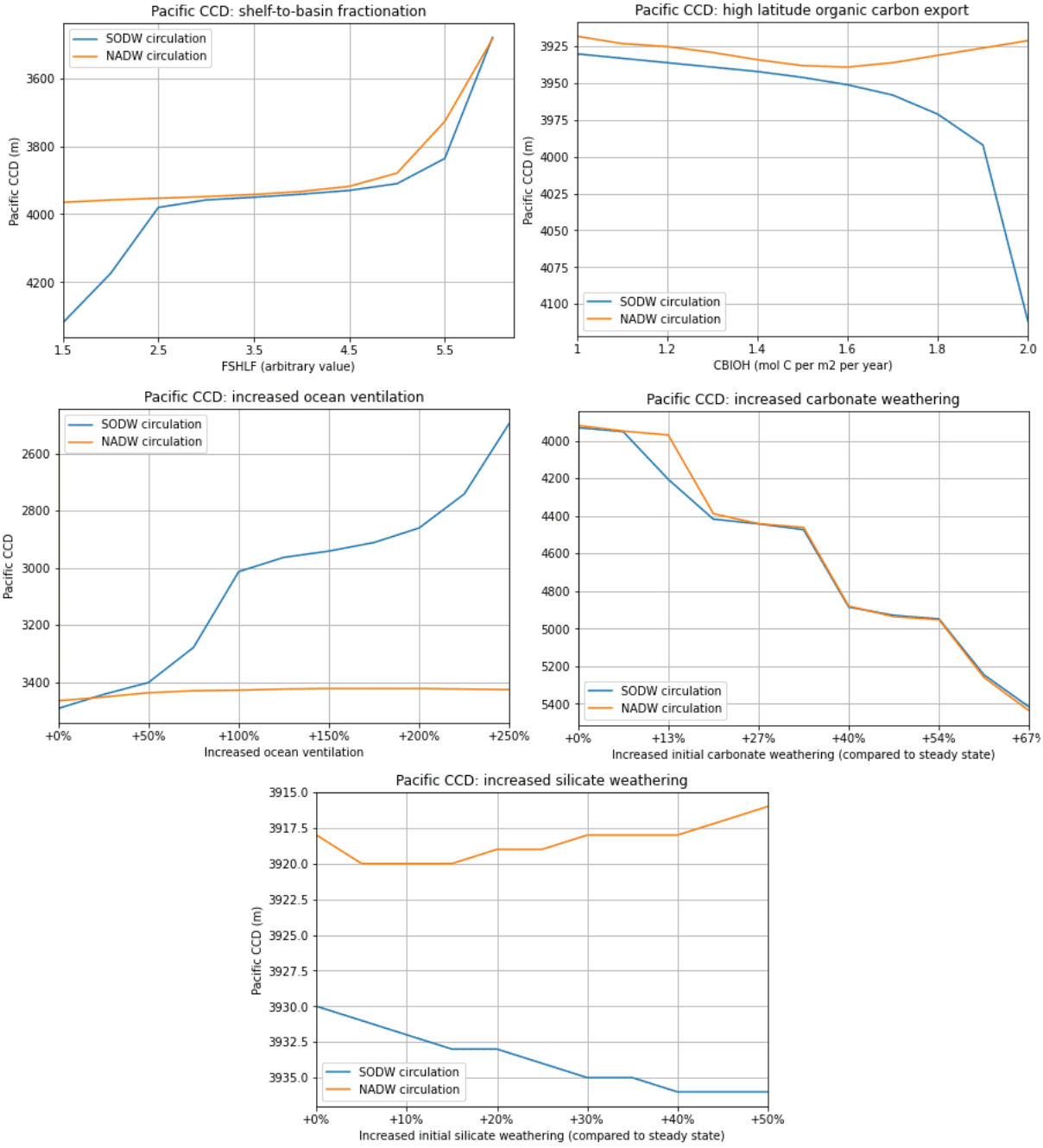
Pacific CCD: shelf-to-basin fractionation
SODW circulation
NADW circulation
Pacific CCD (m)
FSHLF (arbitrary value)
Pacific CCD: high latitude organic carbon export
CBIOH (mol C per m2 per year)
Pacific CCD: increased ocean ventilation
Pacific CCD
Increased ocean ventilation
Pacific CCD: increased carbonate weathering
Increased initial carbonate weathering (compared to steady state)
Pacific CCD: increased silicate weathering
Increased initial silicate weathering (compared to steady state)

Benthic Atlantic $\delta^{13}C$

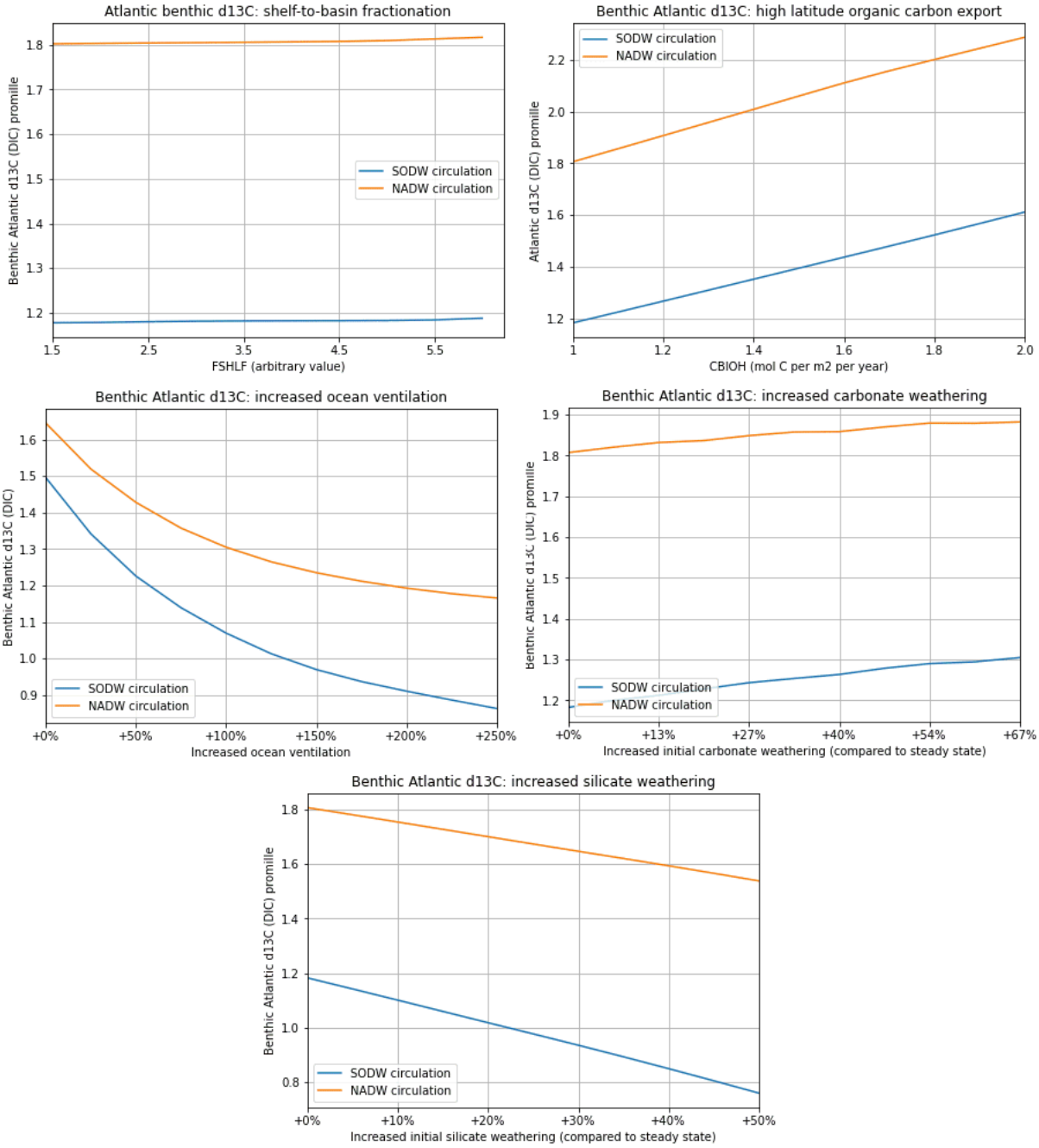

Benthic Pacific $\delta^{13}C$

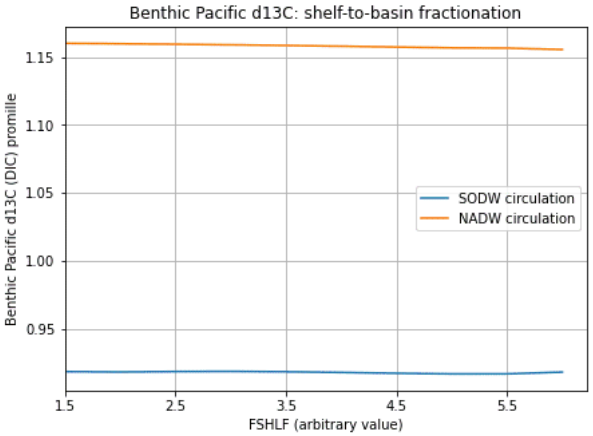

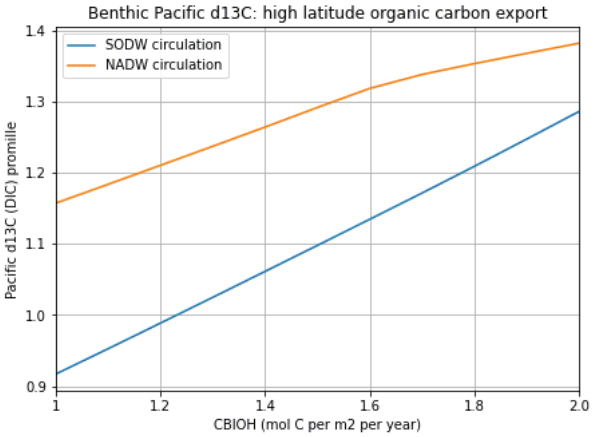

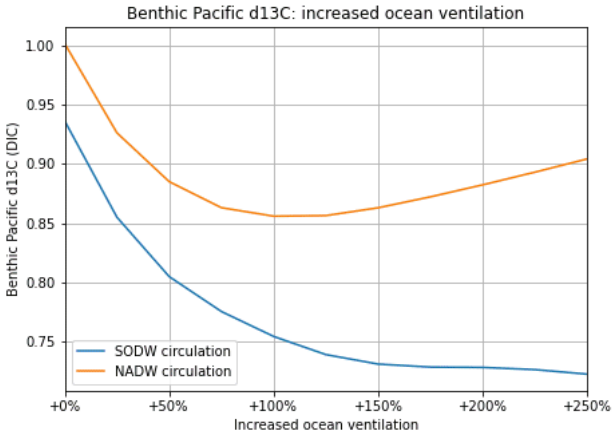

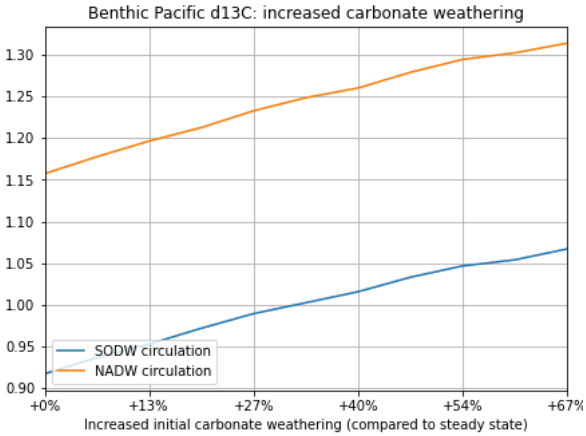

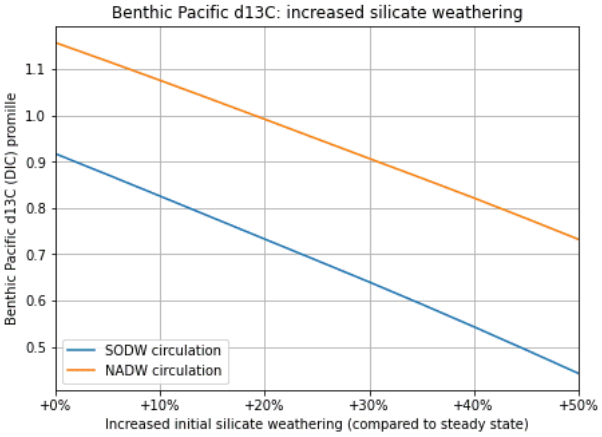

Atmospheric pCO2

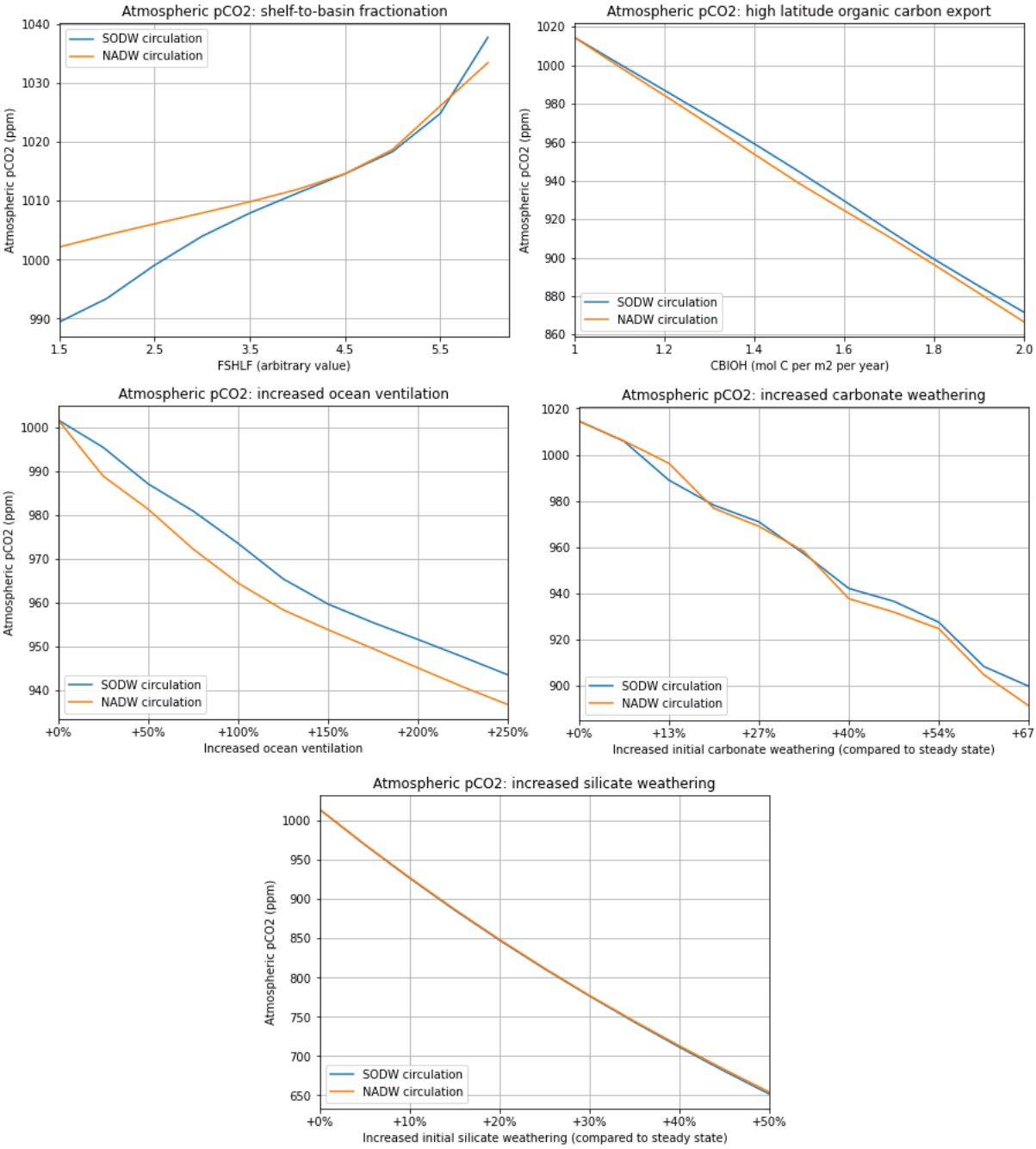

Appendix B: other proxies modelled

OCC:

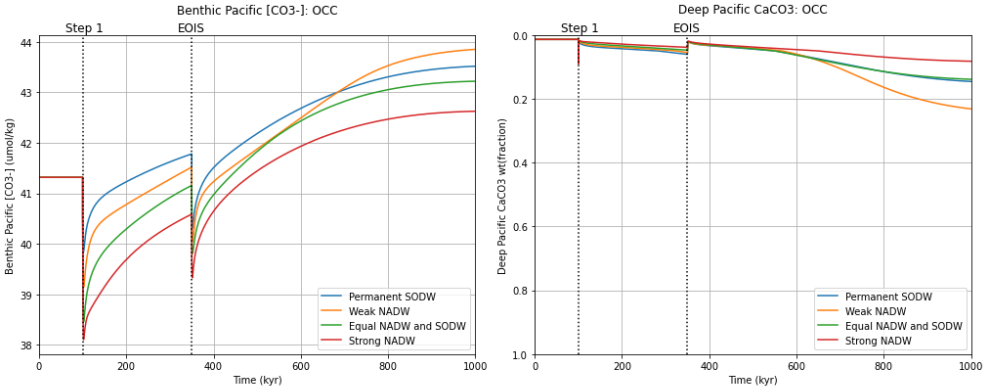

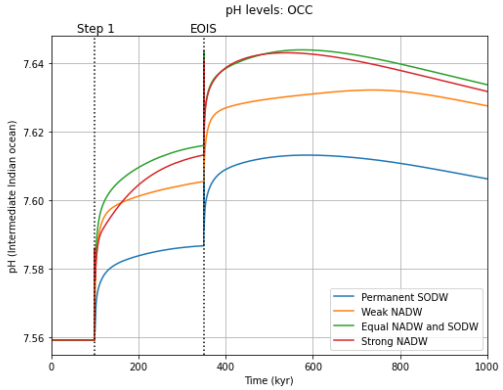

SBFC:

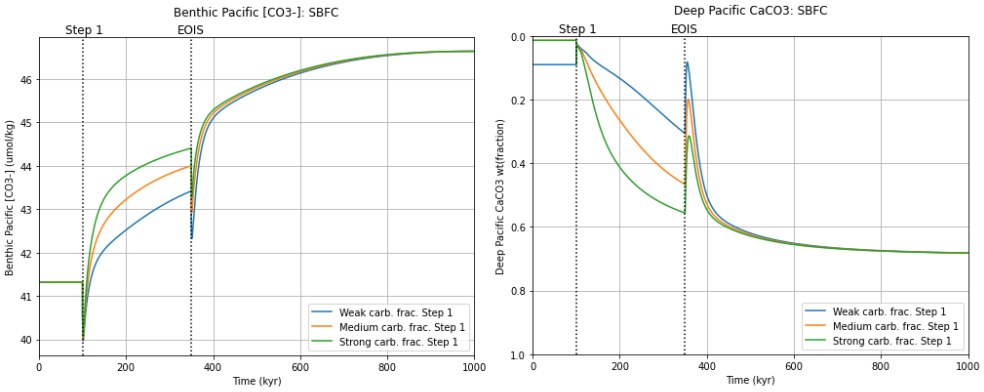

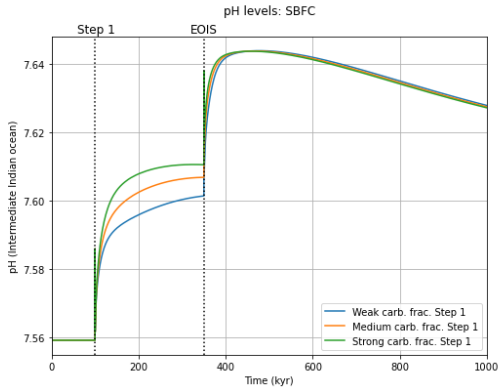

IHBP:

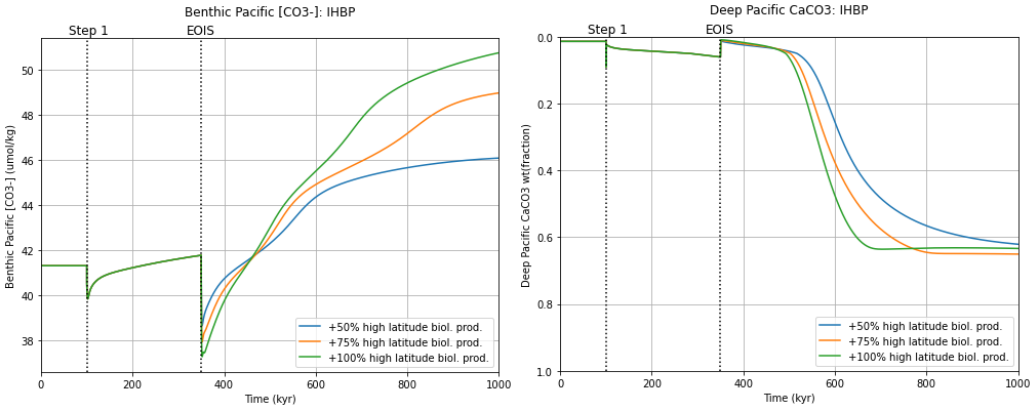
Benthic Pacific [CO3-]: IHBP
Step 1
EOIS
Benthic Pacific [CO3-] (umol/kg)
Time (kyr)
+50% high latitude biol. prod.
+75% high latitude biol. prod.
+100% high latitude biol. prod.
Deep Pacific CaCO3: IHBP
Deep Pacific CaCO3 wt(fraction)

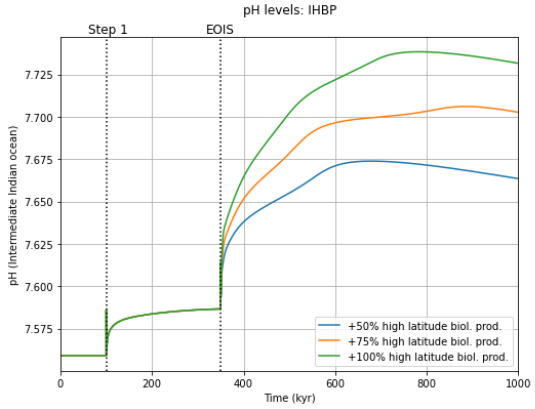
pH levels: IHBP
Step 1
EOIS
pH (Intermediate Indian ocean)
Time (kyr)
+50% high latitude biol. prod.
+75% high latitude biol. prod.
+100% high latitude biol. prod.

IOV:

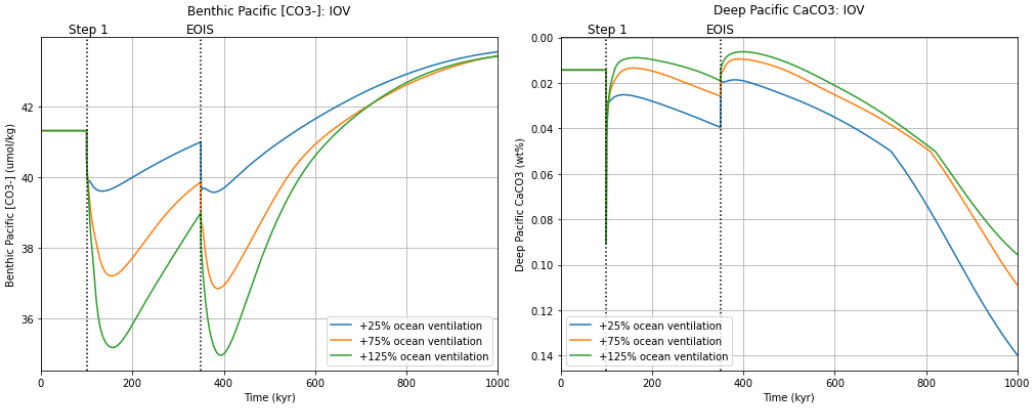
Benthic Pacific [CO3-]: IOV
Step 1
EOIS
Benthic Pacific [CO3-] (umol/kg)
Time (kyr)
+25% ocean ventilation
+75% ocean ventilation
+125% ocean ventilation
Deep Pacific CaCO3: IOV
Deep Pacific CaCO3 (wt%)

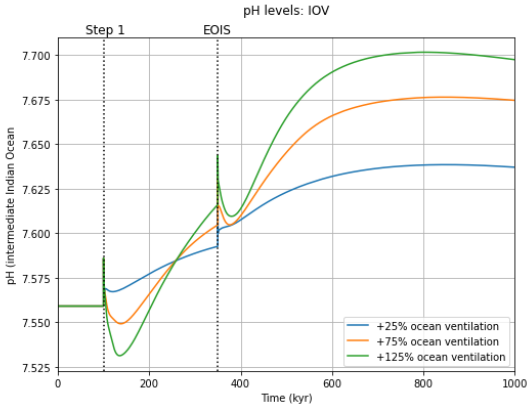
pH levels: IOV
Step 1
EOIS
pH (intermediate Indian Ocean
Time (kyr)
+25% ocean ventilation
+75% ocean ventilation
+125% ocean ventilation

ICW:

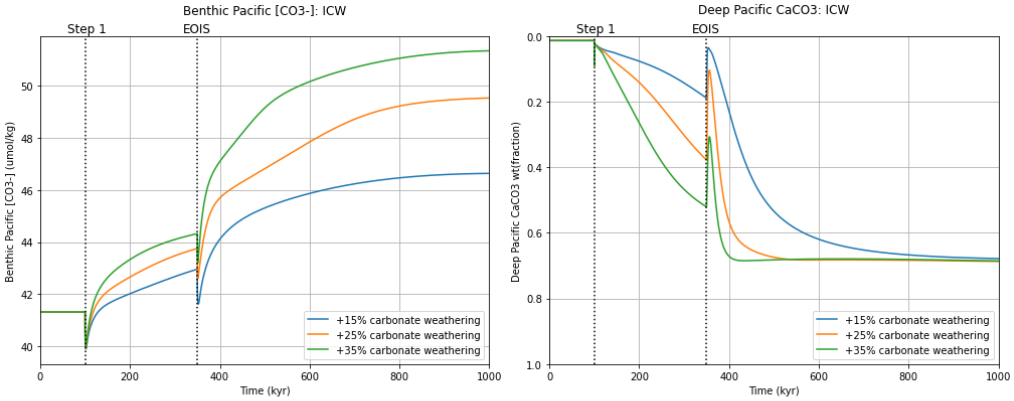
Benthic Pacific [CO3-]: ICW
Step 1
EOIS
Benthic Pacific [CO3-] (umol/kg)
Time (kyr)
+15% carbonate weathering
+25% carbonate weathering
+35% carbonate weathering
Deep Pacific CaCO3: ICW
Deep Pacific CaCO3 wt(fraction)

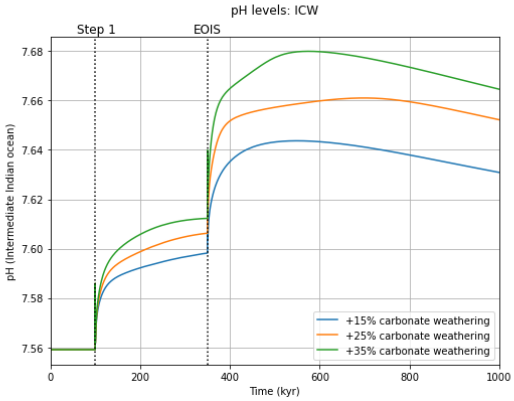
pH levels: ICW
Step 1
EOIS
pH (Intermediate Indian ocean)
Time (kyr)
+15% carbonate weathering
+25% carbonate weathering
+35% carbonate weathering

ISW:

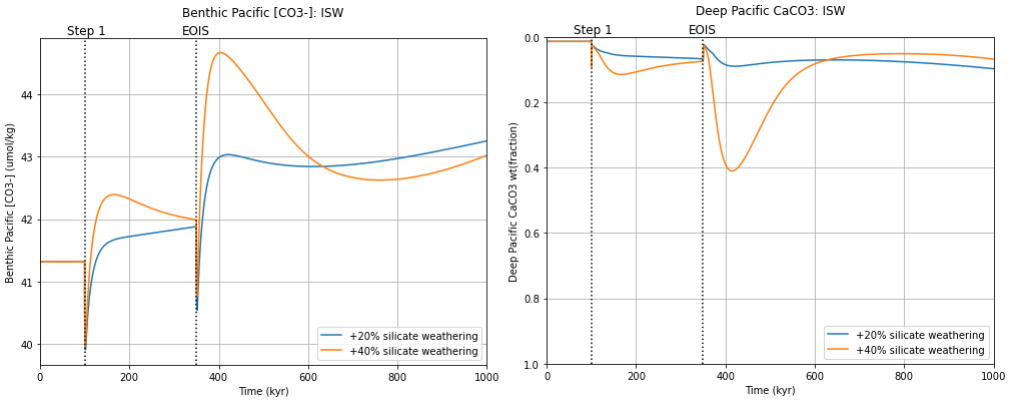
Benthic Pacific [CO3-]: ISW
Step 1
EOIS
Benthic Pacific [CO3-] (umol/kg)
Time (kyr)
+20% silicate weathering
+40% silicate weathering
Deep Pacific CaCO3: ISW
Deep Pacific CaCO3 wt(fraction)

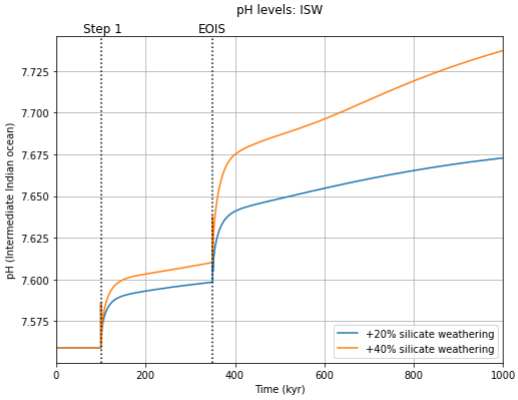
pH levels: ISW
Step 1
EOIS
pH (Intermediate Indian ocean)
Time (kyr)
+20% silicate weathering
+40% silicate weathering

CFW:

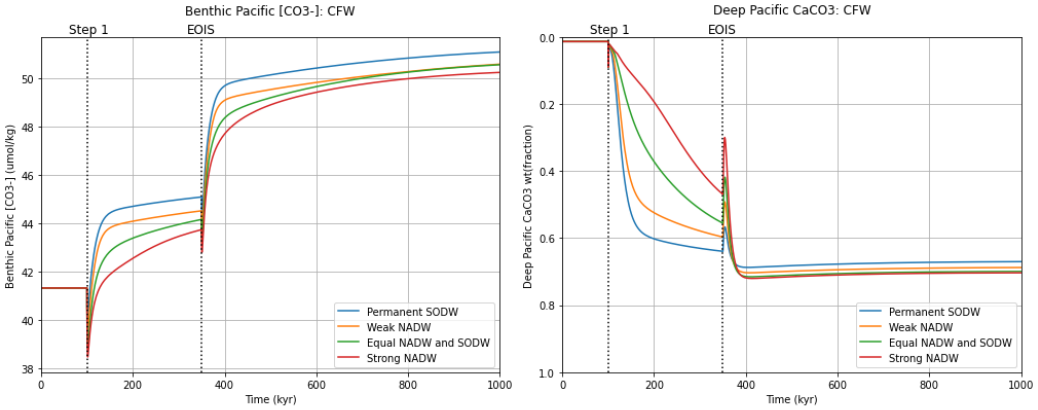
Benthic Pacific [CO3-]: CFW
Step 1
EOIS
Benthic Pacific [CO3-] (umol/kg)
Time (kyr)
Permanent SODW
Weak NADW
Equal NADW and SODW
Strong NADW

Deep Pacific CaCO3: CFW
Step 1
EOIS
Deep Pacific CaCO3 wt(fraction)
Time (kyr)
Permanent SODW
Weak NADW
Equal NADW and SODW
Strong NADW

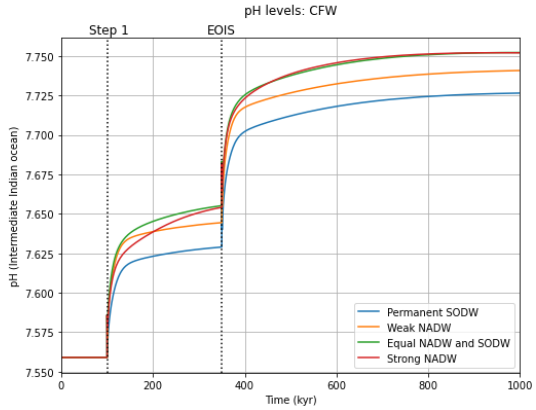
pH levels: CFW
Step 1
EOIS
pH (Intermediate Indian ocean)
Time (kyr)
Permanent SODW
Weak NADW
Equal NADW and SODW
Strong NADW

IBV:

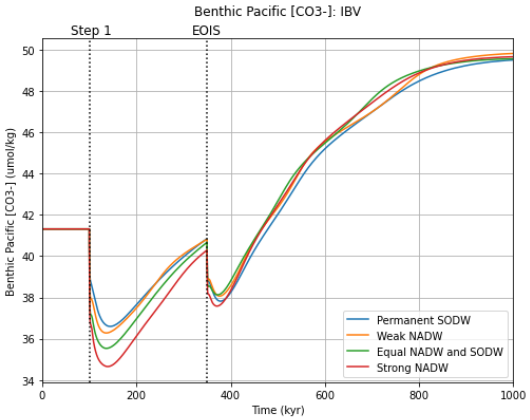
Benthic Pacific [CO3-]: IBV
Step 1
EOIS
Benthic Pacific [CO3-] (umol/kg)
Time (kyr)
Permanent SODW
Weak NADW
Equal NADW and SODW
Strong NADW

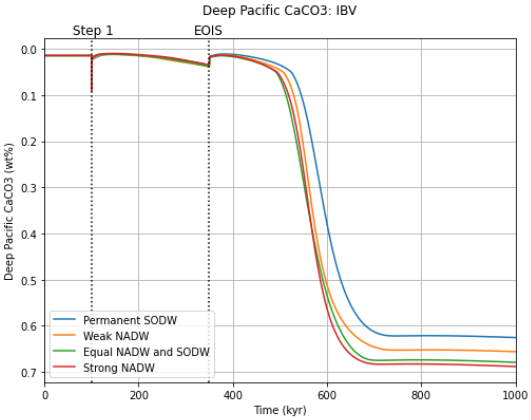
Deep Pacific CaCO3: IBV
Step 1
EOIS
Deep Pacific CaCO3 (wt%)
Time (kyr)
Permanent SODW
Weak NADW
Equal NADW and SODW
Strong NADW

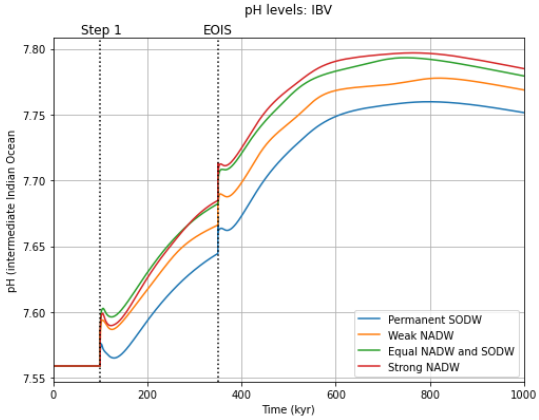
pH levels: IBV
Step 1
EOIS
pH (Intermediate Indian Ocean)
Time (kyr)
Permanent SODW
Weak NADW
Equal NADW and SODW
Strong NADW

Appendix C: Synthesis scenarios

Synthesis scenario 1 includes the following set-up:

Synthesis scenario 1 (first figure of Appendix) is an adapted version of the CFW scenario. Unlike the second synthesis scenario, which includes every hypothesis tested, synthesis scenario 1 only follows up on the CFW scenario. Silicate weathering is increased at Step 1 with 20%, and FSHLF declines to 3.0, just like synthesis scenario 2. Carbonate weathering increases with one-third of 25%, similarly to the CFW scenario. At EOIS, carbonate weathering increases with 50% (from initial steady state), but declines in about 300 kyr (similarly to biological productivity in synthesis scenario 1) to initial steady state. The extra weathered carbonate has a d13C signature of +4‰, higher than the +3‰ used in the CFW scenario. Further at EOIS, FSHLF declines to 1.5 from 3.0. Plots may exhibit "jagged" lines as to reduce model run time, the transient behaviour of carbonate weathering is applied every 25 kyr.

Synthesis scenario 2 includes the following set-up:

In general, Synthesis scenario 2 (second figure of Appendix) is an adapted version of the IBV scenario. At Step 1, a 15% increase in carbonate weathering, a 20% increase in silicate weathering and a FSHLF decline to 3.0 are added, to increase the severity of Step 1 on model output such as CCD and $CaCO_3$ (wt%). Just as the IBV scenario, at Step 1 half of a 75% increase in ocean ventilation and high latitude biological productivity are included as well. At EOIS, ventilation increases to 1.75x of initial steady state level (same as IBV scenario), while high latitude biological productivity is increased to 3.0x of initial steady state level (compared to a 1.75x increase from initial steady state in the IBV scenario). After EOIS, high latitude biological productivity is linearly decreased, such that it reaches initial steady state level again after about 300 kyr, to produce a transient response in biological productivity. Again, note that (some) plots exhibit jagged behaviour, as this linear decrease is enforced on a 25 kyr scale to increase model run time speed.

Both synthesis scenarios offer a good match with proxy records. The CCD deepens too much (>1.0 km) after EOIS, but due to the transient behaviour (of carbonate weathering and high latitude biological productivity in synthesis scenario 1 and 2, respectively), the CCD eventually shallows to position in the order of 1 km deeper than at initial steady state. Benthic $\delta^{13}C$ increases more in synthesis scenario 1 (in the order of 0.7 to 0.9‰), while benthic $\delta^{13}C$ in synthesis scenario 1 increases less severe (0.25 to 0.5‰, depending much on ocean circulation state). Both scenarios show a subsequent decrease, following proxy data, ca. 250 kyr after EOIS. Synthesis scenario 2 shows a somewhat stronger control on atmospheric pCO_2, $[CO_3^{-}]$ and pH levels, while synthesis scenario 1 shows a more stable $CaCO_3$ wt(%) modelled record. Both scenarios are capable of hitting an atmospheric pCO2 of <800 ppm before EOIS, roughly in the range of modelled Antarctic glaciation threshold levels.

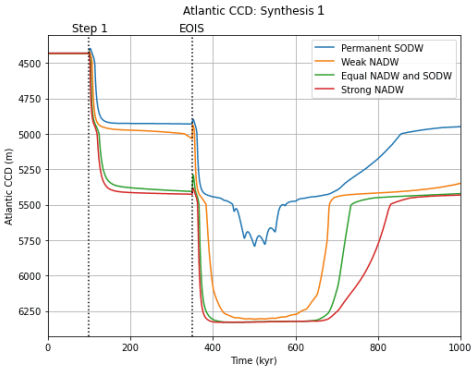
Atlantic CCD: Synthesis 1
Step 1
EOIS
Permanent SODW
Weak NADW
Equal NADW and SODW
Strong NADW
Atlantic CCD (m)
Time (kyr)

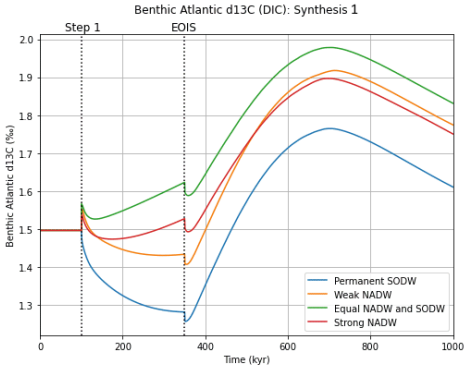
Benthic Atlantic d13C (DIC): Synthesis 1
Step 1
EOIS
Permanent SODW
Weak NADW
Equal NADW and SODW
Strong NADW
Benthic Atlantic d13C (‰)
Time (kyr)

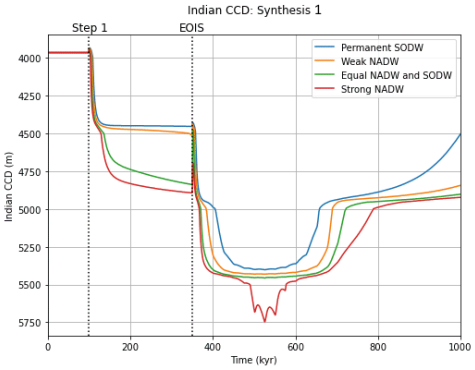
Indian CCD: Synthesis 1
Step 1
EOIS
Permanent SODW
Weak NADW
Equal NADW and SODW
Strong NADW
Indian CCD (m)
Time (kyr)

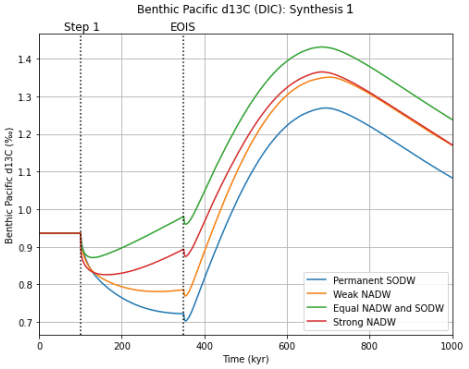
Benthic Pacific d13C (DIC): Synthesis 1
Step 1
EOIS
Permanent SODW
Weak NADW
Equal NADW and SODW
Strong NADW
Benthic Pacific d13C (‰)
Time (kyr)

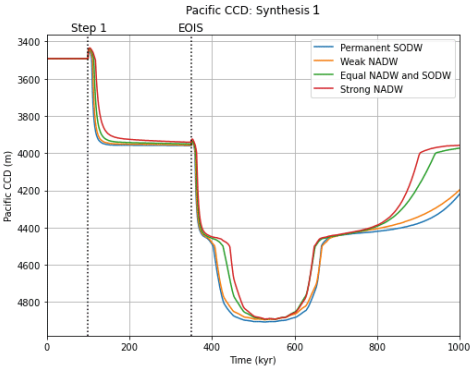
Pacific CCD: Synthesis 1
Step 1
EOIS
Permanent SODW
Weak NADW
Equal NADW and SODW
Strong NADW
Pacific CCD (m)
Time (kyr)

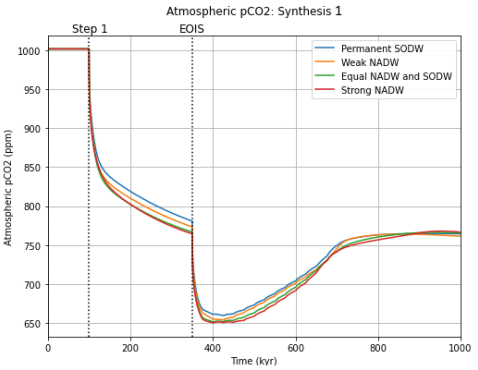
Atmospheric pCO2: Synthesis 1
Step 1
EOIS
Permanent SODW
Weak NADW
Equal NADW and SODW
Strong NADW
Atmospheric pCO2 (ppm)
Time (kyr)

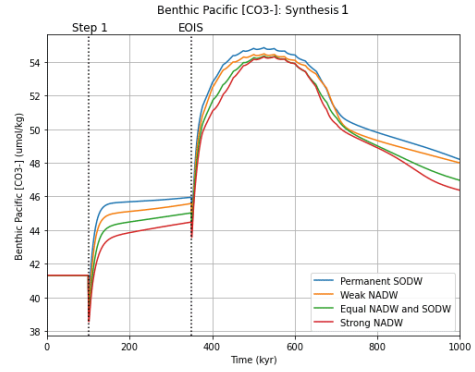
Benthic Pacific [CO3-]: Synthesis 1
Step 1
EOIS
Permanent SODW
Weak NADW
Equal NADW and SODW
Strong NADW
Benthic Pacific [CO3-] (umol/kg)
Time (kyr)

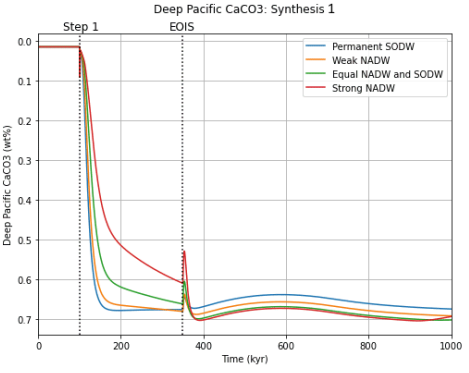
Deep Pacific CaCO3: Synthesis 1
Step 1
EOIS
Permanent SODW
Weak NADW
Equal NADW and SODW
Strong NADW
Deep Pacific CaCO3 (wt%)
Time (kyr)

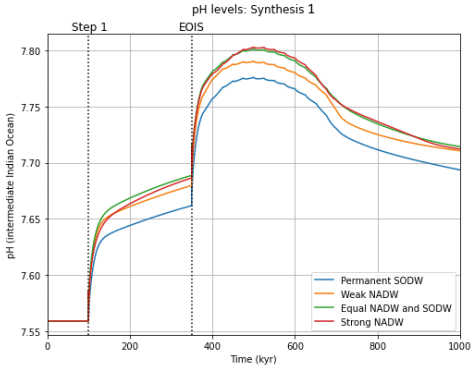
pH levels: Synthesis 1
Step 1
EOIS
Permanent SODW
Weak NADW
Equal NADW and SODW
Strong NADW
pH (intermediate Indian Ocean)
Time (kyr)

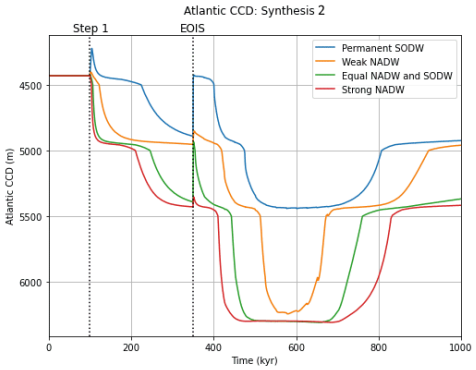
Atlantic CCD: Synthesis 2
Step 1
EOIS
Permanent SODW
Weak NADW
Equal NADW and SODW
Strong NADW
Atlantic CCD (m)
Time (kyr)

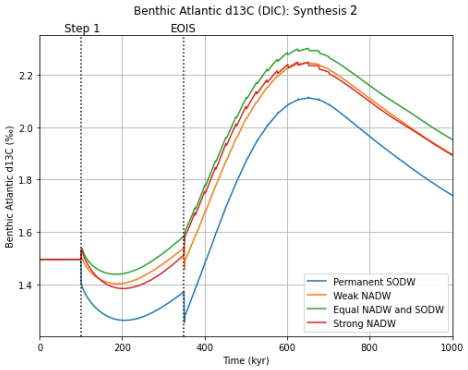
Benthic Atlantic d13C (DIC): Synthesis 2
Step 1
EOIS
Permanent SODW
Weak NADW
Equal NADW and SODW
Strong NADW
Benthic Atlantic d13C (‰)
Time (kyr)

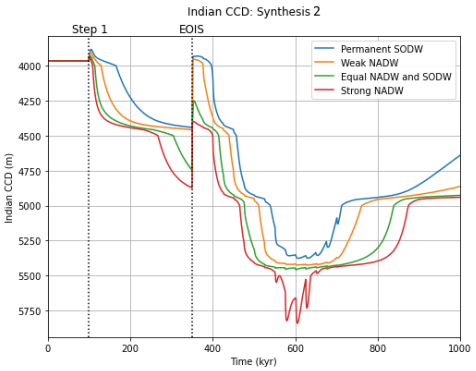
Indian CCD: Synthesis 2
Step 1
EOIS
Permanent SODW
Weak NADW
Equal NADW and SODW
Strong NADW
Indian CCD (m)
Time (kyr)

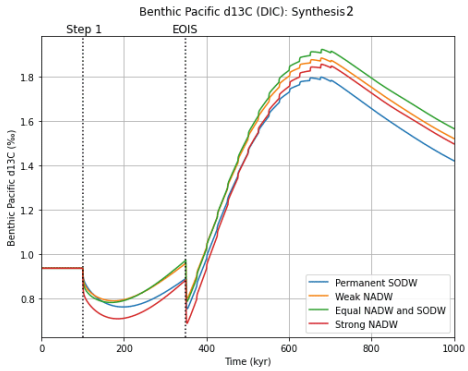
Benthic Pacific d13C (DIC): Synthesis 2
Step 1
EOIS
Permanent SODW
Weak NADW
Equal NADW and SODW
Strong NADW
Benthic Pacific d13C (‰)
Time (kyr)

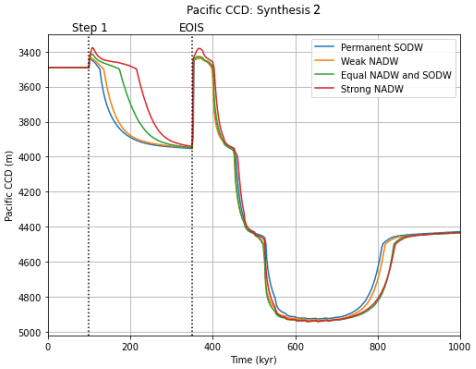
Pacific CCD: Synthesis 2
Step 1
EOIS
Permanent SODW
Weak NADW
Equal NADW and SODW
Strong NADW
Pacific CCD (m)
Time (kyr)

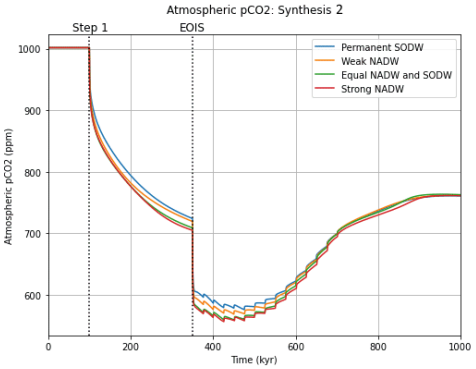
Atmospheric pCO2: Synthesis 2
Step 1
EOIS
Permanent SODW
Weak NADW
Equal NADW and SODW
Strong NADW
Atmospheric pCO2 (ppm)
Time (kyr)

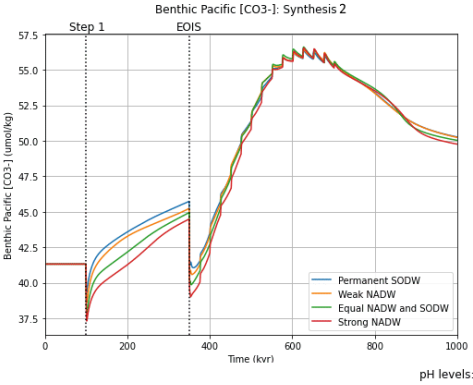
Benthic Pacific [CO3-]: Synthesis 2
Step 1
EOIS
Permanent SODW
Weak NADW
Equal NADW and SODW
Strong NADW
Benthic Pacific [CO3-] (umol/kg)
Time (kyr)

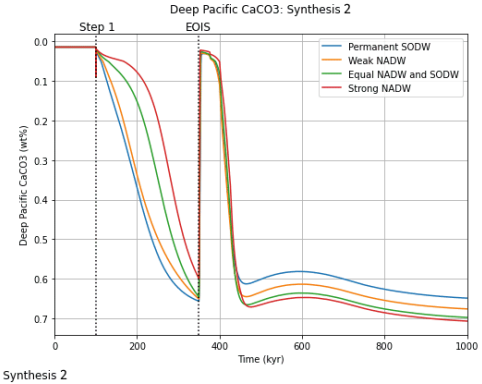
Deep Pacific CaCO3: Synthesis 2
Step 1
EOIS
Permanent SODW
Weak NADW
Equal NADW and SODW
Strong NADW
Deep Pacific CaCO3 (wt%)
Time (kyr)

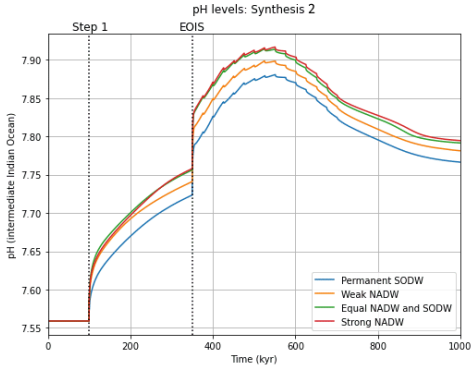
pH levels: Synthesis 2
Step 1
EOIS
Permanent SODW
Weak NADW
Equal NADW and SODW
Strong NADW
pH (intermediate Indian Ocean)
Time (kyr)